INTELLIGENT COMPUTATIONAL SOLUTIONS FOR CONSTITUTIVE MODELLING OF MATERIALS IN FINITE ELEMENT ANALYSIS

Asaad Faramarzi

PhD in Engineering

University of Exeter
October 2011

College of Engineering, Mathematics and Physical Sciences

INTELLIGENT COMPUTATIONAL SOLUTIONS FOR CONSTITUTIVE MODELLING OF MATERIALS IN FINITE ELEMENT ANALYSIS

Submitted by

ASAAD FARAMARZI

to the University of Exeter as a thesis for the degree of

Doctor of Philosophy in Engineering

October 2011

I certify that all material in this thesis which is not my own work has been identified and that no material has previously been submitted and approved for the award of a degree by this or any other University.

.....

To My Family

ACKNOWLEDGEMENTS

First of all I would like to express my deepest gratitude to my supervisor, Prof. Akbar A. Javadi for his support, guidance, great inspiration, and encouragement during my PhD studies in University of Exeter. The completion of this thesis would not have been possible without his enthusiasm for the ideas and concepts developed in this thesis.

I wish to thank the former and present members of the Computational Geomechanics Group in University of Exeter and in particular Mr. Alireza Ahangar-Asr for their supports throughout my study.

I would like to thank my mother and my father who have loved me and supported me for long time. I am deeply indebted to my brother Dr. Amir Faramarzi, who always has encouraged me and supported me during my studies. Indeed, he has been the greatest inspiration of my life. I wish to gratefully thank my sisters Zhila and Mitra and their family for their abiding loves, encouragements and helps. I also would like to thank my sister-in-law Dr. Aviz Rahimzadeh and all other member of my family for their kindnesses and supports.

At last but not least I would like to thank my wife, Moura, whose love, patience, help and support made the work possible.

ABSTRACT

Over the past decades simulation techniques, and in particular finite element method, have been used successfully to predict the response of systems across a whole range of industries including aerospace, automotive, chemical processes, geotechnical engineering and many others. In these numerical analyses, the behaviour of the actual material is approximated with that of an idealised material that deforms in accordance with some constitutive relationships. Therefore, the choice of an appropriate constitutive model that adequately describes the behaviour of the material plays an important role in the accuracy and reliability of the numerical predictions. During the past decades several constitutive models have been developed for various materials.

In recent years, by rapid and effective developments in computational software and hardware, alternative computer aided pattern recognition techniques have been introduced to constitutive modelling of materials. The main idea behind pattern recognition systems such as neural network, fuzzy logic or genetic programming is that they learn adaptively from experience and extract various discriminants, each appropriate for its purpose.

In this thesis a novel approach is presented and employed to develop constitutive models for materials in general and soils in particular based on evolutionary polynomial regression (EPR). EPR is a hybrid data mining technique that searches for symbolic structures (representing the behaviour of a system) using genetic algorithm and estimates the constant values by the least squares method. Stress-strain data from experiments are employed to train and develop EPR-based material models. The developed models are compared with some of the existing conventional constitutive material models and its advantages are highlighted. It is also shown that the developed EPR-based material models can be incorporated in finite element (FE) analysis. Different examples are used to verify the developed EPR-based FE model. The results of the EPR-FEM are compared with those of a standard FEM where conventional constitutive models are used to model the material behaviour. These results show that EPR-FEM can be successfully employed to analyse different structural and geotechnical engineering problems.

TABLE OF CONTENTS

LIST OF FIGURES

LIST OF TABLES

LIST OF ABBREVIATIONS

ANN	Artificial Neural Network
BPNN	Back-Propagation Neural Network
COD	Coefficient of Determination
EEP	Extended End Plate connection
EPR	Evolutionary Polynomial Regression
EPRCM	Evolutionary Polynomial Regression based Constitutive Model
EPR-FEM	Evolutionary Polynomial Regression based Finite Element Method
FE	Finite Element
FEA	Finite Element Analysis
FEM	Finite Element Method
GA	Genetic Algorithm
GP	Genetic Programming
GUI	Graphical user interface
LS	Least Square
MC	Mohr-Coulomb
MCC	Modified Cam Clay
MOGA	Multi-Objective Genetic Algorithm
MO-EPR	Multi-Objective approach in Evolutionary Polynomial Regression
NN	Neural Network
NNCM	Neural Network based Constitutive Model
PCS	Penalisation of Complex Structures
PDE	Partial Differential Equations
PSSP	Plane-strain strain probe
SOGA	Single-Objective Genetic Algorithm
SPSW	Steel plate shear wall
SSE	Sum of Squared Errors
TSADWA	top-and-seat angle with double web-angle connection
TTSP	True triaxial strain probe
UMAT	User Material Subroutine

LIST OF SYMBOLS

ε_{11}	Strain in 11 direction
ε_{22}	Strain in 22 direction
ε_{33}	Strain in 33 direction
γ_{12}	Strain in 12 direction
$\boldsymbol{\varepsilon}$	Vector of strain
$\dot{\varepsilon}$	Strain rate
ε_v	Volumetric strain
$\Delta\varepsilon_1$	Increment of major principal strain
ε_1	Major principal strain
ε_3	Minor principal strain
ε_x	Strain in x direction
ε_y	Strain in y direction
ε_z	Strain in z direction
γ_{xy}	Shear strain
ε_a	Axial strain in triaxial apparatus
ε_r	Radial strain in triaxial apparatus
ε_q	Distortional strain
$\Delta\varepsilon_q$	Increment of distortional strain
σ_{11}	Stress in 11 direction
σ_{22}	Stress in 22 direction
σ_{33}	Stress in 33 direction
τ_{12}	Stress in 12 direction
$\boldsymbol{\sigma}$	Vector of stress
$\dot{\sigma}$	Stress rate
σ_1	Major principal stress
σ_3	Minor principal stress
σ_x	Stress in x direction
σ_y	Stress in y direction

σ_z	Stress in z direction
τ_{xy}	Shear stress
σ_d	Deviator stress
$\acute{\sigma}_3$	Effective confining pressure
σ_a	Axial stress in triaxial apparatus
σ_r	Radial stress in triaxial apparatus
D_{50}	Median grain size
h	Hardness of mineral
n_s	Shape factor
e	Void ratio
C_u	Coefficient of uniformity
C_c	Coefficient of curvature
d_b	Depth of beam
t_b	Thickness of end plate
f_b	Diameter of bolt
θ	Rotational displacement
M	Rotational moment
$\mathrm{D_{NN}}$	Neural network stiffness matrix
E	Elastic modulus
ν	Poisson's ratio
G	Shear modulus
$\acute{p}$	Mean stress
q	Deviator stress
$\acute{C}$	Cohesion intercept
$\acute{\phi}$	Friction angle
M	Slope of critical line in the $\acute{p} - q$ space
λ	Slope of the normal consolidation line
κ	Slope of the unloading-reloading line
e_0	Initial void ratio
γ	Unit weight of soil
v	Specific volume

p_0	Isotropic pre-consolidation pressure
K	Bulk modulus
$\mathbf{D}$	Stiffness matrix
$\mathbf{D}^{\mathrm{e}}$	Elastic stiffness matrix
$\mathbf{D}^{\mathrm{p}}$	Plastic stiffness matrix
$\mathbf{D}^{\mathrm{ep}}$	Elasto-plastic stiffness matrix
$\mathbf{J}$	Jacobian Matrix

Chapter 1

INTRODUCTION

1.1 General Background

Constitutive models are relationships between two or more physical quantities that represent different aspects of material behaviour and predict the response of that material to applied loads, displacements, etc. Constitutive models play an important role in modelling the behaviour of materials. In the past decades several constitutive models have been developed to predict the behaviour of different materials including soils. Among these model there are simple elastic models (Hooke, 1675); or more complex material models such as cam clay model (Schofield & Worth, 1968) or Lade's single hardening model (Lade & Jakobsen, 2002). Most of these models involve determination of material parameters. Generally in conventional constitutive material modelling, the parameters of the model are identified from appropriate physical tests on representative samples.

One of the most fundamental functions of a constitutive model is its application in numerical modelling techniques such as finite element method (FEM). Finite element

method is a numerical technique to find approximate solutions of partial differential equations (PDE). Most of the problems in engineering design and analysis can be modelled as a single or a set of differential equations. These differential equations describe the response of a system subjected to external influences. Many differential equations can not be solved analytically and usually numerical techniques are used to find their approximate solutions. Among numerical techniques the finite element method is known to be one of the most powerful general techniques for the numerical solution of variety of problems encountered in engineering. The basic idea behind finite element method is to divide the structure, body, or region being analysed into a large number of elements (Stasa, 1986).

It is known that the accuracy of the finite element analyses results is mostly dependant on the choice of an appropriate constitutive model that represents the material behaviour. Therefore one of the crucial aspects of FE analysis is selecting the appropriate constitutive model. Despite the large number of existing conventional constitutive models and their complexity, none of these models can completely describe the real behaviour of some materials (e.g., soils, rocks, composites, etc.) under different loading conditions due to the erratic and complex nature of these materials. Therefore alternative and different methods for developing material models seem to be vital.

For the first time, Ghaboussi and his co-workers (1991) proposed to use artificial neural network (ANN) for modelling the behaviour of concrete. After that other researchers continued to apply this technique to modelling the behaviour of other materials. Some of these works have proposed to incorporate the neural network material models in finite element method to analysis engineering boundary value problems. Researchers like Ghaboussi et al., (1998), Shin & Pande, (2000) and Hashash et al., (2006) proposed autoprogressive or self learning approach to train neural network material models via sequences of training an embeded neural network (NN) in a FEM using measured displacements and forces of a structural or geotechnical test. These works indicated that NNs can be used to model the behaviour of materials. They also showed that if the trained NN is used in FEM, it can provide reasonable and good predictions for analysing engineering problems in comparison to the conventional FEM. However NNs suffer from some shortcomings. One of the disadvantages of the NNCM is that the optimum structure of the NN (such as number of inputs, hidden layers, transfer

functions, etc.) must be identified a priori which is usually obtained using a time consuming trial and error procedure (Giustolisi & Savic, 2006). Another main drawback of the NN approach is the large complexity of the network structure, as it represents the knowledge in terms of a weight matrix together with biases which are not accessible to user. In other words NN models give no information on the way the inputs affect the output and therefore are considered as a black box class of models. The lack of interpretability of NN models has stopped them from achieving their full potential in real world problems (Lu et al., 2001 and Javadi & Rezania, 2009a).

For the reasons mentioned above, an alternative data mining technique which can dispel the drawbacks of NN would be very benefitial. Among other data mining techniques a novel and recently developed technique named evolutionary polynomial regression (EPR) is considered here as a strong alternative for NN since it express the model being studied in terms of structured mathematical equations. EPR was first introduced and used by Giustolisi & Savic, (2006) to study the hydroinformatics and environmental related problems. EPR is a two-step technique where in the first step it searches for symbolic structures using a genetic algorithm and in the second step EPR estimates constant values by solving a linear least square problem. The application of EPR in modelling and analysing different discipilines of engineering and in particular geotechnical and structural engineering have also been investigated by the author of this thesis and his co-workers.

1.2 Objectives

The potential of EPR in pattern recognition and data mining as well as its capability in returning transparent mathematical expressions to describe systems, have been an inspiration to employ this technique in constitutive material modelling soils. Therefore the objective of this PhD thesis can be outlined in the following items:

- Review the main and recent developments in using data mining techniques in material modelling and their implementation in FE.
- Introduce and develop different approaches of material modelling using EPR.
- Present a technique to extract additional data from a single standard test in order to prepare adequate data for training EPR.

- Develop different material models for different purposes and different materials. In particular develop material models for soils in order to simulate both its stress-strain and volumetric behaviour.
- Develop a model to predict cyclic behaviour of soils.
- Construct Jacobian matrix using partial derivatives of developed constitutive models.
- Incorporate the developed EPR material models in FEM.
- Verify the EPR-based FEM using a number of illustrative examples.

1.3 Layout of the thesis

The thesis consists of six chapters; a brief description of the contents of each chapter is given in the following paragraphs.

Chapter two provides a literature review of the key and recent developments in the use of data mining techniques in material modelling. This chapter begins with the historical background of conventional constitutive material modelling as well as first and latest developments in using data mining techniques and in particular neural networks in material modelling and its incorporation in finite element analysis.

Chapter three presents a complete explanation of the new data mining technique, evolutionary polynomial regression (EPR). This chapter starts with a general introduction on most popular data mining techniques, artificial neural network (ANN) and genetic programming (GP). In addition a brief description of evolutionary algorithms and genetic algorithms is outlined since it is the main idea behind EPR. The main focus of this chapter is on description of the EPR and its key features.

In chapter four, EPR based modelling of materials and in particular soil is introduced. Two different approaches are introduced to train and develop EPR-based model. Also finding the optimum EPR models will be discussed in this chapter. The developed EPR-based models are compared with other conventional constitutive material models and its advantages are highlighted. Moreover an EPR-based model for cyclic behaviour of material is developed and presented.

In chapter five, a procedure is presented for construction of the Jacobian matrix from the EPR models using their partial derivatives. Also a methodology is presented for incorporating of EPR-based model in FEM and in particular ABAQUS (FE software). A number of different examples are provided to validate the developed EPR-based FEM. The presented examples range from simple to complex geometry and from monotonic to cyclic loading conditions with both linear and nonlinear material behaviour. The results of the EPR-based FEM are compared to those obtained from standard FEM using conventional constitutive models.

The final chapter 6 presents the main conclusions of the thesis and recommendations for further research.

Chapter 2

REVIEW OF DATA MINING BASED CONSTITUTIVE MODELLING

2.1 Introduction

During the recent decades, simulation techniques and particularly the finite element method (FEM) have been extensively and successfully used as a robust tool in the analysis of a wide range of engineering problems including aerospace, structural engineering, automotive, biomedical, geotechnical engineering and many others. In this numerical analysis, the behaviour of the actual material is approximated with that of an idealised material that deforms in accordance with some constitutive relationships. Therefore, the choice of an appropriate constitutive model that adequately describes the behaviour of the material plays an important role in the accuracy and reliability of the numerical predictions.

This chapter review some of the application of the recently developed data mining techniques in material modelling and discuss their advantages and shortcomings.

2.2 Conventional Constitutive Modelling

In the past few decades several constitutive models have been developed for various materials including soils. Among theses models there are simple elastic models (Hooke, 1675); plastic models (e.g., Drucker and Prager, 1952), models based on critical state of soils (Schofield & Worth, 1968), single or double hardening models (Lade & Jakobsen, 2002; Lade, 1977), etc. Most of these models involve determination of material parameters, many of which have little or no physical meaning (Shin & Pande, 2000).

In conventional constitutive material modelling, an appropriate mathematical model is initially selected and the parameters of the model (material parameters) are identified from appropriate physical tests on representative samples to capture the material behaviour. When these constitutive models are used in finite element analysis, the accuracy with which the selected material model represents the various aspects of the actual material behaviour and also the accuracy of the identified material parameters affect the accuracy of the finite element predictions. In spite of considerable complexities of constitutive theories, due to the erratic and complex nature of some materials such as soils, rocks, composites, etc., none of the existing constitutive models can completely describe the real behaviour of these materials under various stress paths and loading conditions.

2.3 Application of data mining techniques in constitutive modelling

In recent years, by rapid and effective developments in computational software and hardware, alternative computer aided pattern recognition approaches have been introduced to constitutive modelling of materials. The main idea behind pattern recognition systems such as neural network, fuzzy logic or genetic programming is that they learn adaptively from experience and extract various discriminants, each appropriate for its purpose. Artificial neural networks (ANNs) are the most widely used pattern recognition procedures that have been employed for constitutive modelling of materials. Recently other data mining techniques such as evolutionary methods have

been utilised to modelling the behaviour of materials. In what follows a review of the key works and the latest development in this field is presented.

The application of ANN for constitutive modelling was first proposed by Ghaboussi et al. (1991) for modelling concrete behaviour. The use of ANN was also continued by Ellis et al. (1992) and Ghaboussi et al. (1994), who applied this technique to modelling of geomaterials. These works indicates that neural network based constitutive models can capture nonlinear material behaviour. These models are versatile and have the ability to continuously learn as additional data become available.

ANN models have the ability to operate on large quantities of data and learn complex model functions from examples, i.e., by training on sets of input and output data. The greatest advantage of ANNs over traditional material models is their ability to capture nonlinear and complex interaction between variables of the system without having to assume the form of the relationship between input and output variables.

The role of the neural network (NN) is to assign a given set of output vectors to a given set of input vectors. When applied to the constitutive description, the physical nature of these input-output data is determined by the measured quantities like stresses, strains, pore pressure, temperature, etc (Javadi et al., 2009).

A typical NN based constitutive model is shown in Figure 2.1.

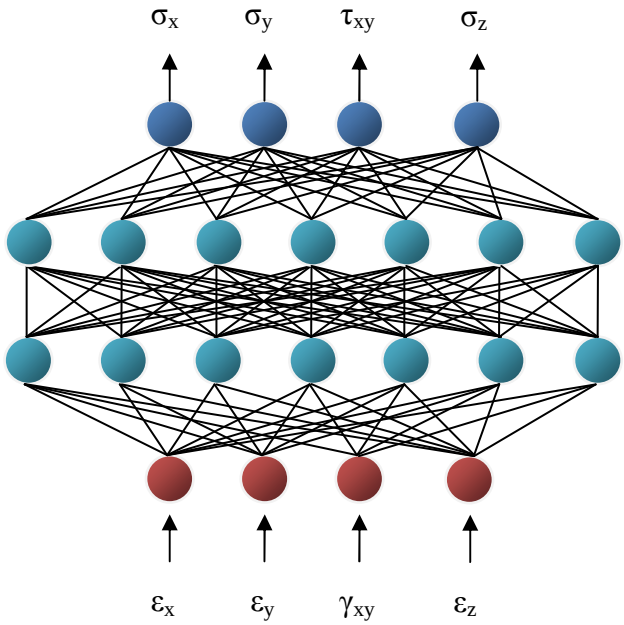

Figure 2.1: A simple neural network based constitutive model (after Shin, 2001)

In this simple network, one input layer, two hidden layers, and one output layer are used to represent a constitutive model. Inputs are four strain components (ε_x, ε_y, ε_{xy}, and ε_z) for a two dimensional problem and a forward pass through the network results in the prediction of four corresponding stresses (σ_x, σ_y, σ_{xy}, and σ_z) at the output layer. Every neuron in each layer is connected to every neuron in the next layer with a "connection weight". The knowledge stored in the developed network is represented by the set of connection weights. The neural network is trained by appropriately modifying its connection weights, through the set of "training cases", until the predicted stress variables agree satisfactory with the correct stress variables. Sometimes the NN developed in this way is called back-propagation NN. The "back-propagation" term refers to the algorithm by which the observed error in the predicted stress variables is used to modify the connection weights.

Ghaboussi and Sidarta (1998) introduced nested adaptive neural network (NANN) and applied this neural network in modelling of the constitutive behaviour of geomaterials. NANNs take advantage of the nested structure of the material test data, and reflect it in the architecture of the neural network. They applied this new type of neural network in modelling of the drained and un-drained behaviour of sand in triaxial tests.

Penumadu & Zhao (1999) modelled the stress-strain and volume change behaviour of sand and gravel under drained triaxial compression test conditions using neural network. They used a vast number of database (around 250 triaxial test data) collected from literature to train the neural network. They performed a trial and error procedure to find the optimum architecture of the neural network. The developed neural network consisted of 3 hidden layers, eleven neuron in input, 15 neurons in each hidden layer and two outputs. The input and output parameters were as follow:

Inputs: $D_{50}, C_u, C_c, h, n_s, e, \varepsilon^i, \Delta\varepsilon^i, \acute{\sigma}_3, \sigma_d^i, \varepsilon_v^i$
Outputs: σ_d^{i+1}, ε_v^{i+1}

where D_{50}, C_u, C_c are equivalent particle size and their distribution, h is hardness of material, , n_s shape factor, e is void ratio, and $\acute{\sigma}_3$ is effective confining pressure. The current state units of stress and strain were represented with three inputs using deviator stress σ_d^i, axial strain ε^i and volumetric strain ε_v^i. For a given specimen conditions and

current state units the objective of neural network was prediction of two outputs, deviator stress σ_d^{i+1} and volumetric strain ε_v^{i+1} of the next state of an input axial strain increment $\Delta\varepsilon^i$. It was observed that the developed NN model has captured the behaviour of soil with an acceptable accuracy in terms of both non-linear stress-strain relationship, and volume change. Despite developing a very comprehensive ANN-based model for granular soils from a large database, the incorporation of this model in a finite element (or another simulation) model was not presented.

Shin and Pande (2002) described a strategy to generate additional data from general homogeneous material tests in order to train NNCM. This was done by taking advantage of isotropy when it is applicable to the material under consideration. Assuming isotropy, transformation of the stress-strain pairs was carried out by rotating the datum axes (X-Y-Z) from the original axes (1-2-3) in which the material test has been done. This resulted in increasing the training data significantly. A boundary value problem of a circular cavity in a plane stress plate was analysed with the FE code using NNCM trained with the enhanced dataset. The NNCM-based FE showed comparable results with FE analyses using conventional constitutive models. As stated by the authors, this strategy has the limitation that it cannot be used for anisotropic materials.

Javadi and his co-workers carried out extensive research on application of neural networks in constitutive modelling of complex materials in general and soils in particular. They have developed an intelligent finite element method (NeuroFE code) based on the incorporation of a back-propagation neural network (BPNN) in finite element analysis. The intelligent finite element model was then applied to a wide range of boundary value problems including several geotechnical applications (e.g., Javadi et al., 2002; Javadi & Zhang, 2003; Javadi et al., 2004a; Javadi & Zhang, 2004b; Javadi et al., 2005; Javadi et al., 2009) and has shown that NNs can be very efficient in learning and generalising the constitutive behaviour of complex materials such as soils, rocks and others.

Hashash et al. (2004a) described some of the issues related to the numerical implementation of a NNCM in finite element analysis and derived a closed-form solution for material stiffness matrix for the neural network constitutive model. They derived a formula to compute consistent Jacobian matrix (stiffness matrix) for NN material models. For validation, the derived formula was implemented in ABAQUS

through its user defined material subroutine (UMAT) to analyse a number of numerical examples including analyses of a beam bending and a deep excavation problem.

Furukawa and Hoffman (2004) proposed an approach to material modelling using neural networks, which can describe monotonic and cyclic plastic deformation and its implementation in a FEA system. They developed two neural networks, each of which was used separately learn the back stress and the drag stress. The back stress represents kinematic hardening Y, and the drag stress represents isotropic hardening R. The architecture of neural networks and their inputs and outputs are illustrated in the following figure.

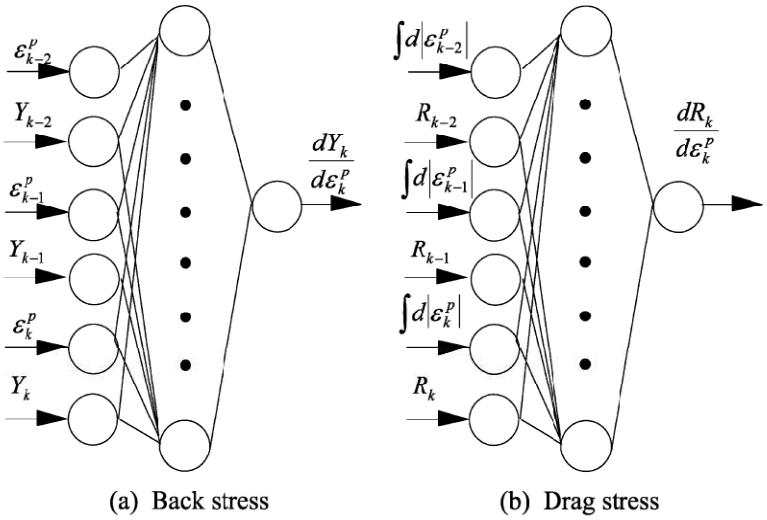

Figure 2.2: Structure of the proposed neural network material model (Furukawa & Hoffman, 2004)

In this figure Y and R represent the kinematic and isotropic hardening respectively and $\boldsymbol{\varepsilon}^p$ is the plastic strain. The subscripts k, k-1 and k-2 are denoting the current and previous states of each variable. After training and validation stages of NNs, the NNCM was implemented in a commercial FEA package, MARC, using its user subroutine for material models. The implementation involves the determination of the **D** matrix, which describes the stress-strain relationship,

$$\boldsymbol{\sigma} = \boldsymbol{D}\boldsymbol{\varepsilon} \qquad 2.1$$

and is given by the sum of the elastic matrix $\mathbf{D}^e$ and the plastic matrix $\mathbf{D}^p$:

$$\mathbf{D} = \mathbf{D}^{e} + \mathbf{D}^{p} \qquad 2.2$$

The elastic matrix is derived from Young's modulus and Poisson's ratio and only the plastic matrix is updated using developed neural networks. In order to appraise the performance of the proposed approach, two material models similar to Figure 2.2 were developed using actual material data with monotonic plastic deformation. The results were compared to one of the conventional material models (Chaboche model) and experimental data. A similar process was also curried out for cyclic plastic deformation and a good agreement was noted. Eventually the developed models were implemented in FEA package (MARC) using the described approach to analyse an axisymmetric FE model, representing the central part of a tensile specimen under a cyclic load. The results are shown in Figure 2.3.

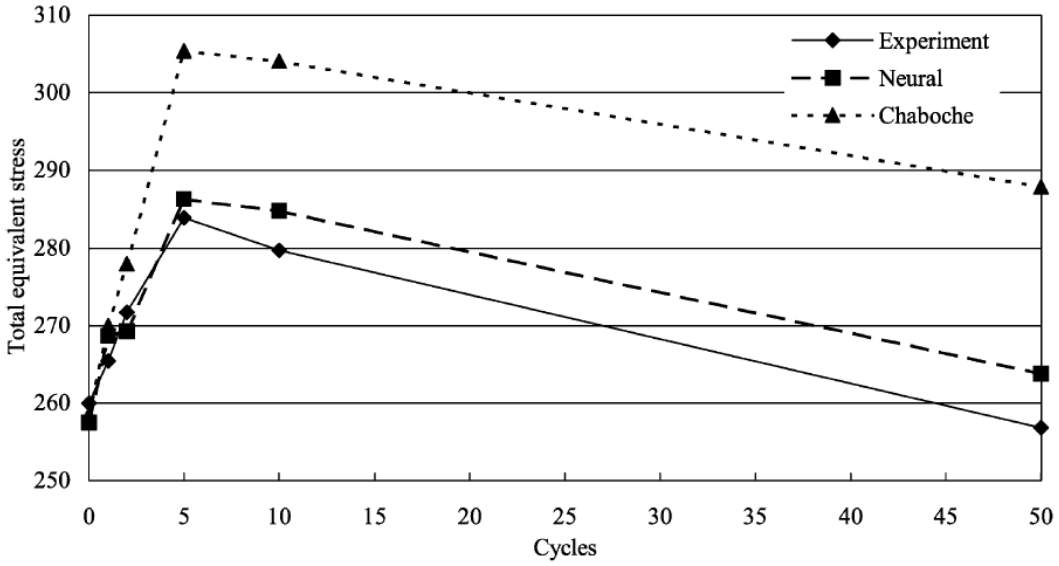

Figure 2.3: Total equivalent stress data of experiment and FEAs with neural network model and best-fit Chaboche model vs. cycles (Furukawa & Hoffman, 2004)

It can be seen in this figure that the results of the developed FE model show a better prediction compared to the conventional method (Chaboche model), however as the number of cycles increases the results of NN based FEA diverge from the actual data.

Nezami et al. (2006) utilized discrete element method (DEM) to generate the stress, strain data to train Neural Network (NN) soil models. The trained NN models were then used in Real Time Simulation (RTSM) framework. Within this framework, model training is done on the non-real time scale (several times faster than actual). This results in a faster simulation run compared with the actual DEM simulation. 2D and 3D examples were used to verify the proposed approach. It was shown that the results of NN models in RTSM framework provide reasonable prediction compared to the DEM results. In addition the results of the NN model in RTSM framework are obtained in a significantly lower time.

Jung and Ghaboussi (2006a) presented a rate dependent NN material model and its implementation in finite element software. In rate dependant materials, the material behaviour is dependant on both strains (stresses) and the rate of strains (rate of stresses). Therefore they developed a NN with the following architecture:

$$\dot{\boldsymbol{\sigma}}^n = \dot{\boldsymbol{\sigma}}^n \mathbf{NN}(\boldsymbol{\varepsilon}^n, \boldsymbol{\varepsilon}^{n-1}, \boldsymbol{\sigma}^{n-1}, \boldsymbol{\sigma}^n, \dot{\boldsymbol{\varepsilon}}^n, \dot{\boldsymbol{\varepsilon}}^{n-1}, \dot{\boldsymbol{\sigma}}^{n-1}) \quad 2.3$$

where the following equations were used to define stress and strain rate.

$$\dot{\sigma}^n = \frac{1}{\Delta t}(\sigma^n - \sigma^{n-1}) \quad 2.4$$

$$\dot{\varepsilon}^n = \frac{1}{\Delta t}(\varepsilon^n - \varepsilon^{n-1}) \quad 2.5$$

The developed NN model was then implemented in FE software ABAQUS through user material (UMAT). The proposed model was verified for a hypothetical material and structure. In addition, laboratory test data obtained by previous researchers were used as an example application of the rate dependent NN material model. The test structure was $1/8^{th}$ scale model of a real bridge, and the time dependent strain changes were measured at the mid span using three strain gauges located at the top, centre, and bottom of the bridge cross section as shown in Figure 2.4.

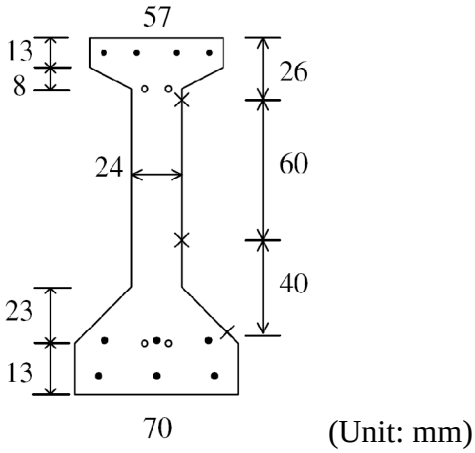

Figure 2.4: Geometry of test specimen (Jung & Ghaboussi, 2006a)

During the experiment, 10 cm by 20 cm cylinders were made with concrete used to construct the beam. These samples were loaded and the time dependant strain was measured. The stress and strain data extracted from these tests were used to train NN material model. UMAT subroutine of ABAQUS was utilized to implement the developed NN model and analysing the beam structure. The results of analysis and measured strains are shown in the following figure.

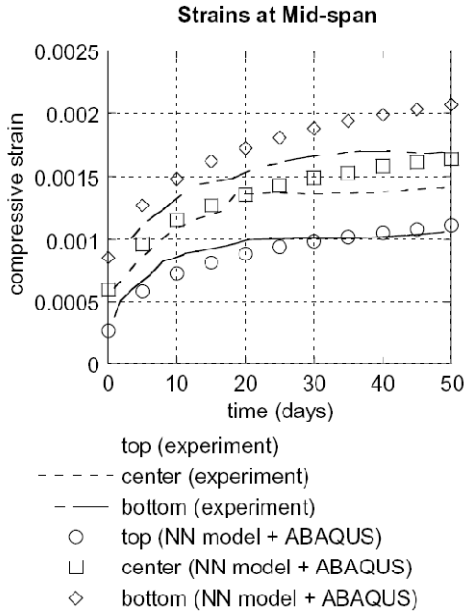

Figure 2.5: Measured and computed strains at mid-span (Jung & Ghaboussi, 2006a)

The figure shows good overall agreement between FE results using the implemented NN model and the experiments. However a significant difference can be seen for the results of the bottom gauge.

Kessler et al. (2007) demonstrated the implementation of a neural network (NN) material model in a finite element code, ABAQUS, through its user subroutine VUMAT. They developed a NN model for 6061 Aluminium under compression and different temperatures. They tried different types of inputs and different NN architectures and at the end the following inputs were selected to train NN.
Inputs:

$$\ln(\varepsilon), \ln(\dot{\varepsilon}), \ln(\sigma), \frac{1}{T}, tabular\ data\ of\ flow\ stresses\ and\ strains$$

where ε and $\dot{\varepsilon}$ are strain and its rate respectively, σ is stress, and T is temperature.
The obtained NN model was implemented in ABAQUS via VUMAT to carry out analysis and the results were compared to the two other conventional build-in models of ABAQUS (power law model and tabular data). The results relieved that the NN-based finite element model can provide a better prediction in comparison to the other two. It was noted that some parameters need to be defined a priori for conventional models, while no parameter identification is required in NN model. No description is provided in this paper on how the NN material model has been implemented in ABAQUS. The way that a constitutive model is implemented in FE analysis is vital and may have significant effect on the output results.

Haj-Ali and Kim (2007) presented a neural network constitutive model for fibre reinforced polymeric (FRP) composites. Four different combinations of NN models were considered in this study. Data for training the NN models were gathered from off-axis compression and tension tests performed with coupons cut from a monolithic composite plate manufactured by pultrusion process. Inputs for NN models were σ_{11}, σ_{22}, τ_{12} and outputs were scalar or vector of inelastic or total strains; which created the four different combinations. The results of NN models were compared to the experimental data and good agreement was observed. Furthermore a notched composite plate with an open hole was tested and the results were used to examine its FE model using the developed NNs model. For this purpose the developed NNs were implemented in ABAQUS material user subroutine. The results of finite element model

were compared to the experimental results in an unknown point where the response of structure was linear. It was shown that the model was capable of predicting the general linear behaviour of the composite at this point but showed a little diversion as strain increased. No comparison was made between the results of the FE model with NN constitutive model and the experimental data around the hole, where the behaviour was more nonlinear.

Najjar and Huang (2007) used a recurrent neural network to develop a model to simulate clay behaviour under plane strain loading conditions. They used this model to investigate the effects of loading rate and stress history on clay response. They showed that developed model was able to assess the effect of strain rate and stress history on clay behaviour. However, as indicated by authors, the model cannot be directly used in the solution of boundary value problems.

Yun et al. (2008a) and Yun et al. (2006a) proposed an approach for NN-based modelling of the cyclic behaviour of materials. In the hysteric behaviour of material, one strain value may correspond to multiple stresses and this can be a major reason that stops NNs from learning hysteretic and cyclic behaviour. To overcome this issue, they introduced two new internal variables in addition to the other ordinary inputs of NN-based constitutive material models to help the learning of the hysteretic and cyclic behaviour of materials. The following two parameters $\xi_{\varepsilon,n}$, $\Delta\eta_{\varepsilon,n}$ are used as the additional inputs of the NN material model:

$$\sigma_n = \hat{\sigma}_{NN}(\varepsilon_n, \varepsilon_{n-1}, \sigma_{n-1}, \xi_{\varepsilon,n}, \Delta\eta_{\varepsilon,n}) \qquad 2.6$$

where ε_n, is current strain; ε_{n-1}, is previous state of strain, σ_{n-1}, is previous state of stress and σ_n is current stress. $\xi_{\varepsilon,n}$, and $\Delta\eta_{\varepsilon,n}$ are the internal variables and are defined in the following equations:

$$\xi_{\varepsilon,n} = \sigma_{n-1}\varepsilon_{n-1} \text{ and } \Delta\eta_{\varepsilon,n} = \sigma_{n-1}\Delta\varepsilon_n \qquad 2.7$$

The above constitutive model was implemented in a general purpose FE code ABAQUS using its user defined subroutine for materials. The following equations were used to construct the material tangent stiffness matrix

$$\boldsymbol{D}^{ep} = \frac{\partial(^{n+1}\Delta\sigma)}{\partial(^{n+1}\Delta\varepsilon)} \qquad 2.8$$

where $^{n+1}\Delta\sigma = {}^{n+1}\Delta\sigma - {}^{n}\Delta\sigma$ and $^{n+1}\Delta\varepsilon = {}^{n+1}\Delta\varepsilon - {}^{n}\Delta\varepsilon$. Two actual and one simulated experimental data were used to verify the proposed NN-based material models. In the first example, data from a cyclic test on plain concrete were employed to train a NN-based material model (equation 2.6). The results of training the NN model together with experimental data and an analytical model are presented in the following figure.

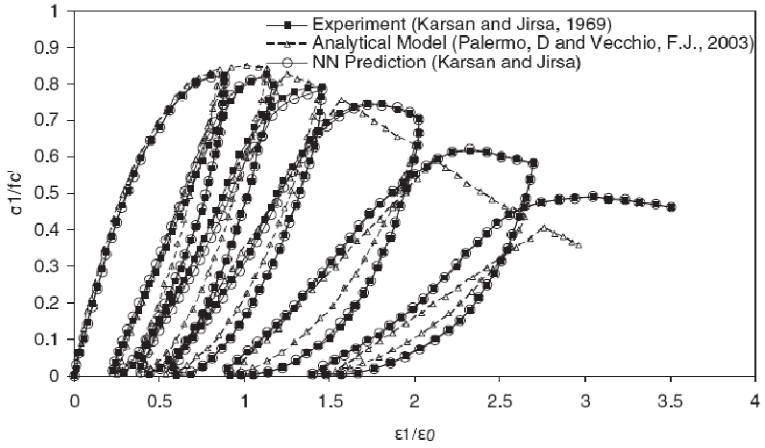

Figure 2.6: Results of training the proposed models and its comparison with an analytical model (Yun et al., 2008a)

The trained NN was used to predict a new series of data in order to explore its generalization capability. The results of this prediction are presented in Figure 2.7.

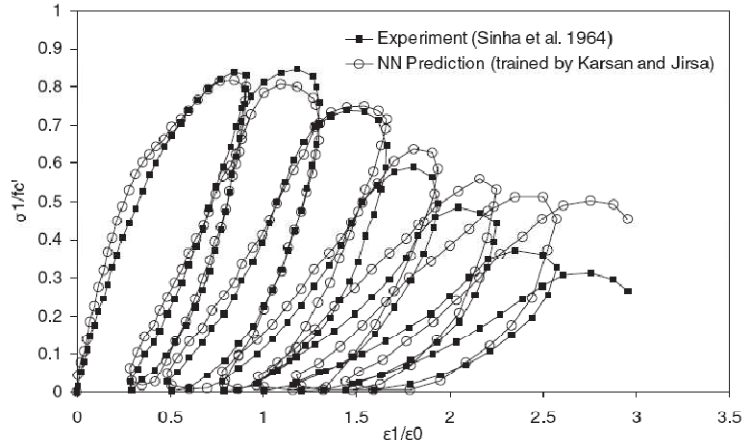

Figure 2.7: Trained neural network tested on different test data (Yun et al., 2008a)

In the second example two experimental data from two different steel beam-column connections were used to train and verify another NN-based cyclic material model. None of the NN-based material models in examples 1 and 2 were implemented in the finite element code. However in the third numerical example a three-floor building was modelled in ABAQUS using Lemaitre-Chaboche as material model and then simulated data were extracted to train NN model. The architecture of the NN is presented in the following equation.

$$\left\{{}^{n+1}\sigma_{11};\ {}^{n+1}\sigma_{22};\ {}^{n+1}\sigma_{12}\right\} = \hat{\sigma}_{NN}({}^{n+1}\varepsilon_{11};\ {}^{n+1}\varepsilon_{22};\ {}^{n+1}\varepsilon_{12};\ {}^{n}\varepsilon_{11};\ {}^{n}\varepsilon_{22};\ {}^{n}\varepsilon_{12};\ {}^{n}\sigma_{11};\ {}^{n}\sigma_{22};\ {}^{n}\sigma_{12};\ {}^{n+1}\varsigma_{\varepsilon,11};\ {}^{n+1}\varsigma_{\varepsilon,22};\ {}^{n+1}\varsigma_{\varepsilon,12}) \quad 2.9$$

where $\varsigma_{\varepsilon,n} = \xi_n + \Delta\eta_{\varepsilon,\mathrm{n}}$ is a combination of the two previously introduced internal variables. The trained NN model was incorporated in a non-linear FE code and used to predict the cyclic behaviour of the beam sections. The results showed a good agreement between the simulated data and predictions; however minor differences can be seen in some of the results. One of the key issues that have not been discussed in this paper is the effect of strain increment (i.e. $\Delta\varepsilon = {}^{n+1}\varepsilon - {}^{n}\varepsilon$) on the results of the NN model. The developed NN models should be examined for different strain increment. Moreover it was not discussed that what range of strain increment was used for training the NN models.

Yun et al. (2008 b) extended the NN-based cyclic material model developed by Yun et al. (2008a) and Yun et al. (2006a) for beam-column connections by adding the mechanical and design parameters. The architecture of new NN model can be presented in the following equation:

$$M_n = \widehat{M}_{NN}(\theta_n, \theta_{n-1}, M_{n-1}, \xi_{\theta,n}, \Delta\eta_{\theta,n}, \mathcal{G}_i(DV_1, \dots, DV_j)) \quad 2.10$$

where n indicates the n^{th} load (or time) step, θ and M indicate the rotational displacement and moment, $\xi_{\theta,n}$=M_{n-1}*θ_{n-1} and $\Delta\eta_{\theta,n} = M_{n-1} \times \Delta\theta_n$ are the two internal variables for accelerating learning capability of hysteretic behaviour and $\mathcal{G}(\mathrm{DV}_1, ...,\mathrm{DV}_j)$ is the i^{th} mechanical parameter as a function of design variables.

For the purpose of validation of the proposed NN model, two different types of connections, extended-end-plate (EEP) and top-and-seat-angle with double web-angle

(TSADWA) connection, under cyclic and earthquake loading condition were considered. Synthetic data were utilized to develop a NN for the EEP connection. Depth of beam (d_b), thickness of end plate (t_p) and diameter of bolt (f_b) were chosen as design variables. Therefore the following equation can describe the NN model.

$$M_n = \widehat{M}_{NN}(\theta_n, \theta_{n-1}, M_{n-1}, \xi_{\theta,n}, \Delta\eta_{\theta,n}, \mathcal{G}(d_b, t_p, f_b)) \qquad 2.11$$

For the TRADWA connection, real experimental data were employed to train and test the NN material model. In both cases good agreement between the NN material models prediction and actual data can be seen; however some discrepancies in results can also be noticed.

Kim et al. (2010) compared two different approaches for modelling of steel beam-to-column connections. The first approach is a component-based model where all components of connection are idealized by using one-dimensional springs. Constitutive relationships for every deformable component (spring) were defined in order to represent the actual comprehensive response of a joint. The idealized component-based model is shown in Figure 2.8.

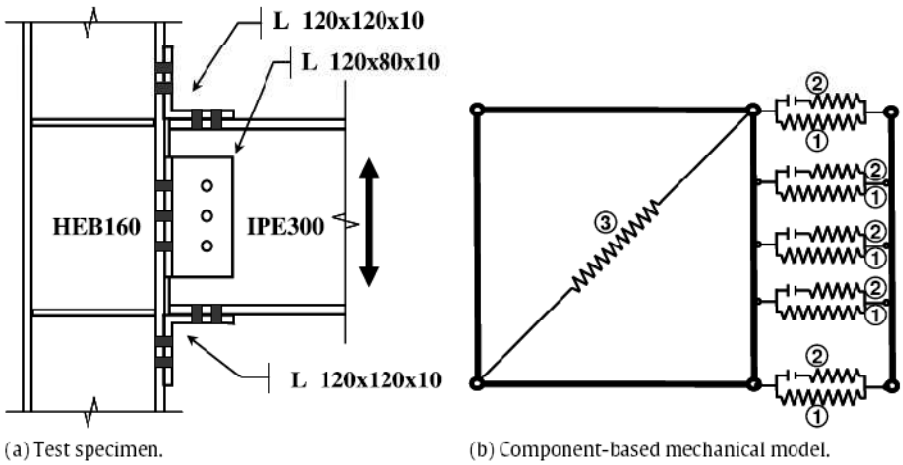

Figure 2.8: A top-and-seat angle connection with double web angles (Kim et al., 2010)

The component-based model approach was verified using two experimental data from literature, Calado et al. (2000) and Kukreti and Abolmali (1999). The experimental and component-based model results for two examples are presented in Figure 2.9 and Figure 2.10.

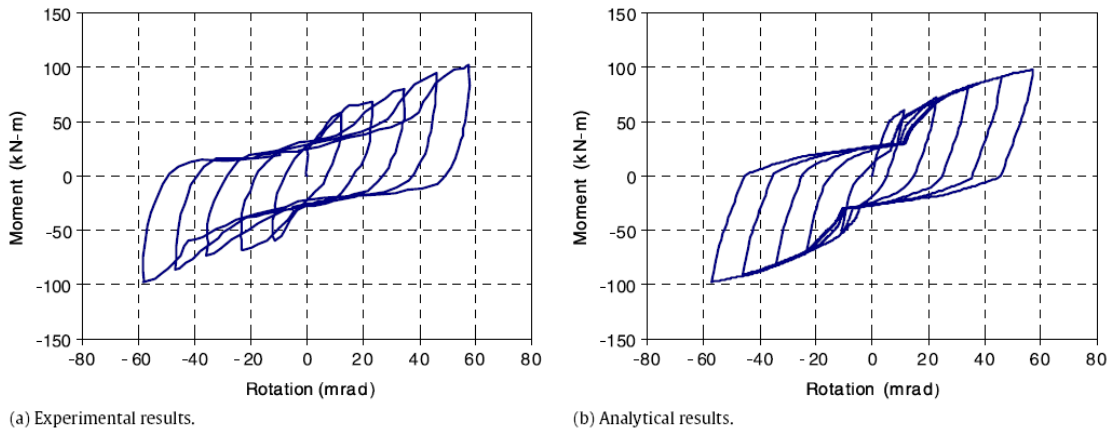

Figure 2.9: Experimental and analytical hysteretic responses for Calado et al. 2000 (Kim et al., 2010)

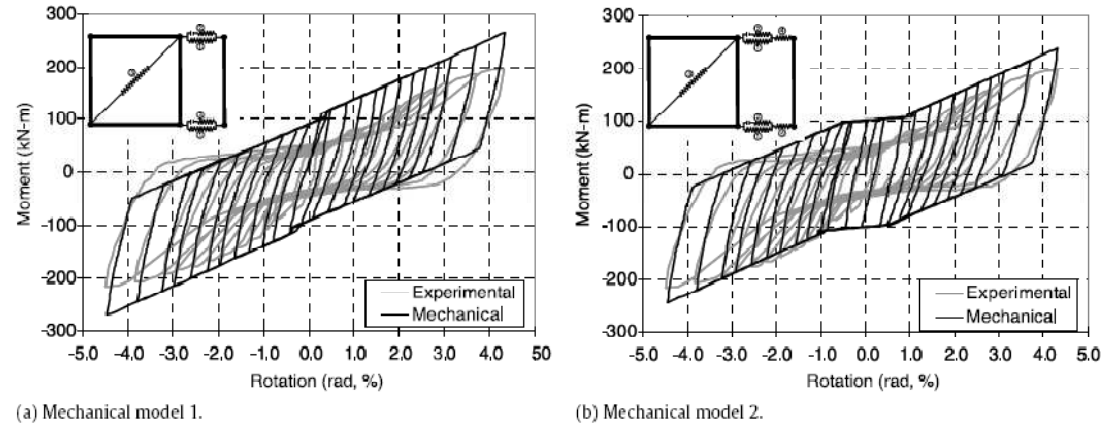

Figure 2.10: Comparisons between experimental and analytical results (Kim et al., 2010)

From these figures it can be seen that the component-based model has been able to predict the general behaviour of connection, however it is not able to capture every detail of connection behaviour.

In the second approach, the nonlinear hysteretic neural network model, proposed by Yun et al. (2008a), was employed to model stress-strain relationship of connections. The NN-based model was first verified by synthetic data (generated by Ramberg-Osgood relationship). The applicability of the NN approach was further appraised by applying to the two experimental data (used to verify component-based model). The architecture, inputs and output of the NN is presented in the following equation.

$$M_n = \widehat{M}_{NN}(\theta_n, \theta_{n-1}, M_{n-1}, \xi_n, \Delta\eta_n, E_{n-1}) \quad 2.12$$

In this equation $\xi_{\theta,n} = M_{n-1}\theta_{n-1}$ and $\Delta\eta_{\theta,n} = M_{n-1}\Delta\theta_n$ are the two internal variables, M=moment, θ=rotation, $\widehat{M}_{NN}$ and $\hat{\theta}_{NN}: R^5 \rightarrow R$ are the functional mapping to be established through NNs and n indicates nth time (or load) step. An additional input variable of E_{n-1} is introduced in this paper to represent the complex hysteric behaviour that includes pinching and degradation. The results of the NN-based model were compared to the experimental data. The comparison showed that the neural network model is capable to predict the overall pinched hysteric loops better than the component-based model presented in this study. The neural network model of the connections is limited only to prediction of the global response of the joint. It can not represent the contribution of individual components and therefore does not give the user an insight into the underlying components mechanics.

At the end, the authors proposed a third approach for future investigation that will be a mixture of the two approaches proposed in this study. The suggested approach would involve the most effective mechanical and informational aspects of the complex behaviour of connections.

2.3.1 Autoprogressive and Self-Learning training of NNCM

After the pioneering work by Ghaboussi and his co-workers (Ghaboussi et al., 1991) on application of ANN for constitutive modelling of materials, Ghaboussi et al. (1998) presented an entirely different approach, termed autoprogressive approach, for training neural network material models. In this approach the information measured from a global load-deflection response of a structural test is employed to enrich the data for training the NN. In general, neural networks require a large amount of data for modelling material behaviour which usually can not be collected from a single test on a sample of material. The proposed approach overcomes this issue and utilizes the fact that a structural test contains a huge and diverse amount of data (e.g., different patterns of stresses and strains) that can be used for training. In this method the material model is extracted from an iterative non-linear finite element analysis of the test specimen and gradually improves stress-strain information with which to train the neural network. Two simple examples were presented in this paper; structural response data from a

simple truss and a laminated structural plate containing an open hole. In this paper, the minimum number of measured structural responses, and their type and locations is an important issue that has not been addressed. This approach requires data from structural tests in priori which may not be available in some practical applications.

Sidarta and Ghaboussi (1998) developed a neural network based constitutive model for geomaterials using autoprogressive training. They used a non-uniform material test (a triaxial test with end friction) which had a non-uniform distribution of stresses and strains. Then the measured boundary forces and displacements were applied in a finite element model of the test to generate the input and output data for training the neural network material model. Using the data generated in that way, the autoprogressive method was used to train the neural network material model.

Shin and Pande (2000) presented a self-learning finite element code with a neural network based constitutive model (NNCM) instead of a conventional material model. The methodology presented in this paper is in fact similar to what Ghaboussi and his co-workers presented as “autoprogressive training” in 1998. Two boundary value problems were used in this paper to validate the methodology. The first was a two-bar structure in which one of the bars is made of an ideally plastic or a strain softening material whilst the second bar is linear elastic. Artificially generated load-deformation data of the structure was used for training of the neural network based constitutive model (NNCM) for the non-linear bar. The second problem simulates a plane stress panel of linear elastic material subjected to a concentrated vertical load at the top. The displacements at a number of monitoring points were used to train a NNCM. It was shown that the choice of the position of monitoring points affects the training programme and consequently the convergence of the NNCM predictions to standard solutions. The position of the load was then changed to demonstrate that the NNCM has been adequately trained to be able to perform analysis of any boundary value problem in which the material law corresponds to the trained NNCM.

Shin and Pande (2001) presented an approach to compute the tangential stiffness matrix of the material using partial derivatives of the NNCM (trained with total stress and strain data). They incorporated the computed stiffness matrix in their self learning finite element code. The potentials of the developed intelligent FE code were examined by analysing a rock specimen under uniaxial cylindrical compression with fixed ends.

Shin and Pande (2003) used the self learning FE code (the finite element code with embedded NNCM) to identify elastic constants for orthotropic materials from a structural test. They proposed a two-step methodology in which, in the first step, the monitored data of a structure are used to train a NN based constitutive model implemented in a finite element code. In the second step, the trained NNCM is used to form the constitutive matrix using the following equation to compute material elastic parameters.

$$D_{NN} = DNN_{ik}(\varepsilon_i, \sigma_k) = \frac{\partial \sigma_k}{\partial \varepsilon_i} \qquad 2.13$$

The input and output of the NN together with its optimal architecture are presented in the following figure. Strain and stress vectors were the input and output of the NN respectively.

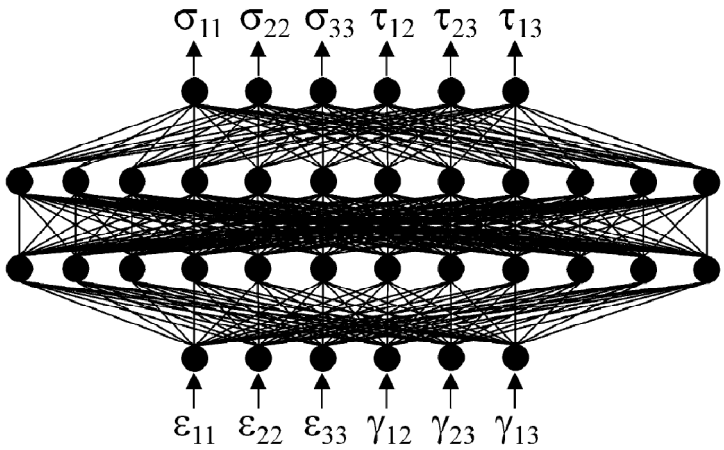

Figure 2.11: Architecture of the NNCM presented in Shin and Pande (2003)

The methodology was then applied to a plane stress panel with a circular hole at its centre under a compressive pressure. A finite element model of the panel with assumed values of the nine independent orthotropic elastic constants was created as a synthetic structural test. Displacements of 66 nodes at 5 load levels, obtained from the FE analysis, were assumed as measured data from the structural test. The material behaviour was linear elastic and after 3rd cycle of self learning approach a good agreement was noted with target results. The orthotropic elastic constants were also

compared and a good prediction was observed. The nine elastic constants were as follow:

$$E_x, E_y, E_z, G_{xy}, G_{yz}, G_{xz}, \nu_{xy}, \nu_{yz}, \nu_{xz}$$

Although it should be noted that the NN based constitutive matrices were not symmetric and therefore 36 elastic constants was achieved. They were symmetrised by averaging the off diagonal terms. A relatively large number of nodes are used to monitor the displacements of a structure with a relatively simple geometry and simple behaviour (linear elastic). This could pose a limitation to this method in more complex and nonlinear problems.

Hashash et al. (2003) extended autoprogressive training methodology to extract soil constitutive behaviour using measurements of lateral wall deflection and surface settlements from a sequence of construction stages of a braced excavation. The input and output for training the neural network model were obtained from a simulated excavation problem using a synthetically generated data. For this simulated FE model, modified cam clay was used as the material model. To start the autoprogressive procedure, two FE model of the problem were created; one used to simulate soil removal and bracing installation of n^{th} excavation stage and the second one to apply monitored deformations of the same excavation stage. From the first FE model stresses were extracted and from the second one the strains. The stress-strain pairs gathered from the two FE model were used to train a NN soil model. It should be mentioned that at the beginning of the procedure the material behaviour is unknown and therefore the two FE model were initialised with a NN model representing linear elastic behaviour. The procedure was repeated until the entire excavation stages are simulated. At the end of the process, a NN material model which has been trained with a rich set of data, will be created through this iterative process. The results showed that the methodology proposed in this paper is capable of extracting relevant material behaviour from a series of finite element analyses of the excavation and incrementally learn from field observation.

Hashash et al. (2004b) presented a systematic and general procedure for probing constitutive models. The following general strain probe equation was utilized to explore constitutive model behaviour.

$$\sqrt{(\Delta\varepsilon_{11})^2 + (\Delta\varepsilon_{22})^2 + (\Delta\varepsilon_{33})^2 + (\Delta\varepsilon_{12})^2 + (\Delta\varepsilon_{23})^2 + (\Delta\varepsilon_{31})^2} = r_{\Delta\varepsilon} \qquad 2.14$$

Two special cases of probing, true triaxial strain probe (TTSP) and plane-strain strain probe (PSSP) are considered to investigate the application of the above equation in studying material behaviour. Three different models, Von Mises, Modified Cam Clay, and MIT-E3 were used to demonstrate the true triaxial probing procedure. But for the plane-strain probing case an artificial neural network (ANN) model was considered. The NN model was trained with the autoprogressive algorithm, in a braced excavation problem using MIT-E3 constitutive model. The NN model showed a good performance in predicting the surface settlement and lateral displacement of excavation problem. However when the probing procedure was performed to find the yield loci of NN model, it was discovered that NN model has not captured the correct shape of the loci but the overall size of response surface was similar to MIT-E3 model. A possible reason for this, as stated by authors, can be the lack of training data for NN model. However as the data were generated synthetically using the results of FE analysis, it is not clear why the model was not verified using additional data.

Hashash et al. (2006a) introduced SelfSim (self-learning simulations) which they called a software analysis framework to implement and extend the autoprogressive algorithm. The procedure and steps of SelfSim are in fact identical to those introduced in Ghaboussi et al. (1998) and (Hashash et al., 2003) as autoprogressive method. The SelfSim performance was validated using a simulated excavation case history. Synthetic data including lateral wall deflections and surface settlements were generated using a FE model employing the MIT-E3 as soil model. Three numerical examples and two actual case histories were used to examine the capability and performance of SelfSim in prediction of deep excavation projects. The results showed that the proposed approach extracts sufficient information on soil behaviour to accurately capture observed field behaviour.

Hashash et al. (2006 b), used the SelfSim method to characterize the constitutive behaviour of granular material and in particular extra-terrestrial soils using load-displacement measurements. The steps of SelfSim presented in this paper are exactly the same as (Hashash et al., 2006a). It was assumed that an in-situ test will be performed on an extra-terrestrial soil in which the applied load and resultant

deformation are recorded. Two FE models of the domain under consideration will be created and measured loads and displacements will be applied incrementally to each of these two models. Stresses will be obtained from the 1st model where measured load are applied, and measured displacements and compatibility will be used to obtain the strains in the second FE model. Since all the measurements can be taken in the place, the costly process of acquiring and transferring the extra-terrestrial soils can be avoided. Also because in the SelfSim method no priori assumption is considered for constitutive relationship of material, this method is a strong candidate to investigate the behaviour of unknown and new materials, such as extra-terrestrial soils.

Jung and Ghaboussi (2006b) extended autoprogressive algorithm to include rate dependant material models. Same NN architecture as Jung and Ghaboussi (2006a) was used to create the NN model. In the autoprogressive algorithm, rate of stresses and strains were added to the values measured from simulated FE models.
A hypothetical cylinder with viscoelastic material and variable diameter as shown in the Figure 2.12 was considered to verify the proposed method.

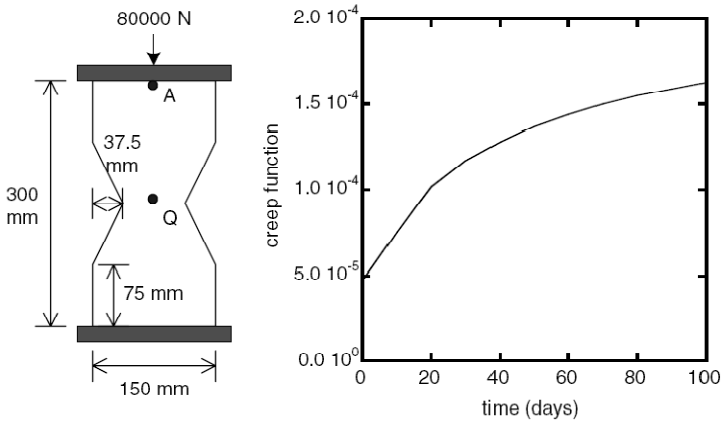

Figure 2.12: The structure and the creep function used in the simulated experiment (Jung & Ghaboussi, 2006 b)

A NN-based rate dependant material model was developed using the global response of the structural test shown in Figure 2.12. The trained NN material model was then employed to solve a new boundary value problem. An important aspect of the NN model was its learning of the time step effects. It was observed by the authors of the paper that if the NN model be trained using only one time step, its prediction for other time steps will be poor. Therefore it was suggested by the authors that the model should

be trained using different time steps. The methodology was applied to the results of actual experiments to capture the non-linear creep behaviour of a superalloy.

Aquino and Brigham (2006) used autoprogressive or self-learning finite element method to develop a NN thermal constitutive model. Like other applications of autoprogressive method, this one also included the following steps. Pre-training or initialising of NN model, two simulated finite element models, and finally training the NN material model.

To verify the methodology a simulated experiment was utilized. The simulated test was a steel plate with a heat flux on one side and 100˚C temperature as boundary condition on the other three sides as shown in Figure 2.13.

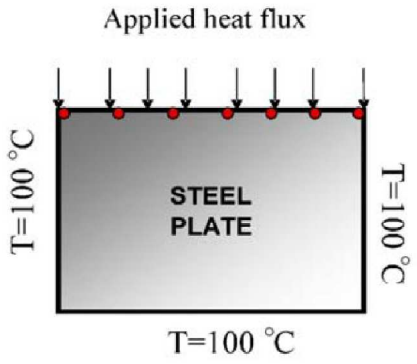

Figure 2.13: Simulated experiment (Aquino & Brigham, 2006)

Synthetic data were generated using the above simulated experiment. Three cases were considered and in order to study the stability of the self-learning FE methodology, a random noise was introduced in the simulated data. Then the self-learning algorithm was started with pre-training of a NN model by generating random temperature, temperature gradient, and their corresponding heat flux using Fourier law. Two finite element models were created. The temperature and temperature gradient as inputs were extracted from the second finite element model, and heat flux vectors from the first FE analysis as output. The NN was trained with the above data set. The inputs and output of the NN model were as following:

Inputs: $\frac{\partial T}{\partial x}$, $\frac{\partial T}{\partial y}$, $and\ T$

Outputs: J_x, J_y

where: $\frac{\partial T}{\partial x}$, $\frac{\partial T}{\partial y}$ are gradients in x and y directions respectively and T is temperature. J_x, and J_y are heat flux vectors in x and y directions.

It was shown that self-learning method is capable of developing a NN thermal constitutive model even in the presence of noisy data.

Jung et al. (2007) used SelfSim to predict the time-dependant behaviour of concrete during the construction of a segmental bridge. They used SelfSim to predict the remaining or future stages of construction using a NN developed with stresses, strains, and their corresponding rates from early stages of construction. The proposed methodology was applied to Pipiral Bridge, a concrete segmental bridge, built by the balanced cantilever method in Colombia. The NN model used in this study had 2 hidden layers 7 inputs and 1 output. Each hidden layer had 14 nodes as shown in Figure 2.14.

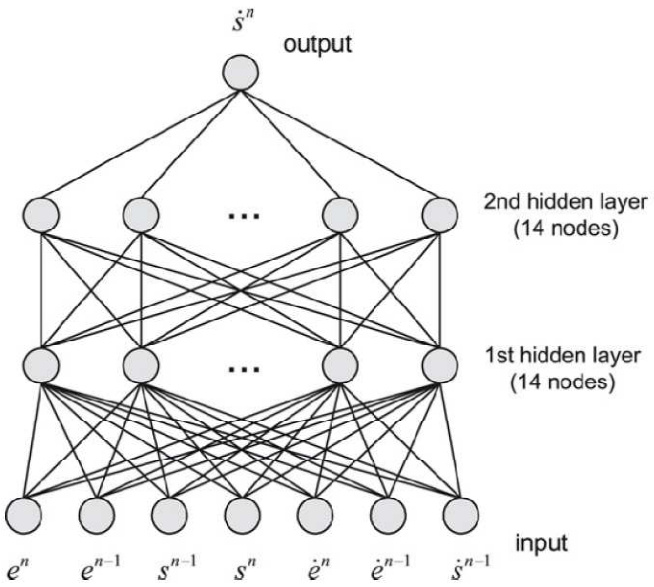

Figure 2.14: Rate-dependent neural network material model used in Jung et al. 2007

The inputs and output of NN were:

$$\dot{s}_{lm}^n = \dot{s}_{lm}^n NN(e_{lm}^n, e_{lm}^{n-1}, s_{lm}^{n-1}, s_{lm}^n, \dot{e}_{lm}^n, \dot{e}_{lm}^{n-1}, \dot{s}_{lm}^{n-1}) \quad 2.15$$

where $s_{lm} = \sigma_{lm} - \delta_{lm}\sigma_v/3,\ e_{lm} = \varepsilon_{lm} - \delta_{lm}\varepsilon_v/3,\ \sigma_v = \sigma_{kk},\ \varepsilon_v = \varepsilon_{kk}, (l, m, k = 1, 2, 3)$. The superscripts n and n-1 represent the current and the previous time steps respectively. The proposed constitutive equation was solved iteratively using the following equation.

$$s_{lm}^{n} = s_{lm}^{n-1} + \Delta t \times NN(e_{lm}^{n}, e_{lm}^{n-1}, s_{lm}^{n-1}, s_{lm}^{n}, \dot{e}_{lm}^{n}, \dot{e}_{lm}^{n-1}, \dot{s}_{lm}^{n-1}) \quad 2.16$$

The current strain and previous steps of other parameters were obtained from the results of finite element analyses. The rate-dependent NN model represents the creep of concrete in this paper.

The method proposed in this paper was used in two different ways to predict the deflection of a segmental bridge (Figure 2.15). In the first case, when a construction case had a repetition of many cantilevers, the NN model was calibrated using the first couple of cantilevers and the remaining ones were predicted using this NN model. In the second case the NN model learned from earlier segments and predicted the deflections of the remaining segments in one cantilever. However it is known that NN models are not reliable when they are used to predict data beyond what they have experienced during training. The authors of the paper have suggested adding previously obtained data from other sources (e.g. data from lab test, field data, and synthetic data generated by conventional models) to the current database in order to improve prediction capability of SelfSim and predict the deflections of remaining segments.

Literally this indicates that the SelfSim method in its current way can not be used to predict unseen range of strains and stresses based only on learning from early stages of construction, and additional data is required. It is therefore can be argued that SelfSim should not claim to be a fully self-simulation technique that can predict future stages of a construction like segmental bridge.

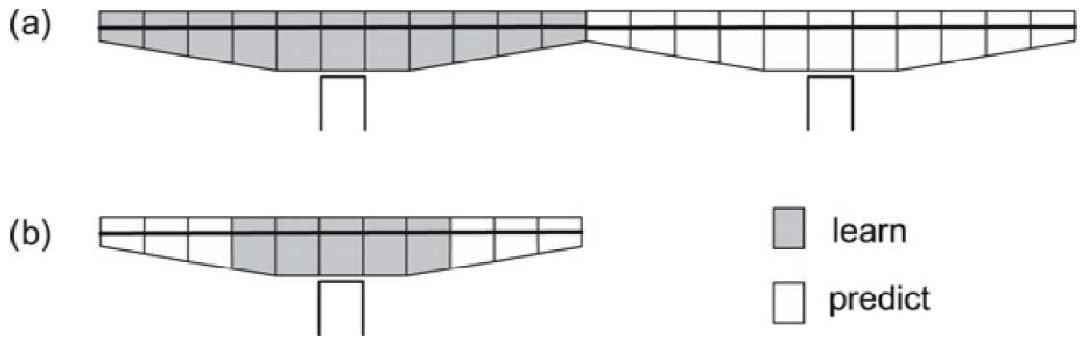

Figure 2.15: Improvement of the camber using SelfSim: (a) learn from the current cantilever and predict deflections of the remaining cantilevers (b) learn from the earlier segments and predict the deflections of the remaining segments (Jung et al., 2007)

Fu et al. (2007) and Hashash et al. (2006 c) continued the use of SelfSim for linking soil laboratory testing and constitutive model development. They applied the methodology to two simulated laboratory tests, a triaxial compression shear test, and a triaxial torsional shear test. Using extracted soil behaviour from laboratory tests, they developed a neural network-based constitutive model. The developed model was then used in the prediction of the load-settlement behaviour of a simulated strip footing.

Yun et al. (2008c) and Yun et al. (2006 b) used self-learning simulation to characterize cyclic behaviour of beam-column connections in steel frames. In these papers, they used similar NN model to Yun et al. (2008a) and (2008 b) to predict the cyclic and hysteretic behaviour of beam-column connection. The architecture of the NN and its input and output is presented in the following form.

$$M_n = \widehat{M}_{NN}(\theta_n, \theta_{n-1}, M_{n-1}, \xi_{\theta,n}, \Delta\eta_{\theta,n}) \qquad 2.17$$

where $\xi_{\theta,n} = M_{n-1}\theta_{n-1}$ and $\Delta\eta_{\theta,n} = M_{n-1}\Delta\theta_n$ are the two internal variables, M=moment, θ=rotation, $\widehat{M}_{NN}$ and $\hat{\theta}_{NN}: R^5 \rightarrow R$ are the functional mapping to be established through NNs and n indicates nth time (or load) step. The two internal variables are described intuitively in the following figures.

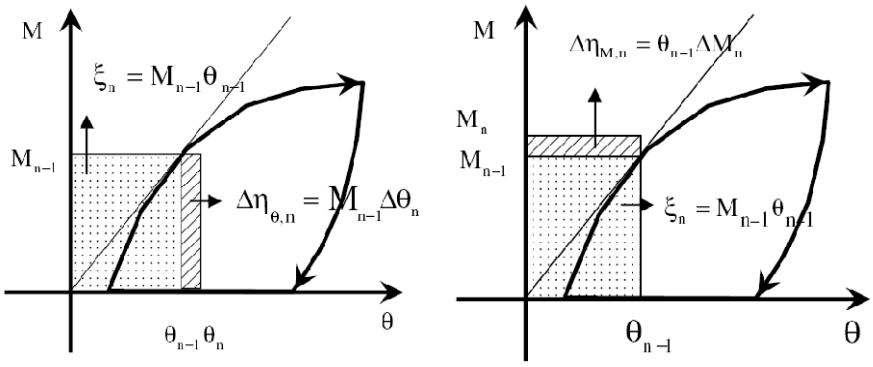

(a) (b)

Figure 2.16: Internal variables defined for NN based cyclic connection model: (a) displacement control form; (b) stress resultant control form (Yun et al. 2008c).

The following equation was used to calculate tangent stiffness of the NN-based connection model.

$$\mathbf{K} = \frac{\partial \Delta \mathbf{M}}{\partial \Delta \boldsymbol{\theta}} \qquad 2.18$$

where $\Delta\mathbf{M} = {}^{n+1}\Delta\mathbf{M} - {}^{n}\Delta\mathbf{M}$ and $\Delta\boldsymbol{\theta} = {}^{n+1}\Delta\boldsymbol{\theta} - {}^{n}\Delta\boldsymbol{\theta}$

Self-learning simulation approach in this paper was enhanced with a new algorithmic formulation of the NN based cyclic material model. Both synthetic and actual data were used to validate the enhanced self-learning simulation method in prediction of cyclic behaviour of connections. As previously described in SelfSim method, in the 2nd step, two parallel finite element models (A, B) run in order to update and improve the NN-based material model. In the model A, measured forces are applied and in the model B the measured displacement are enforced. Two different cases were considered to construct the stiffness matrix based on the FEM-A and FEM-B as shown in following figure.

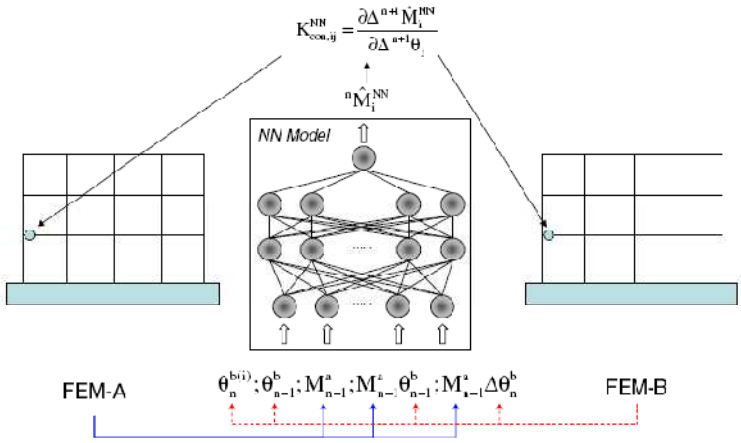

Figure 2.17: Case I: algorithmic tangent stiffness formulation during self-learning simulation (Yun et al., 2008c)

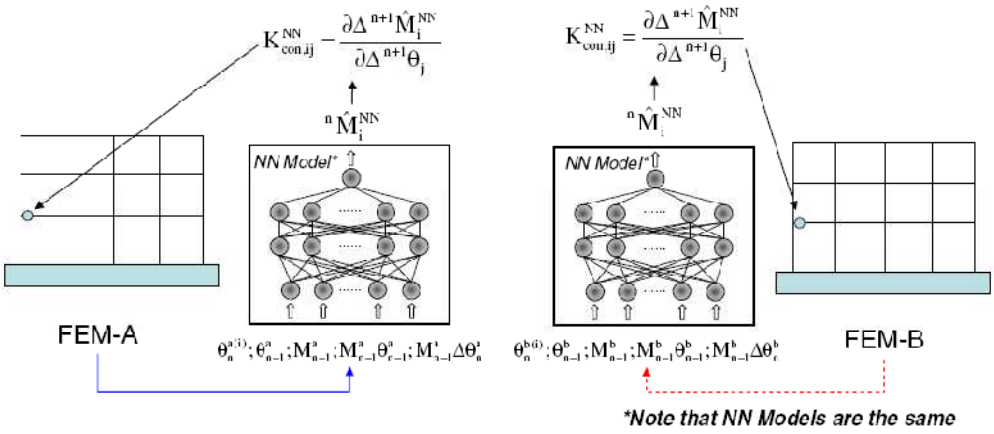

Figure 2.18: Case II: algorithmic tangent stiffness formulation during self-learning simulation (Yun et al., 2008c)

It is shown in this paper that the NN model from the case I provides a better prediction than case II for the examples presented in this study.

Hashash and Song (2008) utilized self-learning simulations (SelfSim) technique to extract soil constitutive behaviour. They used this approach to model three different problems; a triaxial test with frictional loading plates, deformation due to deep excavations, and site response as a result of horizontal shaking. Although they showed that developed model can predict the soil behaviour with a very good accuracy, however as stated by the authors, selecting SelfSim and neural network parameters is an empirical task and needs personal experiences. This shows the lack of interpretability of neural network models as extracting their optimum parameters could be a protracted trial and error procedure and in some cases can be subjective.

Tsai and Hashash (2008) presented the application of SelfSim method in analysis of dynamic soil behaviour. The paper describes the implementation of SelfSim to integrate field data measurements and numerical simulations of seismic site response to obtain the underlying cyclic soil response. They applied the SelfSim to study 1D seismic site response in the following steps.

Step 1: The ground response corresponding to a base shaking is measured in selected depths within soil profile. The input base shaking and the resultant measurements create sets of field data. Initially an NN soil model is pre-trained using stress-strain data that represent linear elastic behaviour over a limited strain range.

Step 2(a): A simulated model of site response using the initial NN model is created and the measured acceleration from the deepest point in a downhole array is applied at the bottom of the soil column. After analysing, the stresses and strains are computed throughout the soil column based on dynamic equilibrium considerations. In the SelfSim approach it is assumed that since the applied boundary forces (due to base acceleration) are accurate then the corresponding computed equilibrium stresses provide an acceptable approximation of the true stress field experienced by the soil. However the computed strains may not match the expected results and will be discarded.

Step 2(b): A similar site response analysis using the same NN model is carried out in which the measured displacements from a downhole array are imposed as additional boundary conditions. In this analysis stresses and strains are also computed in the soil column. It is assumed that the applied displacements are accurate and therefore the corresponding computed strains are an acceptable approximation of the true strain field experienced by the soil.

The stresses from step 2a and the strains from step 2b form stress-strain pairs that approximate the soil constitutive response. A material constitutive model is updated by training and retraining the NN-based material model using the extracted stress-strain pairs. The entire process is repeated several times using the full ground motion time series until analyses of step 2a provide ground response similar to the measured response. This process is shown in the following figure.

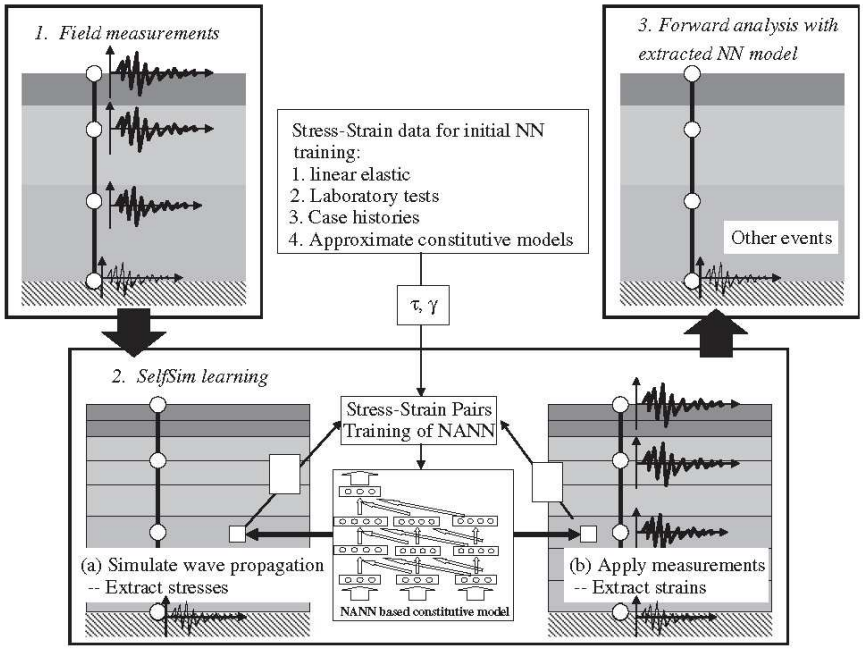

Figure 2.19: SelfSim algorithm applied to a downhole array (Tsai and Hashash, 2008)

Later in this paper they applied this procedure to a synthetically generated downhole array data. The methodology was applied to three different cases in order to evaluate its capability to extract dynamic soil behaviour. A single soil layer under a sinusolidal motion, a uniform but multilayer soil profile under seismic motion, and a non-uniform multilayer soil profile under seismic motions were the 3 synthetic cases. It was shown that SelfSim is able to provide a good prediction of the site response in all three cases. Eventually to evaluate the predictive capability of the extracted material model from individual events it was assumed there are two more recordings available in profile 3. Site response analyses (with FE incorporated NN material model obtained from a given event) were performed using input motions of the other two events. The results of these analyses are presented in Figure 2.20. In this figure it can be noticed that in some cases the prediction of surface response is very poor.

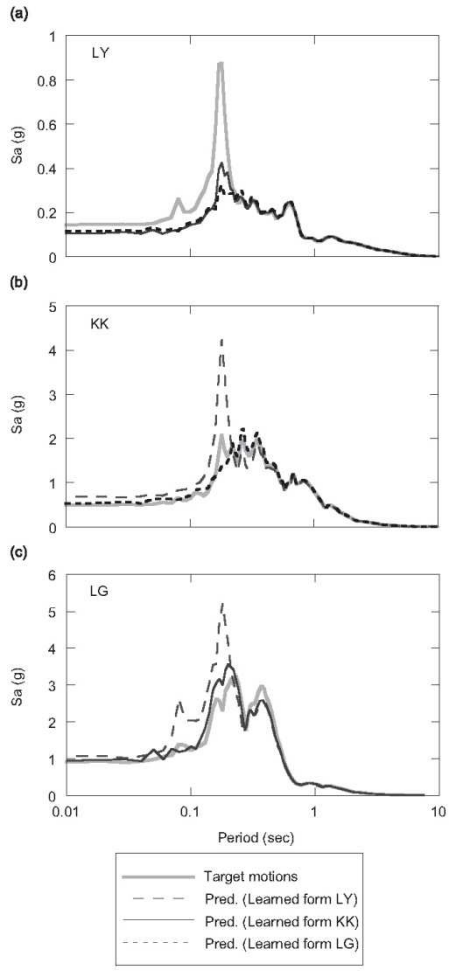

Figure 2.20: Predicted surface response spectra of a given event using SelfSim extracted NN material models from other events (Tsai and Hashash, 2008)

As stated by the authors, this difference is caused because the site response analyses experienced a range of unseen strains which was not introduced to the NN model during the training stage. After this, the individual extracted stress-strain behaviour from three events were combined together in one single database to train a new NN material model. It was shown that the prediction of the new NN material model was improved compared to the previous results however there was still a significant difference in one of the predicted response spectra. Therefore further SelfSim training using all three events were performed to increase the accuracy of the results.

Hashash et al. (2009) employed the SelfSim method to interpret the drained behaviour of sand from triaxial test with fully frictional loading platens. Three series of isotropically consolidated drained triaxial tests were performed on loose, medium, and

dense specimens. The triaxial tests were simulated using FE method and SelfSim method was used to extract the non-uniform stress-strain behaviour from external load and displacement measurements. It was shown that the SelfSim was capable of capturing the exact behaviour of the specimens. The authors claimed that using the proposed approach (integration of SelfSim and laboratory testing) it is possible to use a single laboratory test to generate a multitude of stress paths, instead of the current practice of a single laboratory test for a single stress path. The presented study did not provide any finite element modelling of a different boundary value problem than the triaxial ones to appraise the capability of the extracted NN model.

Hashash et al. (2010) compared two different approaches for learning the behaviour of deep excavations in urban environment. In this paper, they utilized genetic algorithm (GA) and SelfSim approaches to learn the behaviour of soil in a deep excavation. In the first approach the material parameters of an existing material model (hardening soil model of PLAXIS) were optimised using a genetic algorithm. In the second approach a combination of finite element method and artificial neural network (ANN) was employed to extract the soil behaviour. In this approach no predefined constitutive model was needed. Both approaches were applied to a case study in Lurie Centre excavation in Chicago, USA. It was shown that GA and SelfSim could reproduce the wall deformations reasonably well; however it appears that the hardening soil model used in the FE model in the GA approach is not capable of reproducing the settlement profile behind the wall, neither in magnitude nor in shape. This is shown in Figure 2.21. In this figure the graph on the right shows the surface settlement. The difference between the results of GA-based approach and measured values can be noticed clearly in this graph; this difference for SelfSim results is negligible. This shows that the GA-based approach highly depends on the selected constitutive model, i.e. the results would differ if a different soil constitutive model was used in the GA approach. On the left side of figure, while both approaches have provided a relatively good prediction, it can be observed that none of the methods have been able to predict the exact wall deformation.

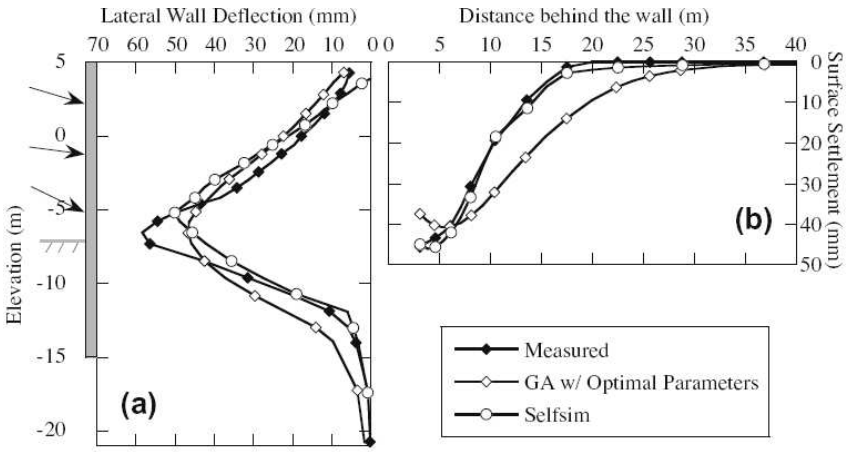

Figure 2.21: Comparison of computed (a) lateral wall deformation and (b) surface settlement using GA and SelfSim for the stage 7 of excavation (Hashash et al., 2010)

Jung and Ghaboussi (2010) presented a similar work to the Jung and Ghaboussi (2006a), Jung and Ghaboussi (2006b) and Jung et al. (2007). In this paper the authors first have explained and verified the rate-dependant neural network model. Then using the autoprogressive method, they trained neural network constitutive models with load-displacement measurements from structural monitoring. After pre-training the NN, the method was applied to inverse identification of creep of a concrete beam. The results of the comparison between the experiment and the autoprogressive method are presented in Figure 2.22.

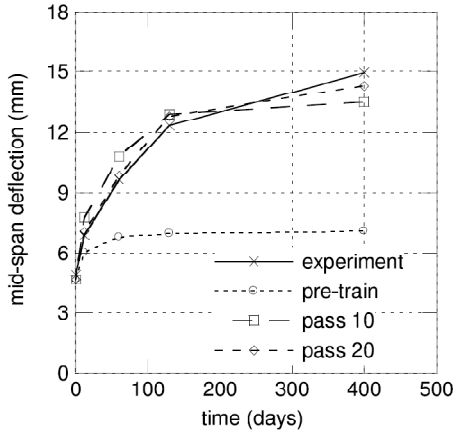

Figure 2.22: Convergence of mid-span deflection during the autoprogressive training (Jung & Ghaboussi, 2010)

In the application of the method it was tried to add the effect of shrinkage to the neural network model in order to improve its prediction. The result is illustrated in Figure 2.23. As it can be seen, including shrinkage effect has improved the prediction of NN model slightly and this improvement is not significant.

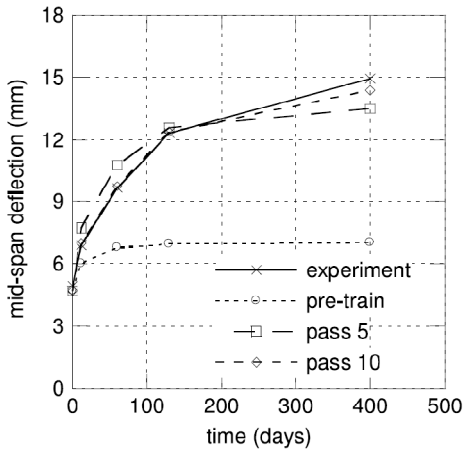

Figure 2.23: Convergence of mid-span deflection during the autoprogressive training (Jung & Ghaboussi, 2010)

The authors of this study attempted to use the autoprogressive methodology to forecast the behaviour of concrete in long-term based on its behaviour in short-term. For this purpose they generated some data from the equation presented for creep in the ACI code. The data from this equation with different time steps and the original database were re-trained again to predict the 4^{th} and 5^{th} load steps of the concrete beam test based on the first three load steps. The best achieved results are presented in Figure 2.24.

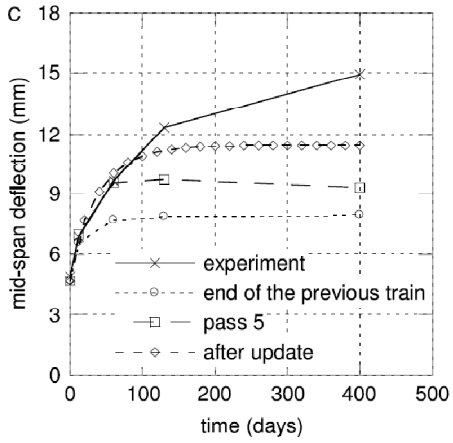

Figure 2.24: prediction after learning the first three steps and the database (Jung & Ghaboussi, 2010)

Although the authors have tried to improve the prediction of NN model using different ways; however, looking at the figure presented above, clearly the proposed method has failed to forecast the prediction of concrete beam behaviour for the 4^{th} and 5^{th} load steps.

Following the suggestion by Kim et al. (2010), Ghaboussi et al. (2010) developed a hybrid modelling framework by using mathematics-based and information-based methods, called HMIM. This hybrid method combines the mathematical models of engineered systems (derived based on physics and mechanical laws) with artificial neural network models using autoprogressive and Self-learning Simulation. In HMIM, neural networks only store information that is in experimental data and mathematical models can not capture them due to their complex relationships. As an example the HMIM method was applied to modelling a steel beam-to-column connection. In this example the components of the connection were divided to mathematical-based or information-based components. The components that their underlying mechanics are well-developed are suitable for the mathematical modelling. Others fit to the informational modelling because their background theories or available representations are too poor or too complex to be implemented in the current computational power. The results of an experimental test on a top-and-seat-angle connection carried out by Kukreti and Abolmaali (1999) were employed to evaluate the capability of the proposed method. In this connection, angles and column panel zone components were classified as mathematics-based components and slip and ovalization as informational-based components. The mathematical-based components were idealized as one-dimensional springs and reliable constitutive equations were defined for each of them. The autoprogressive method was utilized to train the neural network model of the informational-based components. The behaviour of the connection under cyclic load predicted by the hybrid model and an analytical model were compared to the experimental results and is presented in Figure 2.25. From this figure it can be seen that the hybrid model has been able to predict the behaviour of this connection better than the analytical method. It should be noted that in the presented example in this paper the entire data has been used to train the neural network while it is common to use only a part of the data for training and the rest for validation.

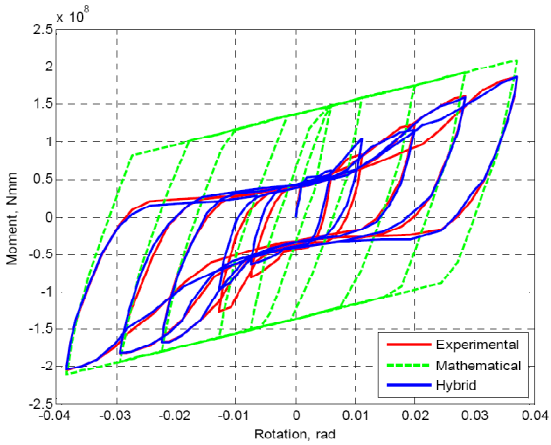

Figure 2.25: Comparison between experiment and hybrid model (Ghaboussi et al., 2010)

Osouli et al. (2010) investigated the influence of different instruments and their locations in an excavation project and the quality of information that can be extracted for excavation modelling using self-learning simulation technique. A set of synthetic data, generated by finite element analysis using MIT-E3 constitutive model, representing the measurement from different locations of the excavation project including surface settlement, wall deflection etc. were considered. These data were utilized to study the relationship between field instrumentation selection and the quality of learned material behaviour. The results showed that in addition to the measurements of lateral wall deflections and surface settlement, inclinometers placed some distance behind the wall and measured forces in the struts can significantly improve the quality of extracted soil behaviour. These findings were verified with an actual case study of a deep excavation project in Taiwan.

Hashash et al. (2011) applied the SelfSim approach to analyse a 3D deep excavation. They described numerical issues related to this problem including those occurred in developing the 3D model. They have shown that the proposed approach can capture the soil behaviour using the measured wall deformation and surface settlement from a 3D problem.

Although it has been shown by various researchers that NNs offer great advantages in constitutive modelling of materials in finite element analysis; however, despite their good performance on the available data, these networks have some shortcomings. One of the disadvantages of the NNCM is that the optimum structure of the NN (such as

number of inputs, hidden layers, transfer functions, etc.) must be identified a priori which is usually obtained using a time consuming trial and error procedure. Also, the main drawback of the NN approach is the large complexity of the network structure, as it represents the knowledge in terms of a weight matrix together with biases which are not accessible to user. In other words NN models give no information on the way inputs affect the output and are therefore considered as a black box class of model. The lack of interpretability of NN models has inhibited them from achieving their full potential in real world problems (Lu et al., 2001 and Javadi & Rezania, 2009a).

2.3.2 Application of evolutionary techniques in constitutive modelling

Feng and Yang (2004) proposed a hybrid evolutionary algorithm to identify the structure of the non-linear constitutive material model and its coefficients. The problem was defined as finding the elements of Jacobian matrix using a combination of genetic programming and genetic algorithm. Genetic programming was used to find the structure of the mathematical relationship between stress and strain and the genetic algorithm then used to find its coefficients. The methodology can be described in the following steps:

Step 1: A set of load-deflection data, obtained in a structural test, is divided in two groups. One is used for training to get the constitutive models and the other as testing to appraise applicability of the learned constitutive model. Then a non-linear finite element analysis is performed to extract stress-strain data set of experimental load-deflection data.

Step 2: A group of mathematical structures for constitutive models are randomly generated as an initial generation of model evolution using genetic programming.

Step 3: The best coefficient set for the generated models at step 2 is found using genetic algorithm.

Step 4: The applicability of each model is evaluated by calculating errors.

Step 5: If the calculated error is less than the tolerable error or cannot be considerably reduced any more, then the procedure is terminated; or else, it goes to the next step (step 6).

Step 6: New mathematical structures of material model are evolved and the process restart again from step 3.

The proposed methodology was applied to modelling the non-linear behaviour of laminated composite materials. The experimental results of a test on a laminated graphite plates with an open hole under compressive load was utilized to verify the methodology. The results showed that the proposed approach is generally capable of learning the behaviour of the laminated composites; however it was less promising for the cases that were used for testing.

The proposed approach also suffers from other issues. For instance in the first step, it is not clear what constitutive equation is used in the FE model to generate the stress-strain data. The choice of the constitutive model has a very strong effect on the outcome results.

2.4 Summary

This chapter reviewed a number of approaches to constitutive material modelling using different data mining techniques. The review indicated that each approach has its own limitation and shortcoming. To overcome the issues and drawbacks associated with this approaches, a further refined approach, called evolutionary polynomial regression (EPR) is proposed in this thesis that provides transparent models in terms of mathematical expressions to describe the material models. It is shown that how material models and in particular models that describes soil behaviour, is developed using EPR. Furthermore the incorporation of the material models (developed by this new data mining technique) in finite element method (FEM) is described in this thesis and different examples are provided to illustrate the potential of the proposed EPR-FEM in analysing boundary value problems in engineering.

Rezania, 2008 and Javadi & Rezania, 2009b were the only works that have used EPR for constitutive modelling of materials. They developed EPR models to predict the behaviour of shear stress in soil using the data from experimental test on soil (triaxial data). They introduced a methodology to incorporate the developed model in FE model and a number boundary value problems were used to verify the methodology. However these works have not addressed some main points. For instance in these studies the volumetric behaviour of soil was not considered and only a model was developed to predict the shear stress of soils. In addition only monotonic loading condition was considered in these studies when modelling the soil behaviour. In these works, the

Jacobian matrix was not developed based on the derivatives of the developed model and instead only elastic modulus was updated. Moreover when the developed models are incorporated in FE analysis the effect of Poisson's ratio was not considered. Furthermore the developed models were incorporated in an in-house FE code and the capability of the developed model in a commercial software was not examined. Only two dimensional examples were used to verify the proposed methodology.

This thesis is biult on the works done by Rezania (2008) and Javadi & Rezania (2009) and address the shortcomings and issues associated with these studies. In this thesis two different strategies are introduced to develop EPR-based material models. The volumetric behaviour of the soil is taken into account when developing the material model (i.e. an additional model is developed to predict the volumetric behaviour of soil). In addition a model is developed to predict the cyclic behaviour of soils. Moreover in this thesis a methodology introduced to construct the Jacobian matrix using the derivatives of the developed models. The incorporation of the developed models in this thesis in a commercial software (ABAQUS) is introduced. Examples including 2D and 3D problems are used to verify the methodology proposed in this thesis.

Chapter 3

Evolutionary Polynomial Regression (EPR)

3.1 Introduction

As discussed in chapter 2, data mining techniques and especially neural networks (NNs) have been successfully trained with synthetic as well as experimental data to obtain constitutive models for materials. It was also shown that various researchers have successfully implemented the obtained material models in different numerical analysis methods such as finite elements (FE).

Generally there are two most well known data-driven techniques, artificial neural networks (ANN) and genetic programming (GP). ANN use highly simplified models composed of many processing elements (neurons) connected by links of variable weights (parameters) to form black box representations of systems. ANNs are capable of dealing with large amount of data and learn complex model functions from examples, i.e. by training using sets of input and output data. ANNs have the ability to model complex, nonlinear processes without having to assume the form of the relationship between input and output variables. However, ANN also has some drawbacks; for example the structure of a neural network (e.g. model inputs, transfer functions, number

of hidden layers, etc) must be identified a priori. Another disadvantage of ANNs is the large complexity of the network structure, as it represents the knowledge in terms of a weight matrix and biases which are not accessible to user. In addition, parameter estimation and over-fitting are other disadvantages of models constructed by ANN (Giustolisi & Savic, 2006; Giustolisi & Laucelli, 2005).

Genetic programming (GP) is another modelling approach that has recently became popular. It is an evolutionary computing method that generates a transparent and structured representation of the system being studied. The most frequently used GP method is symbolic regression, which was proposed by Koza (1992). This technique creates mathematical expressions to fit a set of data points using the evolutionary process of genetic programming. Like all evolutionary computing techniques, symbolic regression manipulates populations of solutions (in this case mathematical expressions) using operations analogous to the evolutionary processes that operate in nature. The genetic programming procedure mimics natural selection as the 'fitness' of the solutions in the population improves through successive generations. The nature of GP allows global explorations and allows the user to resolve further information on the system behaviour, i.e. gives an insight into the relationship between input and output data. However, the GP also has some limitations. It is proven that GP is not very powerful in finding constants and, more importantly, that it tends to produce functions that grow in length over time (Giustolisi & Savic, 2006).

To avoid the problems associated with ANN and GP, a new data mining technique called evolutionary polynomial regression (EPR) is introduced in this chapter. EPR is a combination of Genetic Algorithm (GA) and Least Square (LS) regression which uses an evolutionary search for exponents of polynomial expressions by means of a GA engine. In what follows a brief description of evolutionary algorithms and especially genetic algorithm will be outlined and later a complete description of EPR will be explained in detail.

3.2 Evolutionary Algorithms

Evolutionary algorithms (EAs) are a subset of artificial intelligence that involve finding optimal solutions from a finite set of solutions. Evolutionary algorithms generate

solutions to optimization problems using techniques inspired by natural evolution, such as mutation, selection, and crossover. Genetic algorithm (GA) and genetic programming (GP) are the main types of evolutionary algorithms. As it was mentioned before EPR is a combination of GA and LS and for that reason a brief description of GA will be outlined in following.

3.3 Genetic Algorithm (GA)

Genetic algorithms are search algorithms based on the mechanics of natural selection and natural genetics. Genetic algorithms are combination of the survival of the fittest between string structures together with a randomized (but controlled and structured) information exchange to create a search algorithm with some of the innovative styles of human search. Genetic algorithms seek to maximize the fitness of the population by selecting the fittest individuals, based on Darwin's theory of survival of the fittest, and using their genetic information in mating and mutation operations to create a new population of solutions. Although the process involves randomized operations, however genetic algorithms are not simple random walk. Genetic algorithms utilize historical information in an efficient way to find new search points with expected improved performance. Genetic algorithms have been developed by John Holland and his co-workers in the University of Michigan (Goldberg, 1989).

Genetic algorithms (GAs) have received much attention regarding their potential as global optimization techniques for problems with large and complex search spaces. GAs have many advantages over the traditional optimization methods. In particular, they do not require function derivatives and work on function evaluations alone. They have a better possibility of locating the global optimum because they search a population of points rather than a single point and they can allow for consideration of design spaces consisting of a mix of continuous and discrete variables.

Application of genetic algorithms in optimization of various engineering problems has been extensively studied by several researchers. The author of this thesis and his co-workers have also performed a study on application of genetic algorithm in optimization of micro-structures of materials with negative Poisson's ratio (Javadi et al., 2011). The

results of these studies have shown that GAs can be successfully employed as strong optimization tool.

3.4 Evolutionary Polynomial Regression

3.4.1 Introduction

Usually colour names are used in order to categorize mathematical modelling techniques based on their level of required prior information (i.e. white-box models, black-box models and grey-box models). A brief description for each of these types of models is as following (Giustolisi & Savic, 2006):

- A white-box model is a model with known variables, parameters, and underlying physical laws. It explains the relationship of the system in form of a set or a single mathematical equation(s).
- Black-box models are systems for which there is no prior information available. These are data-driven or regressive models, for which the functional form of relationships between variables and the numerical parameters in those functions are unknown and need to be estimated.
- Grey-box models are conceptual models whose mathematical structure can be derived through conceptualisation of physical phenomena or through simplification of differential equations describing the phenomena under consideration. These models usually need parameter estimation by means of input/output data analysis, though the range of parameter values is normally known.

From the above it is clear that white-box models have the advantage of describing the underlying relationships of process being modelled based on the principles of physics. However, the construction of white-box models can be difficult because the underlying mechanisms may not always be wholly understood, or because experimental results obtained in the laboratory environment may not completely represent the real sample environment. Because of these reasons, approaches based on data-driven techniques are gaining large attention.

In the context of modelling classification, EPR is classified as a symbolic grey box technique which can identify and construct structured model expressions for a given data. A schematic representation of EPR classification in comparison with other modelling methods is shown in Figure 3.1.

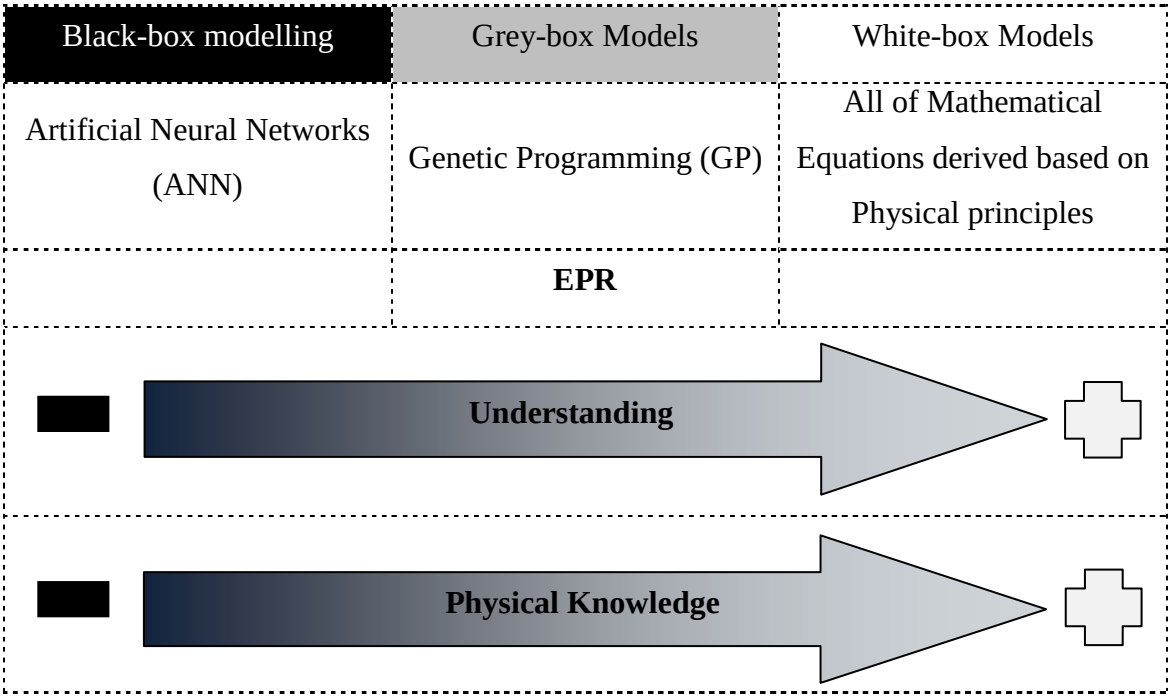

Figure 3.1: Classification of EPR among modelling techniques

3.4.2 The EPR scheme

EPR is a two-step technique in which in the first step it searches for symbolic structures using an ad hoc but simple GA and in the second step EPR estimates constant values by solving a linear Least Square (LS) problem. These two steps will be discussed in details in following.

3.4.2.1 Evolutionary structural identification

A typical formulation of the EPR expression is given as (Giustolisi & Savic, 2006):

$$y = \sum_{j=1}^{m} F(\mathbf{X}, f(\mathbf{X}), a_j) + a_0 \qquad 3.1$$

where y is the estimated output of the system; a_j is a constant value; F is a function constructed by the process; $\mathbf{X}$ is the matrix of input variables; f is a function defined by the user; and m is the number of terms of the expression excluding bias a_0.

The first step to identify the model structure is to transform equation (3.1) in to the following vector form:

$$\mathbf{Y}_{N\times1}(\boldsymbol{\theta},\mathbf{Z}) = \left[\mathbf{I}_N \quad \mathbf{Z}^j_{N\times m}\right] \times [a_0 \quad a_1 \quad \dots \quad a_m]^T = \mathbf{Z}_{N\times d} \times \boldsymbol{\theta}^T_{d\times1} \qquad 3.2$$

where

$\mathbf{Y}_{N\times1}(\boldsymbol{\theta},\mathbf{Z})$ is the least square estimate vector of N target values

$\boldsymbol{\theta}_{1\times\mathrm{d}}$ is the vector of $d = m + 1$ parameters $a_j, j = 1{:}\,m, and\ a_0$

$\mathbf{Z}_{N\times d}$ is a matrix formed by $\mathbf{I}$, for bias a_0, and m vector of variables $\boldsymbol{Z}^j$ that for a fixed j are a product of the independent predictor vectors of variables/inputs, $\mathbf{X} = \langle \mathbf{X}_1 \quad \mathbf{X}_2 \quad \dots \quad \mathbf{X}_k \rangle$.

EPR starts from equation 3.2 and searches first for the best structure, i.e. a combination of vectors of independent variables (inputs) $\mathbf{X}_{S=1:k}$. The matrix of inputs $\mathbf{X}$ is given as:

$$\mathbf{X} = \begin{bmatrix} x_{11} & x_{12} & x_{13} & \dots & x_{1k} \\ x_{21} & x_{22} & x_{23} & \dots & x_{2k} \\ x_{31} & x_{32} & x_{33} & \dots & x_{3k} \\ \dots & \dots & \dots & \dots & \dots \\ x_{N1} & x_{N1} & x_{N1} & \dots & x_{Nk} \end{bmatrix} = [\mathbf{X}_1 \quad \mathbf{X}_2 \quad \mathbf{X}_3 \quad \dots \quad \mathbf{X}_k] \qquad 3.3$$

where the k^{th} column of $\mathbf{X}$ represents the candidate variable for the j^{th} term of equation 3.2. Therefore the j^{th} term of equation 3.2 can be written as

$$\mathbf{Z}^j_{N\times1} = \left[(\mathbf{X}_1)^{\mathbf{ES}(j,1)} \cdot (\mathbf{X}_2)^{\mathbf{ES}(j,2)} \cdot (\mathbf{X}_3)^{\mathbf{ES}(j,3)} \cdot \ldots \cdot (\mathbf{X}_k)^{\mathbf{ES}(j,k)}\right] \qquad 3.4$$

where, $\mathbf{Z}^j$ is the j^{th} column vector in which its elements are products of candidate independent inputs and $\mathbf{ES}$ is a matrix of exponents. Therefore, the problem is to find the matrix $\mathbf{ES}_{k\times m}$ of exponents whose elements can be values within user-defined bounds. For example, if a vector of candidate exponents for inputs, $\mathbf{X}$, **(**chosen by user) is $\mathbf{EX} = [0, \quad 1, \quad 2]$ and number of terms (m) (excluding bias) is 4, and the number of

independent variables (k) is 3, then the polynomial regression problem is to find a matrix of exponents $\mathbf{ES}_{4\times3}$. An example of such a matrix can be as following:

$$\mathbf{ES} = \begin{bmatrix} 0 & 1 & 2 \\ 0 & 1 & 1 \\ 1 & 2 & 0 \\ 1 & 1 & 0 \end{bmatrix} \qquad 3.5$$

When this matrix is substituted into equation 3.4 the following set of mathematical expression is obtained

$$\begin{aligned} \mathbf{Z}_1 &= (\mathbf{X}_1)^0 \cdot (\mathbf{X}_2)^1 \cdot (\mathbf{X}_3)^2 = \mathbf{X}_2 \cdot \mathbf{X}_3^2 \\ \mathbf{Z}_2 &= (\mathbf{X}_1)^0 \cdot (\mathbf{X}_2)^1 \cdot (\mathbf{X}_3)^1 = \mathbf{X}_2 \cdot \mathbf{X}_3 \\ \mathbf{Z}_3 &= (\mathbf{X}_1)^1 \cdot (\mathbf{X}_2)^2 \cdot (\mathbf{X}_3)^0 = \mathbf{X}_1 \cdot \mathbf{X}_2^2 \\ \mathbf{Z}_4 &= (\mathbf{X}_1)^1 \cdot (\mathbf{X}_2)^1 \cdot (\mathbf{X}_3)^0 = \mathbf{X}_1 \cdot \mathbf{X}_2 \end{aligned} \qquad 3.6$$

Thus the expression of equation 3.2 is:

$$\begin{aligned} \mathbf{Y} = {} & a_0 + a_1 \cdot \mathbf{Z}_1 + a_2 \cdot \mathbf{Z}_2 + a_3 \cdot \mathbf{Z}_3 + a_4 \cdot \mathbf{Z}_4 \\ = {} & a_0 + a_1 \cdot \mathbf{X}_2 \cdot \mathbf{X}_3^2 + a_2 \cdot \mathbf{X}_2 \cdot \mathbf{X}_3 + a_3 \cdot \mathbf{X}_1 \cdot \mathbf{X}_2^2 + a_4 \cdot \mathbf{X}_1 \cdot \mathbf{X}_2 \end{aligned} \qquad 3.7$$

It should be noted that each row of **ES** determines the exponents of the candidate variable of the j^{th} term in equations 3.1 and 3.2. Each of the exponents in matrix **ES** corresponds to a value from user-defined vector **EX**. This allows the transformation of the symbolic regression problem into one of finding the best **ES**, i.e. the best structure of the EPR equation, e.g. in equation 3.7.

It should also be mentioned that EPR can construct non-polynomial mathematical expression. It is possible to assume a function f, such as natural logarithm, hyperbolic tangent, hyperbolic secant and exponential and a structure among the following (Doglioni, 2004):

$$\begin{aligned} \mathbf{Y} = {} & a_0 + \sum_{j=1}^{m} a_j \cdot (\mathbf{X}_1)^{\mathbf{ES}(j,1)} \cdot \ldots \cdot (\mathbf{X}_k)^{\mathbf{ES}(j,k)} \\ & \cdot f\left((\mathbf{X}_1)^{\mathbf{ES}(j,k+1)}\right) \cdot \ldots \cdot f\left((\mathbf{X}_k)^{\mathbf{ES}(j,2k)}\right) \end{aligned} \qquad \text{case 1}$$

$$\mathbf{Y} = a_0 + \sum_{j=1}^{m} a_j \cdot f\left((\mathbf{X}_1)^{\mathbf{ES}(j,1)} \cdot \ldots \cdot (\mathbf{X}_k)^{\mathbf{ES}(j,k)}\right) \quad \text{case 2}$$

$$\mathbf{Y} = a_0 + \sum_{j=1}^{m} a_j \cdot (\mathbf{X}_1)^{\mathbf{ES}(j,1)} \cdot \ldots \cdot (\mathbf{X}_k)^{\mathbf{ES}(j,k)} \cdot f\left((\mathbf{X}_1)^{\mathbf{ES}(j,k+1)} \cdot \ldots \cdot (\mathbf{X}_k)^{\mathbf{ES}(j,2k)}\right) \quad \text{case 3} \qquad 3.8$$

$$\mathbf{Y} = g\left(a_0 + \sum_{j=1}^{m} a_j \cdot (\mathbf{X}_1)^{\mathbf{ES}(j,1)} \cdot \ldots \cdot (\mathbf{X}_k)^{\mathbf{ES}(j,k)}\right) \quad \text{case 4}$$

The global search for the best form of equation 3.7 is performed using a standard GA. The parameters being optimised are coded using 'chromosomes', i.e. a set of character strings that are analogous to the chromosomes found in DNA. Standard GAs use binary codes (characters are 0's or 1's) to form chromosomes. Instead, integer GA coding is used here to determine the location of the candidate exponents of **EX** in the matrix **ES** (Doglioni, 2004). For example the positions in $\mathbf{EX} = [0, \ 1, \ 2]$ correspond to the following string for the matrix of equation 3.5 and the expression of equation 3.7:

$$\mathbf{EX} = [1\ 2\ 3, \quad 1\ 2\ 2, \quad 2\ 3\ 1, \quad 2\ 2\ 1] \qquad 3.9$$

It is clear that the presence of a zero in **EX** ensures the ability to exclude some of the inputs and/or input combinations from the regression equation.

After the evolutionary identification of the structure, EPR computes the values of the adjustable parameters a_j by means of the linear Least Square (LS) method using the minimisation of the sum of squared errors (SSE) as the cost function.

3.4.2.2 Least square solution

Computing a_j in equation 3.7 is an inverse problem that corresponds to solving an over-determined linear system in form of a LS problem. This problem is traditionally solved by Gaussian elimination. However, an evolutionary search procedure may generate

candidate solutions (e.g. a combination of exponents of $\mathbf{X}$) that correspond to an ill-conditioned inverse problem. This often means that the rectangular matrix $\mathbf{Z}_{N\times d}$:

$$\mathbf{Z} = [\mathbf{I}_{N\times 1} \quad \mathbf{Z}^{1}_{N\times 1} \quad \mathbf{Z}^{2}_{N\times 1} \quad \mathbf{Z}^{3}_{N\times 1} \quad \dots \quad \mathbf{Z}^{\mathrm{m}}_{N\times 1}]_{N\times(m+1)=N\times d} \tag{3.10}$$

may not be of full rank (if a solution contains a column of zeros) or the columns $\mathbf{Z}^{j}$ are linearly dependent. This can cause serious problems to Gaussian elimination and therefore a more robust method is required. For this purpose parameters estimation of a_j (or $\boldsymbol{\theta}$) in EPR is achieved using Singular Value Decomposition (SVD) of the matrix $\mathbf{Z}$. This approach makes the process of finding the solution to the LS problem more robust, although in general SVD is a slower technique than Gaussian elimination method(Golub & Van Loan, 1993).

3.4.3 Objective functions of EPR

In order to get the best symbolic model(s) of the system being studied, EPR is provided with different objective functions to optimise. EPR can work both in single as well as multi-objective configurations. Figure 3.2 shows a summary of main available objective functions/strategies in EPR.

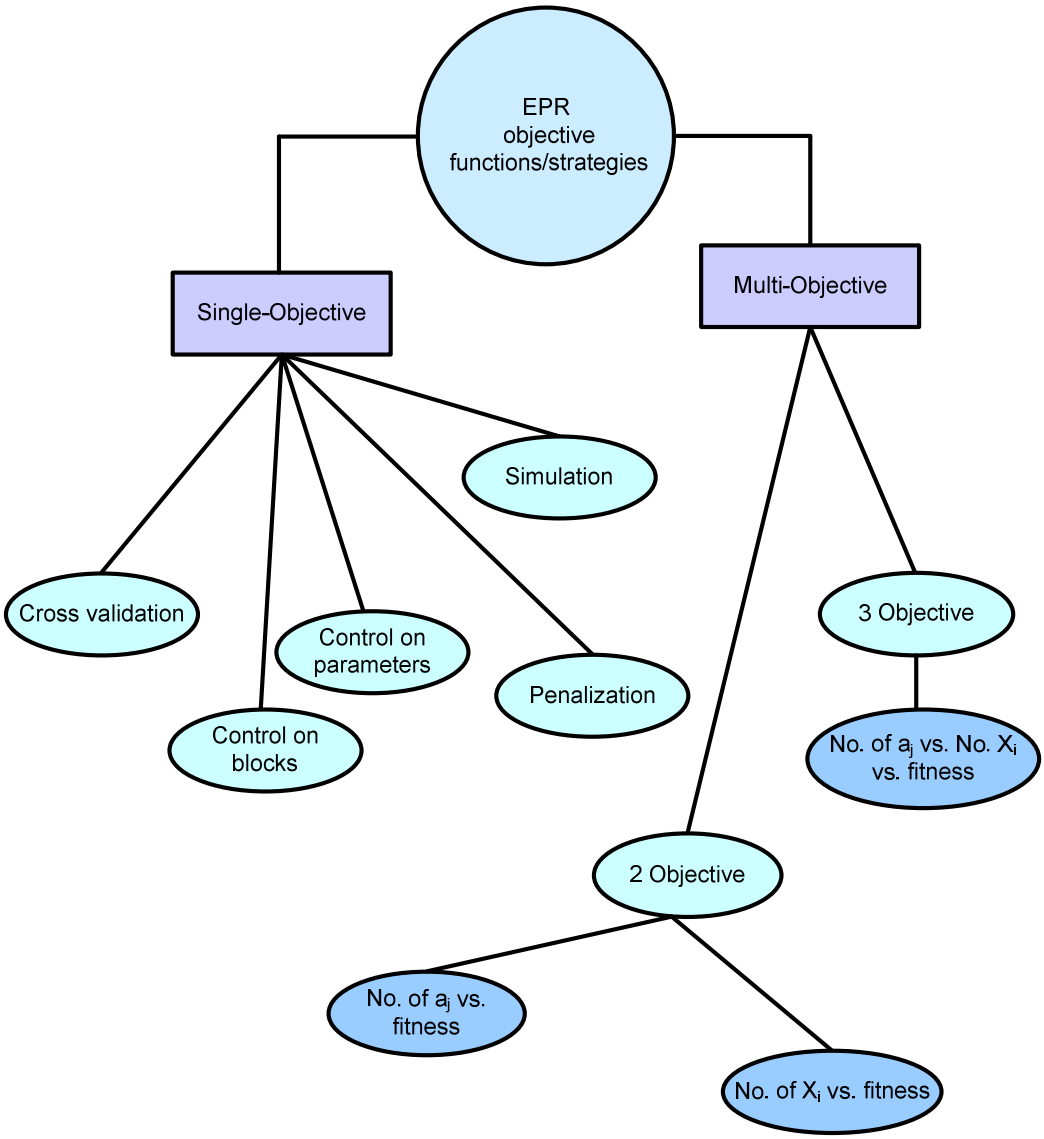

Figure 3.2: Overview of main objective functions/strategies in EPR (after Doglioni, 2004)

EPR introduces a set of multidimensional strategies for model selection, based on a comprehensive analysis of complexity (including number of terms, number of inputs) and fitness of models. It is widely accepted that the best modelling approach is also the simplest that fits the purpose of the application. The so-called principle of parsimony states that for a set of equivalent models of a given phenomenon one should choose the simplest one to explain a set of data. Therefore, the fitness in regression-based models should also include a measure of trade-off between the model complexity (i.e. addition of new parameters) and the quality of fit. This can be achieved in two ways:

I. Single-objective: an objective function is used to control the fitness of the models without allowing unnecessary complexities enter in the models.

II. Multi-objectives: at least two objective functions are introduced; in this case one objective function will control the fitness of the models, while at least one objective function controls the complexity of the models. This approach implies the advantage of returning a set of non-dominated models each one presenting fitting and complexity features which vary along the Pareto front representative of the model solutions. Therefore, the user is not required to assume the number of building blocks a-priori, but he/she just sets the maximum number of building blocks, while the control on the complexity will let them vary according to the fitness. Then, the Pareto front represents the trade-off surface (or line), of complexity vs. fitness, which is required. The trade-off surface allows the user to achieve a lot of purposes of the modelling approach to the phenomenon studied.

3.4.3.1 Single-objective strategy

For a given set of observations or data, a regression-based technique needs to search among a large if not an infinite number of possible models to explain those data. By varying the exponents for the columns of matrix **X** and searching for the best-fit set of parameters $\boldsymbol{\theta}$, the EPR methodology searches among all those models. However it requires an objective function that will ensure the best fit, without the introduction of unnecessary complexity. Unnecessary complexity is here defined as the addition of new terms or combinations of inputs that fit some noise in the raw data rather than the underlying phenomenon. Therefore, the key objective here is to find a systematic means to avoid the problem of over-fitting. There are three possible approaches to this problem:

I. To penalise the complexity of the expression by minimising the number of terms.

II. To control the variance of a_j constants (the variance of estimates) with respect to their values.

III. To control the variance of $a_j \cdot \mathbf{Z}_j$ terms with respect to the variance of residuals.

In addition to the above, two more strategies can be used:

(1) Cross-validation of the models

(2) Optimisation of the SSE evaluated on the simulation (off-line prediction) of the phenomenon performed by the models. These two strategies are more general purposed and the Cross-validation proved to be effective in those cases where a long data set is available and data are affected by a low disturbance (Giustolisi & Savic, 2006; Doglioni, 2004). In what follows description of the first three strategies will be given. A full and detailed description of the last two strategies can be found in Doglioni, (2004).

I. Complexity Penalisation

To choose a model with optimum complexity corresponding to the best prediction for unseen data, a strategy is required to compare two models with different levels of complexity and model fit. The sum of squared errors (SSE) is normally used to conduct the search toward the best-fit model;

$$\mathrm{SSE} = \frac{\sum_{i=1}^{N}(y_a - y_p)^2}{N} \qquad 3.11$$

where y_a are the actual values (target values) in the training dataset and y_p are the model predictions computed by using polynomial expression obtained by EPR. In order to allow a compromise between the quality of fit (SSE) and the model complexity (number of input combinations), the following penalization of complexity (PCS) fitness function was used by Doglioni (2004):

$$PCS = \frac{\mathrm{SSE}}{(Nd - px + 1)^{\alpha}} \qquad 3.12$$

where $Nd = k \cdot m$ is the maximum number of inputs that can be considered, px is the actual number of inputs selected by GA and α is an adjustable exponent that controls the amount of pressure to control complexity. In order to better understand this form of the fitness function, the derivative of the fitness function with respect to px can be presented as following:

$$\frac{\partial}{\partial px}\left(\frac{\mathrm{SSE}}{(Nd - px + 1)^{\alpha}}\right) = \left(\frac{1}{(Nd - px + 1)^{\alpha}}\right)\left(\frac{\partial \mathrm{SSE}}{\partial px} + \frac{\alpha \cdot \mathrm{SSE}}{Nd - px + 1}\right) \qquad 3.13$$

The fitness decreases with respect to px if the derivative in equation 3.13 is negative. This has been shown in Figure 3.3.

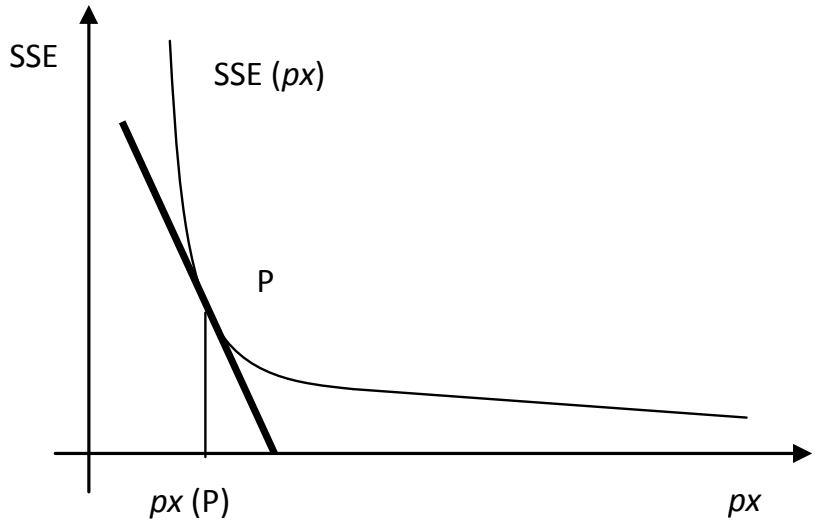

Figure 3.3: SSE variation vs. *px* (Doglioni, 2004)

Therefore the following inequality should hold:

$$\frac{\alpha \cdot \mathrm{SSE}}{Nd - px + 1} \leq -\frac{\partial \mathrm{SSE}}{\partial px} = -VAR_{px}(\mathrm{SSE}) \qquad 3.14$$

This means, adding another combination of inputs **X**, needs not only to be justified on the basis of decreasing SSE, but also need to take into account the terms (*Nd-px*) and $\alpha \cdot \mathrm{SSE}$ (see Figure 3.3). The bold line is the derivative of SSE with respect to *px*(P), while the curve is the natural SSE variation due to the increase in the number of input parameters. Equation 3.14 requires a value of the SSE derivative at P greater than or equal to the term on the left side of the inequality. Equation 3.14 shows that when the actual number of inputs px approaches the maximum Nd, the left term of the inequality increases and, therefore, a high absolute variation of SSE will be required ($VAR_{px}(\mathrm{SSE})$ is always negative) which results in penalisation of complex structures by controlling the total number of inputs in the formula.

II. Variance of a_j

It is possible in EPR to control the polynomial term contribution to variance of **Y** expressed through their parameters during GA search. Indeed, it may be argued that low constant value with respect to variance of estimates corresponds to terms that begin to describe noise in preference to the underlying function of phenomena. Therefore Doglioni, (2004) suggested to use the variance of estimated constant values to eliminate

those parameters with a value that is not sufficiently larger than the variance of the estimated value. Hence, the variance in estimation of parameters obtained by EPR can be computed as

$$var(\boldsymbol{\theta}) = [var(a_0) \quad var(a_1) \quad var(a_2) \quad \dots \quad var(a_m)] \tag{3.15}$$

Assuming that constants are from a Gaussian probability density function, the following expression is used

$$\gamma \cdot \sqrt{\left|var(a_j)\right|} = \gamma \cdot \left|\mathrm{StD}(a_j)\right| > \left|a_j\right| \implies a_j = 0 \tag{3.16}$$

where StD is the standard deviation of estimated constants, a_j (from the diagonal elements of the covariance matrix) and $\gamma = 2.578$ is the value from the table of the standard normal distribution related to the confidence interval of 99%.

III. Variance of $a_j \cdot \mathbf{Z}_j$

EPR can control the polynomial term contribution to variance of **Y** explaining through evaluating the monomial building blocks $a_j \cdot \mathbf{Z}_j$ with respect to variance of the noise in the raw data during GA search. Of course, a level of noise may exist under which the variance of the terms $a_j \cdot \mathbf{Z}_j$ will describe noise, causing over-fitting related problems. This level of noise is not known a priori and, therefore, a residual vector could be used to estimate noise. In this manner, it is possible to compare the standard deviation of this residual vector with the standard deviation of terms $a_j \cdot \mathbf{Z}_j$, in the following form:

$$\left|\mathrm{StD}(a_j \cdot \mathbf{Z}_j)\right| < \beta \cdot |\mathrm{StD}(\mathbf{E})| \implies a_j = 0 \tag{3.17}$$

where β is a user selected adjusting parameter and **E** is the vector of residual ($\mathbf{E} = \mathbf{Y} - \mathbf{Y}(\boldsymbol{\theta}, \mathbf{Z})$). It is not easy to choose β, but it is possible to consider $\beta = 1$ as giving a pressure to EPR for formulæ having variance of each term greater than the variance of the residuals.

3.4.3.2 Multi-objective strategy

The original and first version of EPR methodology (which has been described so far) is using single-objective genetic algorithm (SOGA) strategy for exploring the formulae space. As it was mentioned before this exploration is achieved by first assuming the maximum number of terms m in the pseudo-polynomial expressions shown in equation 3.2 and then sequentially exploring the formulae space having one, two, … and m terms. However, the SOGA-based EPR methodology has the following drawbacks.

a) Its performance exponentially decreases by increasing number of polynomial terms m (more terms means more GA runs).
b) The results of SOGA-based EPR are sometimes difficult to interpret. The identified models can either be ranked based on their fitness to data or according to their structural complexity. However, ranking models based on structural complexity requires some subjective judgment, and therefore this process can be biased by the analyst's experience rather than being purely based on some mathematical criteria that in our case are the objectives.
c) When searching for the formulae with j terms, those formulae that have fewer terms are not presented. However these formulas could have a better accuracy than the previously found ones with $j-1$ terms (Giustolisi & Savic, 2009).

To overcome these drawbacks, multi-objective genetic algorithm strategy (MOGA)(Goldberg, 1989) has been added to EPR. The multi-objective approach in EPR (MOGA-EPR) is aimed at searching for those model structures, which on one hand comply with the fitness and on the other hand with limiting the structural complexity. In this approach the control of fitness and complexity are demanded to different singly acting objective functions. The objectives represented by the functions are mutually conflicting, and then their optimisation returns a trade-off surface of models. The multi-objective strategy in hybrid evolutionary computing enables the user to

a) Find a set of feasible symbolic models.
b) Make a robust choice.
c) Get a set of models with variable parsimony levels in an efficient computational time.

MOGA-EPR tackles a multi-model strategy by varying the structural parsimony (i.e. the number of constant values in the equation) and working on the objective function used in Single-Objective EPR. Then, MOGA-EPR finds the set of symbolic expressions that perform well according to two (or more) conflicting criteria considered simultaneously, the level of agreement between simulated and observed measurements, and structural parsimony of the expressions obtained. The objective functions used are

a) Maximization of the fitness.
b) Minimization of the total number of inputs selected by the modelling strategy.
c) Minimization of the length of the model expression.

The obtained models are ranked according to the Pareto dominance criterion. MOGA-EPR reduces the computational time required by the multiple executions of EPR, which would otherwise be required for one of each of the objective functions introduced in the previous section. The models that dominate others in the population of solutions are presented to the user. The Pareto set of solutions is likely to be the best set of expressions required for the analysis of the problem.

The objective functions commonly used to measure the fitness of the symbolic structures are based on the Sum of Squared Errors (SSE) or on the Penalisation of Complex Structures (PCS). The result of the single-objective EPR optimization consists of a set of equally good models. They might be easily ranked according to their SSE, rather than according to their structural complexity. In fact, sorting models according to their structural complexity is usually a complex task. The multi-objective strategy is implemented to improve both the post-processing phase and the general modelling framework of EPR. Such strategy allows ranking models according both to the Coefficient of Determination (CoD) and structural complexity. The three objective functions implemented in MOGA-EPR are:

a) (1-CoD), which has the same meaning as the SSE,

$$\mathrm{CoD} = 1 - \frac{N-1}{N} \frac{\sum_N \left[(\mathbf{Y}_\mathrm{p} - \mathbf{Y}_\mathrm{a})^2 \right]}{\sum_N \left[\left(\mathbf{Y}_\mathrm{a} - \frac{1}{N} \sum_N \mathbf{Y}_a \right)^2 \right]} = 1 - k \cdot \mathrm{SSE} \qquad 3.18$$

$$k = \frac{2(N-1)}{\sum_N \left[(\mathbf{Y}_a - \frac{1}{N}\sum_N \mathbf{Y}_a)^2 \right]}$$

where $\mathbf{Y}_a$ is the vector of actual data, $\mathbf{Y}_\mathrm{p}$ are the corresponding predicted values and N is the number of data on which the CoD is computed.

b) The number of constant values a_j (# of a_j) and

c) The total number of inputs involved in the symbolic expression (% of $\mathbf{X}_\mathrm{i}$).

Note that the total number of inputs corresponds to the number of times that each input is involved in the symbolic expression. The user must set the maximum number of constant values, which puts an upper limit on the maximum number of the symbolic expression inputs. Therefore, MOGA-EPR looks for the best non-dominated models with respect to both structural complexity and fitness performance, i.e. placed on the best Pareto front. Therefore, a direct multi-model approach is provided where the post-processing phase is improved by MOGA-EPR, which returns models ranked according to both their fitness and their structural complexity.

A further advantage of MOGA-EPR is the increased pressure to achieve structural parsimony because a large number of a_j values or a large total number of inputs must be justified by the fitness of the model (note that the Pareto dominance criterion and the function are to be minimised). The introduced objective functions can be used in a two-objective configuration or all together:

a) CoD vs. (% of $\mathbf{X}_\mathrm{i}$)

b) CoD vs. (% of a_j)

c) CoD vs. [(% of $\mathbf{X}_\mathrm{i}$) and (% of a_j)]

The choice of the Pareto dominance criterion for the multi-objective optimisation implies the following main advantages:

a) It is reasonably fast for few objective functions in comparison with the total amount of time required by multiple single-objective sessions.

b) It deals simultaneously with multiple solutions.

c) It is capable to provide a uniformly distributed range of Pareto solutions.

A typical flow diagram for the EPR procedure is shown in Figure 3.4.

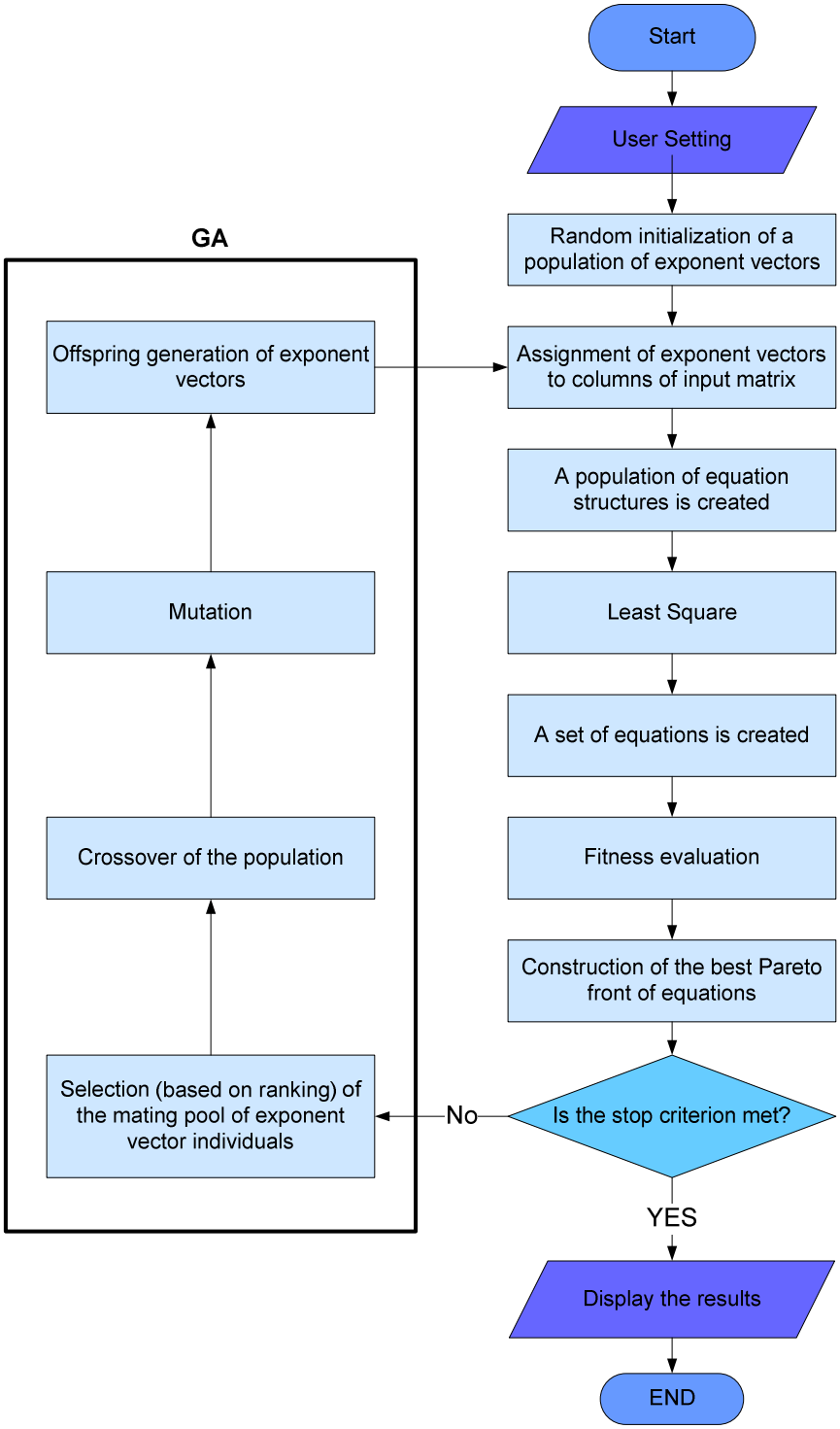

Figure 3.4: Typical flow diagram for the EPR procedure (after Doglioni, 2004)

A typical outlook of EPR during its operation is presented in the following figure. It can be seen in this figure that EPR is performing a multi-objective strategy since it simultaneously optimising CoD, $\boldsymbol{X}_{\mathrm{i}}$ and a_j.

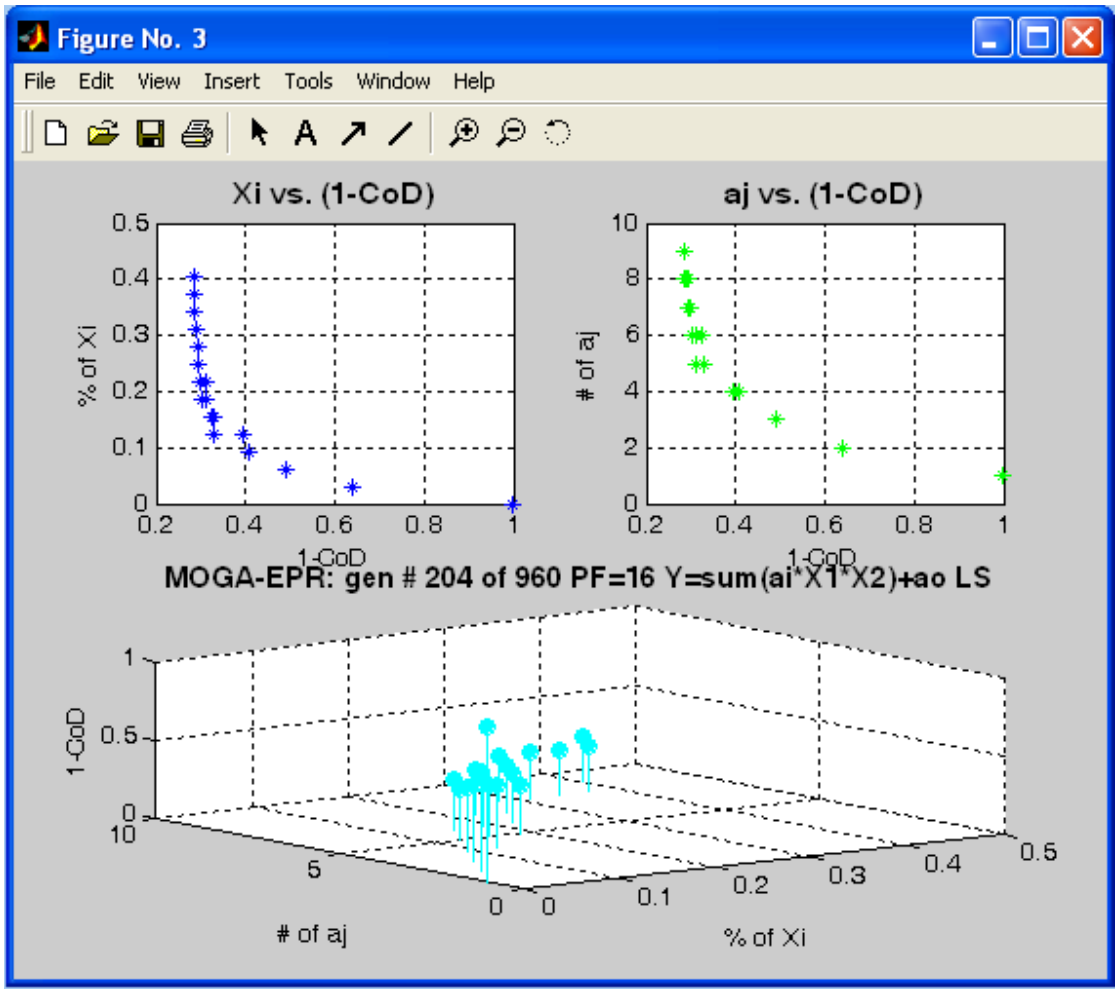

Figure 3.5: A typical outlook of EPR during a multi-objective operation

3.4.4 Multi-Case Strategy for Evolutionary Polynomial Regression

Models returned by the EPR usually contain a certain combination of explanatory variables which are common to the majority of Pareto optimal models, whereas other variables or even entire terms are selected in just a few models. In the case of individual systems, the balancing between model accuracy, complexity and prior insight on the phenomenon can help in selecting the most suitable model to avoid over-fitting. However when the same phenomenon is modelled for several separate systems significant differences may exist among relevant failure models. Such observation

makes it difficult to separate the description of the underlying physical phenomenon from other variables/terms which have been affected by local effects and the particular realization of the noise into each system. As a consequence, this poses doubts about the correctness of individual system models identified and their use as general performance indicators. The Multi-Case Strategy for EPR (MCS-EPR) aims at overcoming the above drawbacks by simultaneously identifying the best model structure and parameter values from the observed data available for multiple systems (cases).

Assume there are C systems (cases) $S_1, S_2, \dots, S_C$ each with the relevant observed dataset containing both system output $\mathbf{Y}_S$ and the corresponding potential k explanatory variables (i.e. $\mathbf{X}_{s,i}$, with $i = 1, \dots, k$ and $S = 1, \dots, C$). Like EPR, MCS-EPR encodes each candidate model structure as a set of polynomial exponents corresponding to potential explanatory variables in all polynomial terms and then uses the MOGA-based search procedure to find the best model structure. The estimate of unknown polynomial coefficients (i.e., model parameters) $a_{s,j}$ $(s = 1, \dots, C \quad j = 1, \dots, m+1)$ is performed by means of numerical regression for all individual systems simultaneously. Evaluation of the last two objectives reported above (i.e., number of polynomial terms and the number of significant explanatory variables) is the same as in EPR, while the value of first objective (model accuracy) depends on how closely each of the C models (with parameters $a_{s,j}$, $(j = 1, \dots, m+1)$ fits in its observed data. Unlike EPR, MCS-EPR employs the following measure of model accuracy:

$$F = 1 - \frac{\sum_{S=1}^{C} \sum_{N_s} (\mathbf{Y}_p - \mathbf{Y}_a)^2}{\sum_N \left[(\mathbf{Y}_a - \frac{1}{N} \sum_N \mathbf{Y}_a)^2 \right]} = 1 - \frac{\sum_{S=1}^{C} N_s \cdot SSE_S}{\sum_N \left[(\mathbf{Y}_a - \frac{1}{N} \sum_N \mathbf{Y}_a)^2 \right]} \qquad 3.19$$

where N is the total number of samples over all C datasets (i.e. $N = \sum N_S$), $\mathbf{Y}_p$ is the value predicted by the model built with the s-th vector of parameters of $a_{s,j}$ and $\mathbf{Y}_a$ is the actual (target) values. Similar to the CoD definition of equation 3.18, the closer to 1 is F; the more suitable the model structure is in describing the overall observed dataset (Berardi & Kapelan, 2007).

3.4.5 EPR user interface

EPR has been coded using MATLAB® in POLITECNICO DI BARI University, Italy, by Professor Giustolisi and his co-workers in collaboration with Professor Savic in University of Exeter, UK. EPR is provided with a friendly user interface, as it can be seen in the following figure.

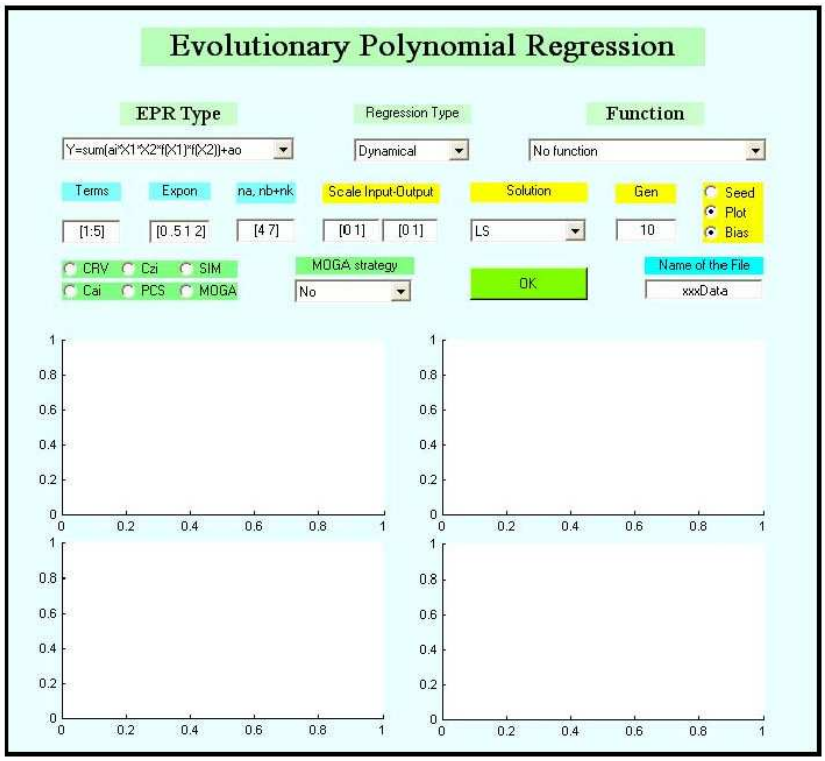

Figure 3.6: EPR Graphical User Interface

Within this graphical user interface (GUI), the user can set up the modelling phase according the features described in the previous sections. Moreover, the user can decide the number of generations of the GA, setting the proper value in the "Generation" box. This value corresponds to a proportionality factor which will be multiplied for the maximum length of the expression (maximum number m of monomial building blocks) and for the total number of inputs. Another option is about the possibility of seeding the population with random elements from the previous parental set. This option efficiently works when large data sets are available and in single-objective configuration. In multi-objective search the seed option does not seem to add any advantage in the GA phase. Finally, the option "bias" refers to the possibility of looking for symbolic expression containing the term a_0. If the bias option is not selected, EPR will automatically exclude

all those expressions containing a_0, otherwise selecting bias EPR will search both for expression with a_0 term and without (Doglioni, 2004).

3.4.6 The application of EPR in modelling engineering problems

Application and potential of EPR in modelling and analysing different disciplines of engineering from structural to geotechnical and environmental engineering have been investigated by different researchers including the author of this thesis. The results of these studies have been published in several conference and journal papers (e.g., Rezania et al., 2011; Ahangar-Asr et al., 2011; Ahangar-Asr et al., 2010; Faramarzi et al., 2011; Javadi et al., 2010).

Rezania et al., 2011 presented the application of EPR in prediction of liquefaction and earthquake-induced lateral displacement. They developed a 3D surface that discriminates between the cases of occurrence and non-occurrence of liquefaction using EPR.

Ahangar-Asr et al, 2010 employed EPR in analysis of stability of soil and rock slopes. EPR models are developed and validated using results from sets of field data on the stability status of soil and rock slopes. The developed models are used to predict the factor of safety of slopes against failure for conditions not used in the model building process. The results show that the proposed approach is very effective and robust in modelling the behaviour of slopes and provides a unified approach to analysis of slope stability problems. It is also shown that the models can predict various aspects of behaviour of slopes correctly.

Faramarzi et al., 2011 proposed to use EPR to predict the behaviour of steel plate shear walls (SPSW) under cyclic behaviour. The results of a number of actual experiments on cyclic behaviour of SPSW structures were used to develop EPR models to predict lateral deformation of SPSW due to the cyclic loading.

Ahangar-Asr et al., 2011 showed that how EPR can be used to predict the mechanical properties of rubber concrete. They used data from 70 cases of experiments on rubber concrete for development and validation of the EPR models.

Chapter 4

EPR Based Material Modelling

4.1 Introduction

As discussed in chapter 2, data mining techniques and especially neural networks (NNs) have been successfully applied in constitutive modelling of different materials. The disadvantages and drawbacks of ANN were discussed both in chapters 2 and 3 and a new data mining technique (evolutionary polynomial regression) was introduced in chapter 3 to overcome these shortcomings. In this chapter the application of the evolutionary polynomial regression (EPR) in material modelling will be discussed in detail.

In material modelling using EPR, the raw experimental or in-situ test data are directly used for training the EPR model. As the EPR learns the constitutive relationships directly from raw data, it is the shortest route from experimental research to numerical modelling. In this approach there are no material parameters to be identified and as more data become available, the material model can be improved by re-training of the EPR using additional data. Furthermore, the incorporation of an EPR in the finite element procedure avoids the need for complex yield/failure functions, flow rules, etc.

An EPR model can be incorporated in a finite element code/procedure in the same way as a conventional constitutive model.

In this chapter two different strategies will be introduced to train EPR and develop material models. In the first approach the total values of stresses and strains will be used to train and develop models while in the second one the incremental values will be employed to construct the constitutive models of materials. Different examples including modelling linear, non-linear, monotonic and cyclic behaviour of materials will be presented to validate both strategies.

One of the main purposes of constitutive modelling of materials is to perform numerical analysis of boundary value problems. This is achieved by incorporation of developed models in numerical methods (for example finite element) analysis. Therefore when developing a constitutive model its suitability for implementation in finite element analysis should be taken into consideration. The material models developed in this chapter are all suitable to be implemented in finite element analysis. This will be shown in the next chapter through different examples.

4.2 Total stress-strain strategy for material modelling

The source of data, the training approach adopted and the way the trained EPR model is to be used have significant effects on the choice of input and output parameters. An EPR model formulated in the form of total stress-strain relationships (total stress-strain strategy) might be used for modelling of materials that are not strongly path-dependent. A similar strategy has been utilised by some researchers such as Ghaboussi et al., (1998) and Shin, (2001) for training neural network based material models. In this approach strain variables (i.e. $\varepsilon_x, \varepsilon_y, \varepsilon_z, \gamma_{xy}$) which represent the strain components in a 2D continuum, can be considered as inputs, and the corresponding stress variables ($\sigma_x, \sigma_y, \sigma_z, \tau_{xy}$) as outputs. It should be noted that due to the nature of EPR which represents the model as a mathematical equation; for each of the output parameters an equation needs to be developed. This is in contrast with artificial neural network (ANN) where you can have more than one parameter in output.

Data from material tests can be used to train EPR models. Usually a single test on a sample of a material provides a set of stress-strain relationships for a single stress path. However generally all the material tests that involve loading along the principal axes result in the shear components (shear strains, shear stresses) being zero. As a result an EPR model trained in this way would not be suitable to be incorporated in a finite element (FE) analysis, since all the components of the stress and strain tensors must be taken into account during analysis. Therefore to obtain an EPR model with the potential to be incorporated in FE framework, the EPR-based model should be trained along global axes with non-zero shear components.

To overcome this issue, a procedure is employed here to generate additional data from an ordinary material test. It should be noted that this procedure can be applied when the material being studied is isotropic or isotropy can be assumed. This procedure was first proposed by Shin, (2001) and Shin & Pande, (2002). The procedure is described here for 2D problems but it can be easily extended to 3D.

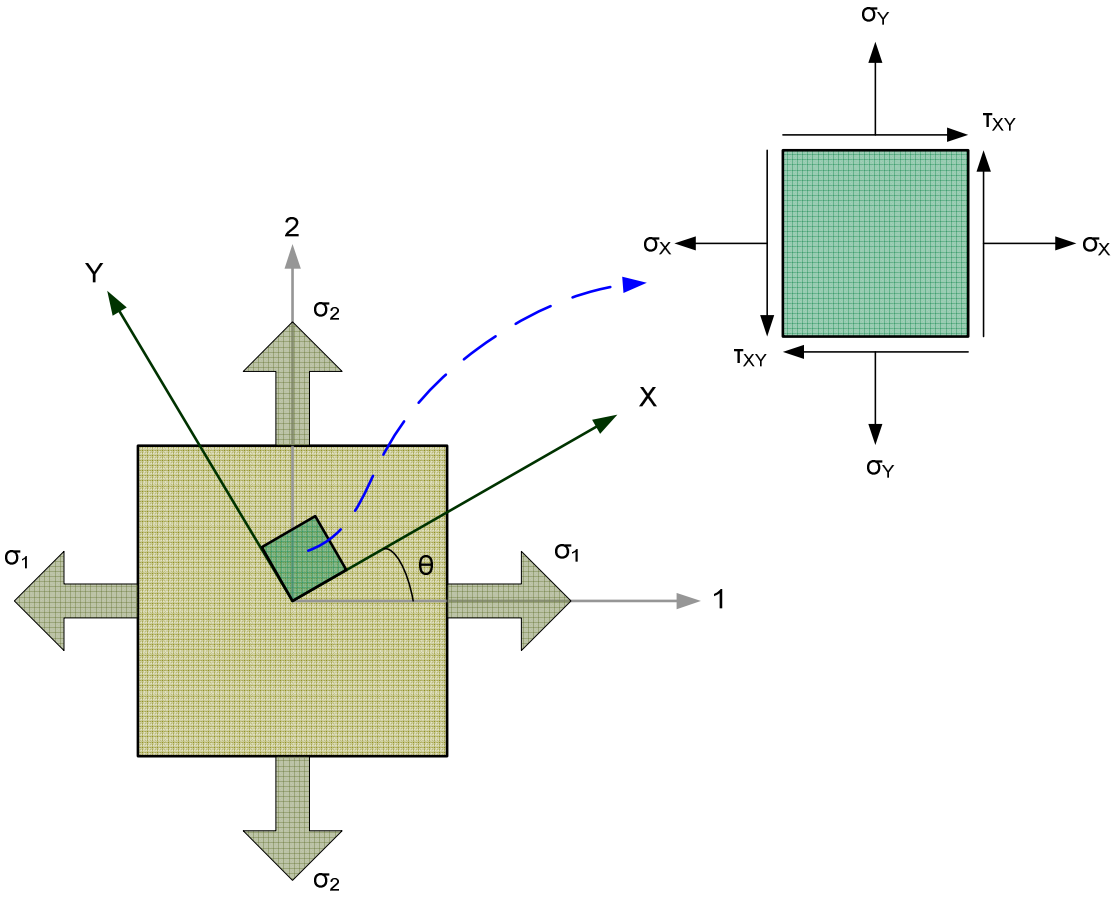

Figure 4.1: Transformation of stress components in a 2D continuum

Figure 4.1 shows a sample of a material under loading along principal axes 1-2. The additional data are generated in two steps. In the first step it is assumed that the material is isotropic. The assumption of isotropy enables to exchange the normal components, thereby to double up the data. Then transformation of each of the exchanged stress-strain pairs is carried out by rotating the datum axes (X-Y) from the original axes (1-2) where the material tests have been carried out. By rotating the axes, non-zero shear stresses and strains and their corresponding normal components can be obtained as a function of the rotation angle θ. Based on Mohr's circle, in the 2D space, the transformation of a principal stress vector by an angle θ measured anti-clockwise from the X axis can be calculated as following:

$$\sigma_X = \frac{\sigma_1 + \sigma_2}{2} + \frac{\sigma_1 - \sigma_2}{2}\cos(2\theta)$$
$$\sigma_Y = \frac{\sigma_1 + \sigma_2}{2} - \frac{\sigma_1 - \sigma_2}{2}\cos(2\theta) \qquad 4.1$$
$$\tau_{XY} = \frac{\sigma_1 - \sigma_2}{2}\cos(2\theta)$$

And for strains:

$$\varepsilon_X = \frac{\varepsilon_1 + \varepsilon_2}{2} + \frac{\varepsilon_1 - \varepsilon_2}{2}\cos(2\theta)$$
$$\varepsilon_Y = \frac{\varepsilon_1 + \varepsilon_2}{2} - \frac{\varepsilon_1 - \varepsilon_2}{2}\cos(2\theta) \qquad 4.2$$
$$\gamma_{XY} = \frac{\varepsilon_1 - \varepsilon_2}{2}\cos(2\theta)$$

This procedure can result in a large amount of training data (depending on the size of the original data and the number of rotational steps) which means additional training time will be required. To avoid any unnecessary training run any duplicated stress-strain pairs in the expanded data must be removed. If the stress or strain components in one the principal direction become zero or have the same value in both directions then in this case some parts of the data become duplicated and have to be eliminated.

To evaluate the potential of using EPR to derive models describing the material behaviour using the above procedure, a feasibility study is performed using synthetically generated data for both linear and non-linear material behaviour.

4.2.1 EPR-based model of a material with linear behaviour

In order to generate the required data for this section, a hypothetical test is conducted as following. The data is obtained from a finite element simulation of this hypothetical test. Figure 4.2 shows a sample of a material tested under a tensile load T along the axis 2 together with its deformed shape. The test is carried out under plane stress conditions. The original shape of the sample is drawn in dashed line. The size of the sample is $10\ \text{cm} \times 5\ \text{cm}$. The sample is made of a linear elastic material with a Young's modulus of $E = 500$ Pa and a Poisson's ratio of $\nu = 0.3$.

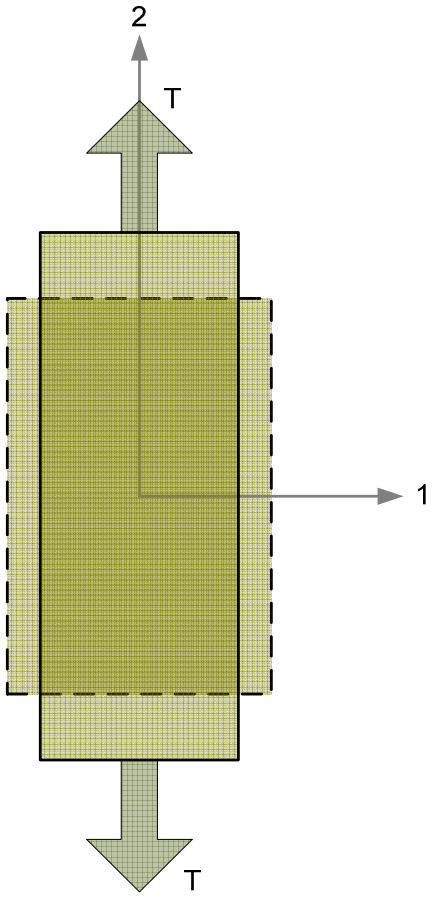

Figure 4.2: A plane stress sample of a material under tension along axis 2

Although the sample is only loaded along axis 2, the deformations are measured along both axes 1 and 2 (note that stress in direction 1 is zero). The sample is loaded up to 20 Pa. Figure 4.3 shows the stress-strain curve along axis 2 obtained from this test. The data from this figure together with the strains measured in axis 1 were employed to extend the data using the procedure described in the previous section.

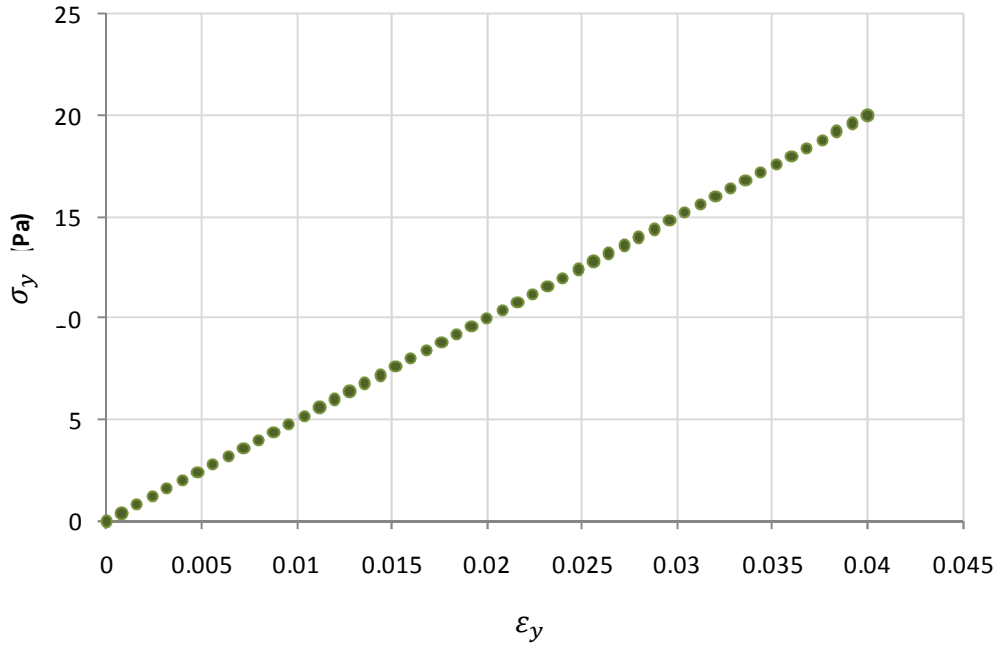

Figure 4.3: Linear stress-strain relationship used to expand data

4.2.1.1 Input and output parameters and data preparation

50 stress-strain pairs were obtained from the hypothetical test described above. The stresses and strains in directions 1 and 2 (which contain zero shear components) were exchanged assuming that the sample in the test is isotropic. This doubled the data (100 pairs); however the shear components of this data are still zero. For that reason, transformation of each stress-strain pair was carried out by an angular step $\Delta\theta$ with θ varying from -45° to 45°. This allowed the generation of all the possible combinations of stresses and strains with non-zero shear components. The transformation was performed in 30 steps (i.e. $\Delta\theta = 3^{\circ}$) from -45° to 45° and therefore the resultant data set of 3000 stress-strain pairs was obtained. These include sets with non-zero shear components. For an efficient training, duplicated data were removed in the expanded data set.

Since the model studied here represents a two dimensional plane stress case, only three components of stresses and three components of strains (out of plane strains are also zero) exist in the model. These are $(\sigma_x, \sigma_y, \tau_{zy})$ for stresses and $(\varepsilon_x, \varepsilon_y, \gamma_{xy})$ for strains. Three EPR models were developed each corresponding to one of the stress components. The inputs and outputs of the three models were:

Model 1 $input: \varepsilon_x, \varepsilon_y, \gamma_{xy}$
$output: \sigma_x$

Model 2 $input: \varepsilon_x, \varepsilon_y, \gamma_{xy}$
$output: \sigma_y$

Model 3 $input: \varepsilon_x, \varepsilon_y, \gamma_{xy}$
$output: \tau_{xy}$

The target is to find a constitutive relationship in the general form of equation 3.1, where the matrix of inputs, **X**, for each model is:

$$\mathbf{X} = \begin{bmatrix} \varepsilon_x^1 & \varepsilon_y^1 & \gamma_{xy}^1 \\ \varepsilon_x^2 & \varepsilon_y^2 & \gamma_{xy}^2 \\ \varepsilon_x^3 & \varepsilon_y^3 & \gamma_{xy}^3 \\ \cdots & \cdots & \cdots \\ \varepsilon_x^i & \varepsilon_y^i & \gamma_{xy}^i \end{bmatrix} \qquad 4.3$$

where superscript i represents the i^{th} row of the data. It should be noted that unlike ANN-based constitutive models (Hashash et al., 2004; Jung & Ghaboussi, 2006 a), in EPR the values of inputs and outputs do not need any normalisation or calibration before or after training and therefore these values can be used as they are. Before training the EPR, the data were randomly shuffled in order to make sure that the obtained models had no bias on a particular part of the data.

4.2.1.2 Training EPR-based constitutive models

The database was divided into two independent sets. One set was used for training to obtain the models and the other one for validation to verify the performance of the obtained constitutive models. Although some researchers have studied the extrapolation capabilities of models developed by EPR (Doglioni et al., 2008; Laucelli & Giustolisi, 2011); however like any other data mining technique EPR does not demonstrate a good performance for data beyond the training range (i.e. extrapolation). It was therefore decided to choose the verification data in the range of the training data to avoid extrapolation as much as possible. Usually around 80% of data is used for training the model and the other 20% is used for validation. Therefore from the 1500 cases, 300 were used for testing the obtained models.

4.2.1.3 EPR procedure and the obtained models

Before starting the EPR process, some of the EPR parameters must be adjusted to control the obtained models. These parameters can control the optimisation techniques (i.e. single-objective or multi-objective), number of terms of the mathematical expressions, range of exponents, EPR structures and the type of the functions used to construct the EPR models. Since in this example the behaviour of material is known a priori (i.e. linear behaviour); therefore no function will be chosen. Also for the same reason the exponents can be limited to $[0 \quad 1]$. As it was mentioned in chapter 3 it is advised to include the value zero, which helps in discarding those variables or inputs that are not useful for models (Doglioni et al., 2008). The EPR type has no effect on the output model if no EPR function or an EPR type that involves a function is chosen. It should be mentioned that most of the times the behaviour of model is not known a priori and therefore different combinations of functions and exponents must be tried to get the best results of EPR. The maximum possible number of terms in a polynomial with above exponents is 8 terms including a constant coefficient and therefore the number of terms is set to 8. Finally as it was discussed in chapter 3, multi-objective strategy of EPR has resolved some of the drawbacks of single-objective EPR including its slow performance. For this reason the multi-objective EPR is used to construct the EPR models. Since the aim of this study is to involve all the components of the strains in the evolved EPR equations, therefore minimising total number of inputs (% of **X**) is not selected but instead to get an efficient equation, minimising the number of constant values (a_j) is chosen as the other objective of EPR. After feeding the training and testing data and setting all the parameters, the EPR can be started. The results of EPR including the obtained equations, and coefficient of determination (CoD) values for training and validation sets are presented in the following equations and Table 4.1.

It should be noted that the coefficients and constants are only valid for the dimension used for each variable and respective equations. For the equations developed in this thesis the units of parameters are provided as footnote on the same page as equation.

Model 1

$$\sigma_x = 5.081 \quad (4.4)$$

$$\sigma_x = 425.0854\varepsilon_x + 2.0669 \quad (4.5)$$

$$\sigma_x = 549.4505\varepsilon_x + 164.8352\varepsilon_y - 5.1338 \times 10^{-12} \quad (4.6)$$

Model 2

$$\sigma_y = 5.119 \quad (4.7)$$

$$\sigma_y = 425.5103\varepsilon_y + 2.0598 \quad (4.8)$$

$$\sigma_y = 164.8352\varepsilon_x + 549.4505\varepsilon_y - 1.2134 \times 10^{-11} \quad (4.9)$$

Model 3

$$\tau_{xy} = -0.0009978 \quad (4.10)$$

$$\tau_{xy} = 192.3077\gamma_{xy} + 3.2319 \times 10^{-12} \quad (4.11)$$

Table 4.1: Summary of results obtained for EPR based models for material with linear behaviour

Equation No.	Model No.	CoD for training (%)	CoD for validation (%)
4.4	Model 1	0.07	5.3
4.5		93.87	86.96
4.6		100	100
4.7	Model 2	0.07	6.74
4.8		93.90	77.97
4.9		100	100
4.10	Model 3	0.07	-
4.11		100	100

* Units: σ (N/m^2)

It can be seen from the obtained equations and Table 4.1 that for each model an equation with 100% accuracy (i.e. CoD = 100%) is achieved. It is also seen that despite the fact that we have fed EPR with three inputs (i.e. $\varepsilon_x, \varepsilon_y, \gamma_{xy}$) in all three models, EPR has only taken the inputs that have greater effects on the models. This is more interesting when we compare them with the equations that we get from classic theory of elasticity.

Equations 4.12, 4.13, and 4.14 describe the relationship between the strains and stresses for an elastic material (Timoshenko & Goodier, 1970).

$$\varepsilon_x = \frac{1}{E}\left[\sigma_x - \nu\left(\sigma_y + \sigma_z\right)\right] \tag{4.12}$$

$$\varepsilon_y = \frac{1}{E}\left[\sigma_y - \nu(\sigma_x + \sigma_z)\right] \tag{4.13}$$

$$\gamma_{xy} = \frac{1}{G}\tau_{xy} \tag{4.14}$$

In these equations E represents elastic modulus, ν is the Poisson's ratio and G is shear modulus which is related to elastic modulus and Poisson's ratio through following equation (Timoshenko & Goodier, 1970):

$$G = \frac{E}{2(1+\nu)} \tag{4.15}$$

If we substitute the values of E and ν from the hypothetical test in equations 4.12 to 4.15 and re-arrange them, then the following equations are obtained:

$$\sigma_x = 549.45\varepsilon_x + 164.83\varepsilon_y \tag{4.16}$$

$$\sigma_y = 164.83\varepsilon_x + 549.45\varepsilon_y \tag{4.17}$$

$$\tau_{xy} = 192.31\gamma_{xy} \tag{4.18}$$

These equations are in an excellent agreement with those obtained from EPR (i.e. equations 4.6, 4.9, and 4.11 respectively). This shows that the EPR models have captured the relationships between stresses and strains with a superior accuracy. This example was deliberately kept simple in order to illustrate the capability of EPR in

modelling material behaviour. In the next example a material with a non-linear behaviour will be used to examine the capabilities of EPR.

4.2.2 EPR-based model of a material with non-linear behaviour

A sample of a material with a non-linear behaviour is utilised here to perform another hypothetical test. The data from FE simulation will be used to illustrate the potential of EPR in modelling of material with nonlinear behaviour.

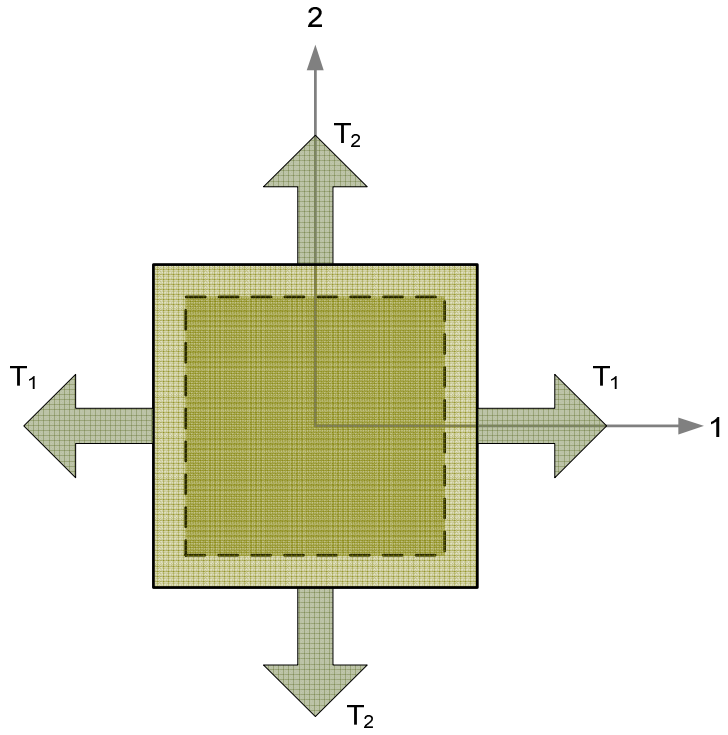

Figure 4.4: A plane stress sample of a material under a biaxial tension loading

Figure 4.4 shows the sample under a biaxial tension loading. The sample corresponds to a plane stress geometrical condition. In this test a value of 15% tensile strain is applied to the sample along axis 2 and 10% tensile strain is applied along axis 1 at the same time. Figure 4.5 and Figure 4.6 show the response of this structure under the loading along axes 1 and 2 respectively. The data from these two curves were extended using the procedure described in previous sections in order to generate the required data for training the EPR model. The rotational steps, number of the data points, number of models and the inputs and outputs are same as the previous example.

In the initial setting of EPR, the exponents were limited to [0 1 2] and no function was selected for EPR. For simplicity the number of terms was limited to 10. The remaining settings of EPR were kept identical to the previous example.

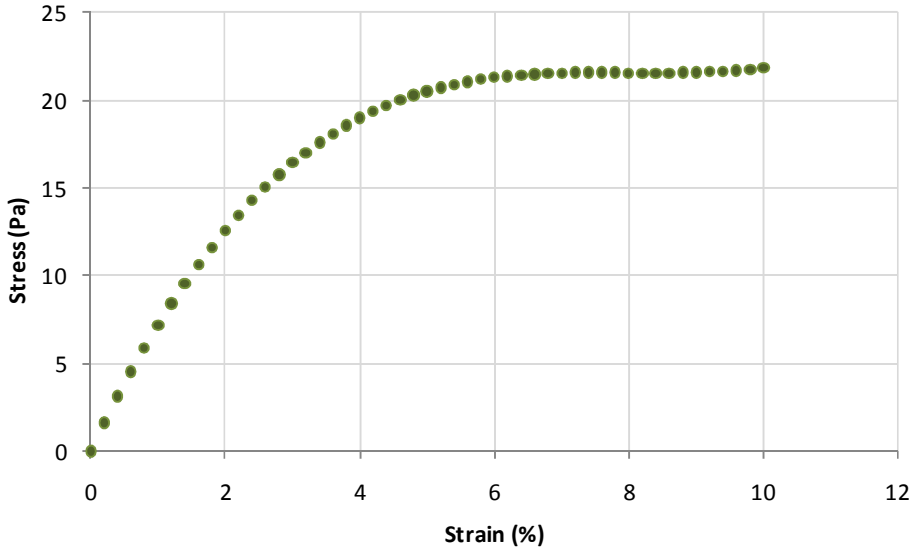

Figure 4.5: Stress-strain response of the structure along axis 1

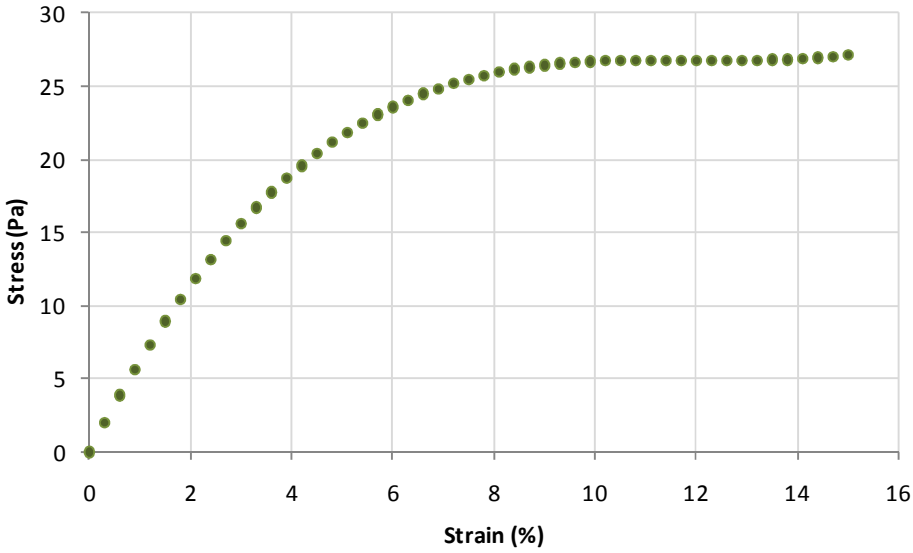

Figure 4.6: Stress-strain response of the structure along axis 2

The results of training of EPR for all three models are presented in the following equations. It can be seen that a wide range of equations from short to long is returned by EPR each having a different CoD value. In all three models, the equations are sorted in order of their CoD values for validation data. The CoD values of each equation for training and validation data sets are presented in

Table **4.2**. In the third model (τ_{xy}), the 7th, 8th, 9th and 10th equations were identical and therefore only one of them is shown.

Model 1 (σ_x)

[*]

$$\sigma_x = 19.70 \quad (4.19)$$

$$\sigma_x = 149.98\varepsilon_x + 10.10 \quad (4.20)$$

$$\sigma_x = -12339.03\varepsilon_x^2\varepsilon_y + 321.29\varepsilon_x + 5.30 \quad (4.21)$$

$$\sigma_x = -1680.01\varepsilon_x^2 - 850.20\varepsilon_x\varepsilon_y + 474.55\varepsilon_x + 3.06 \quad (4.22)$$

$$\sigma_x = 96948.66\varepsilon_x^2\varepsilon_y^2 - 5327.67\varepsilon_x\varepsilon_y + 404.95\varepsilon_x + 259.16\varepsilon_y + 0.57 \quad (4.23)$$

$$\sigma_x = 24133.50\varepsilon_x^2\varepsilon_y - 4455.67\varepsilon_x\varepsilon_y - 2768.33\varepsilon_x^2 + 584.59\varepsilon_x + 138.97\varepsilon_y + 0.09 \quad (4.24)$$

$$\sigma_x = 21341.35\varepsilon_x^2\varepsilon_y + 3673.06\varepsilon_y^2\varepsilon_x - 2321.70\varepsilon_x^2 - 5079.49\varepsilon_x\varepsilon_y + 576.05\varepsilon_x + 154.9\varepsilon_y + 0.02 \quad (4.25)$$

$$\sigma_x = 19240.12\varepsilon_x^2\varepsilon_y + 5875.12\varepsilon_x\varepsilon_y^2 - 4495.79\varepsilon_x^2 - 2535.63\varepsilon_y^2 - 2419\gamma_{xy}^2 + 562.29\varepsilon_x + 169.70\varepsilon_y \quad (4.26)$$

$$\sigma_x = 19888.41\varepsilon_x^2\varepsilon_y + 5755.47\varepsilon_x\varepsilon_y^2 - 5676.00\varepsilon_x\gamma_{xy}^2 - 4544.66\varepsilon_x^2 - 2542.35\varepsilon_y^2 - 1848.63\gamma_{xy}^2 + 564.09\varepsilon_x + 168.41\varepsilon_y \quad (4.27)$$

$$\sigma_x = 19780.05\varepsilon_x^2\varepsilon_y + 5934.19\varepsilon_x\varepsilon_y^2 - 4945.01\varepsilon_x\gamma_{xy}^2 - 1483.55\varepsilon_y\gamma_{xy}^2 - 9837.68\varepsilon_x\varepsilon_y + 2956.03\gamma_{xy}^2 + 563.52\varepsilon_x + 169.06\varepsilon_y \quad (4.28)$$

[*] Units: σ (N/m^2)

Model 2 (σ_y)

[*]

$$\sigma_y = 19.61 \tag{4.29}$$

$$\sigma_y = 150.50\varepsilon_y + 10.05 \tag{4.30}$$

$$\sigma_y = -12366.03\varepsilon_x\varepsilon_y^2 + 322.10\varepsilon_y + 5.30 \tag{4.31}$$

$$\sigma_y = -1686.65\varepsilon_y^2 - 858.05\varepsilon_x\varepsilon_y + 476.08\varepsilon_y + 3.05 \tag{4.32}$$

$$\sigma_y = 96555.76\varepsilon_x^2\varepsilon_y^2 - 5304.64\varepsilon_x\varepsilon_y + 258.68\varepsilon_x + 403.70\varepsilon_y + 0.56 \tag{4.33}$$

$$\sigma_y = 24220.93\varepsilon_x\varepsilon_y^2 - 4463.08\varepsilon_x\varepsilon_y - 2773.55\varepsilon_y^2 + 138.99\varepsilon_x + 584.97\varepsilon_y + 0.09 \tag{4.34}$$

$$\sigma_y = 21393.01\varepsilon_x\varepsilon_y^2 + 3656.64\varepsilon_x^2\varepsilon_y - 5081.24\varepsilon_x\varepsilon_y - 2325.47\varepsilon_y^2 + 154.99\varepsilon_x + 576.1718\varepsilon_y + 0.02 \tag{4.35}$$

$$\sigma_y = 5847.65\varepsilon_x^2\varepsilon_y + 19266.97\varepsilon_x\varepsilon_y^2 - 2534.24\varepsilon_x^2 - 4496.89\varepsilon_y^2 - 2417.57\gamma_{xy}^2 + 169.72\varepsilon_x + 562.25\varepsilon_y \tag{4.36}$$

$$\sigma_y = 5752.44\varepsilon_x^2\varepsilon_y + 19892.15\varepsilon_x\varepsilon_y^2 - 5679.26\varepsilon_y\gamma_{xy}^2 - 2542.30\varepsilon_x^2 - 4544.92\varepsilon_y^2 - 1849.22\gamma_{xy}^2 + 168.42\varepsilon_x + 564.09\varepsilon_y \tag{4.37}$$

$$\sigma_y = 5934.19\varepsilon_x^2\varepsilon_y + 19780.05\varepsilon_x\varepsilon_y^2 - 1483.55\varepsilon_x\gamma_{xy}^2 - 4945.01\varepsilon_y\gamma_{xy}^2 - 5533.73\varepsilon_x\varepsilon_y - 1986.44\varepsilon_y^2 + 886.82\gamma_{xy}^2 + 169.06\varepsilon_x + 563.52\varepsilon_y \tag{4.38}$$

[*] Units: σ (N/m^2)

Model 3 (τ_{xy})

$$\tau_{xy} = -0.14 \quad (4.39)$$

$$\tau_{xy} = 72.64\gamma_{xy} - 0.02 \quad (4.40)$$

$$\tau_{xy} = -791.75\varepsilon_x\gamma_{xy} + 147.64\gamma_{xy} - 0.11 \quad (4.41)$$

$$\tau_{xy} = 7341.59\varepsilon_x^2\gamma_{xy} - 2078.58\varepsilon_x\gamma_{xy} + 198.56\gamma_{xy} - 0.10 \quad (4.42)$$

$$\tau_{xy} = 18899.81\varepsilon_x\varepsilon_y^2\gamma_{xy} + 2142.83\varepsilon_x^2\gamma_{xy} - 954.47\varepsilon_x\gamma_{xy} - 703.60\varepsilon_y\gamma_{xy} + 190.17\gamma_{xy} \quad (4.43)$$

$$\tau_{xy} = 6557.03\varepsilon_x\varepsilon_y\gamma_{xy} - 978.10\varepsilon_x\gamma_{xy} - 982.61\varepsilon_y\gamma_{xy} + 196.26\gamma_{xy} \quad (4.44)$$

$$\tau_{xy} = 1661.50\varepsilon_x^2\gamma_{xy} + 1661.50\varepsilon_y^2\gamma_{xy} + 3323\varepsilon_x\varepsilon_y\gamma_{xy} - 993.22\varepsilon_x\gamma_{xy} - 993.22\varepsilon_y\gamma_{xy} + 197.23\gamma_{xy} \quad (4.45)$$

Table 4.2: CoD values of training and validation data set for all equations developed for all three models

Model 1			Model 2			Model 3		
Eq. No	CoD (%)	CoD_v (%)	Eq. No	CoD (%)	CoD_v (%)	Eq. No	CoD (%)	CoD_v (%)
4.19	0.07	5.97	4.29	0.07	7.37	4.39	0.07	-
4.20	74.96	72.77	4.30	74.96	72.34	4.40	91.76	0.97
4.21	94.14	93.15	4.31	94.12	94.43	4.41	99.05	81.99
4.22	97.56	97.16	4.32	97.54	97.56	4.42	99.76	96.72
4.23	99.25	99.44	4.33	99.25	99.54	4.43	100.00	99.96
4.24	99.96	99.97	4.34	99.96	99.98	4.44	99.99	99.98
4.25	99.99	99.99	4.35	99.99	100.00	4.45	100.00	100.00
4.26	99.99	100.00	4.36	99.99	100.00	4.45	100.00	100.00
4.27	100.00	100.00	4.37	100.00	100.00	4.45	100.00	100.00
4.28	100.00	100.00	4.38	100.00	100.00	4.45	100.00	100.00

In order to assess the quality of the prediction provided by EPR equations, the stress-strain relationship predicted by EPR equations for model 1 along axis 1 versus the actual data is presented in Figure 4.7. In the first graph the predictions provided by the first 5 models are plotted together with actual data. In this graph, it can be seen that as the evolutionary steps are increasing the accuracy of the models are getting better. In the second graph where the second 5 EPR models are shown, it is very difficult (if not impossible) to distinguish the EPR models from the actual data as they all have provided excellent predictions. This makes it difficult to choose the most suitable EPR model among them.

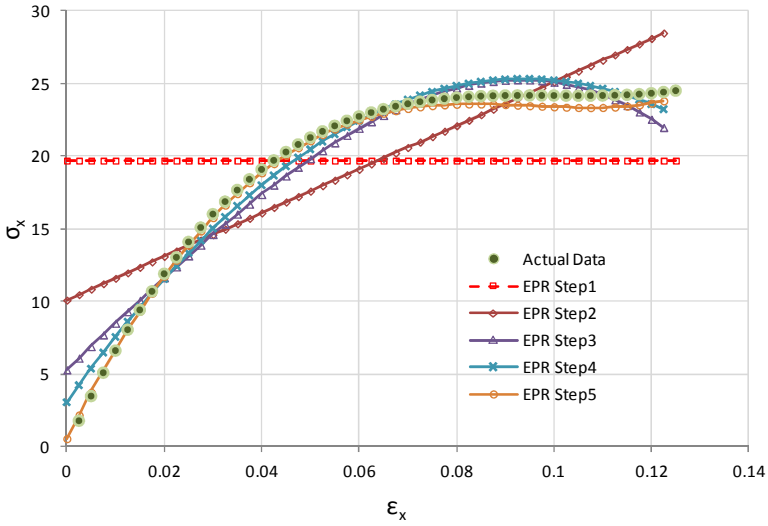

(a)

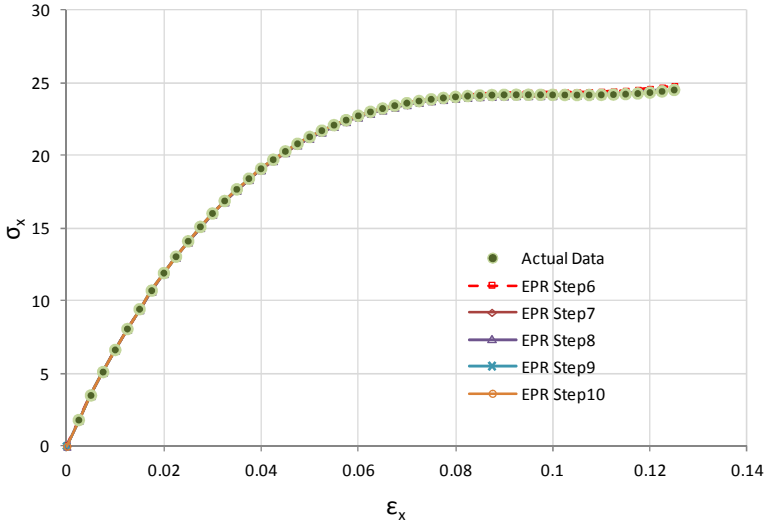

(b)

Figure 4.7: Comparison of EPR equations and actual data for model 1 (σ_x)

(a) Eq. 1-5 (b) Eq. 6-10

The model selection from results of EPR analysis requires some subjective judgment and may be often biased by analyst's experience. As it can be seen the first four equations returned by EPR for all three models have presented a poor CoD values and therefore can be simply discarded. In order to select the best model among the remaining models, the performance of the equations in a finite element model will be observed. Based on the prediction capability of the EPR models in the finite element model, the best EPR model representing the material behaviour will be chosen. The incorporation of the developed EPR models in finite element and their performance will be discussed in the next chapter.

4.3 Incremental stress-strain strategy for material modelling

4.3.1 Input and output parameters

Another strategy to train EPR-based material models includes an input set providing the EPR with the information relating to the current state units (current stresses and current strains) and an output that predicts the next state of stress and/or strain relevant to an input strain or stress increment. This is a typical scheme to train most of the neural network based models (Ghaboussi et al., 1998). A similar scheme is utilised in this section and different examples are provided to demonstrate the potential of this strategy for training EPR-based material models.

In this section invariants of stresses and strains are used unlike the previous section where we used their values in the spatial directions. This means that mean stress $\acute{p}^i$, deviator stress q^i, volumetric strain ε_v^i, and distortional strain ε_q^i are used as the input parameters representing the current state of stresses and strains in a load increment i, and deviator stress q^{i+1}, and/or volumetric strain ε_v^{i+1} corresponding to the input incremental distortional strain $\Delta\varepsilon_q^i$ are used as the output parameters. The definition of the stress and strain invariants is as follow (Muir Wood, 1990):

$$\acute{p} = \frac{\acute{\sigma}_x + \acute{\sigma}_y + \acute{\sigma}_z}{3} \quad 4.46$$

$$q = \left[\frac{\left(\acute{\sigma}_y - \acute{\sigma}_z\right)^2 - (\acute{\sigma}_z - \acute{\sigma}_x)^2 - \left(\acute{\sigma}_x - \acute{\sigma}_y\right)^2}{2} + 3(\tau_{yz}^2 + \tau_{zx}^2 + \tau_{xy}^2)\right]^{1/2} \quad 4.47$$

$$\varepsilon_v = \varepsilon_x + \varepsilon_y + \varepsilon_z \quad 4.48$$

$$\varepsilon_q = \frac{1}{3}\left\{2\left[\left(\varepsilon_y - \varepsilon_z\right)^2 + (\varepsilon_z - \varepsilon_x)^2 + \left(\varepsilon_y - \varepsilon_z\right)^2\right] + 3\left(\gamma_{yz}^2 + \gamma_{zx}^2 + \gamma_{xy}^2\right)\right\}^{1/2} \quad 4.49$$

4.3.2 EPR-based material model of soils under monotonic loading

To demonstrate the capability of EPR to obtain mathematical expressions describing the constitutive behaviour of soils using the incremental strategy, the results from a series of triaxial tests (Cekerevac & Laloui, 2004) are utilized in this section. The work done by Cekerevac & Laloui, (2004) contains information on both shear and volumetric behaviour of the soil samples studied which makes it a suitable collection of data for this purpose.

Triaxial apparatus is one of the most widely used experimental systems for investigating the stress-strain behaviour of soils. A schematic diagram of a triaxial apparatus is presented in Figure 4.8. In this experiment a cylindrical sample of soil is located in a cell filled with a fluid (usually water). The sample is surrounded by rubber membrane to isolate it from direct contact with the surrounding fluid. The cell fluid can be pressurised to cause the confining pressure around the sample. The sample sits in the cell between a rigid base and a rigid top cap. The quantities that are usually measured during the test are pressure in the cell fluid (the cell pressure σ_r) which provides an all-round pressure on the soil sample; the axial stress σ_a, axial strain ε_a, the volumetric strain ε_v, if drainage from the soil sample is allowed or pressure in the pore fluid u, if drainage is prevented.

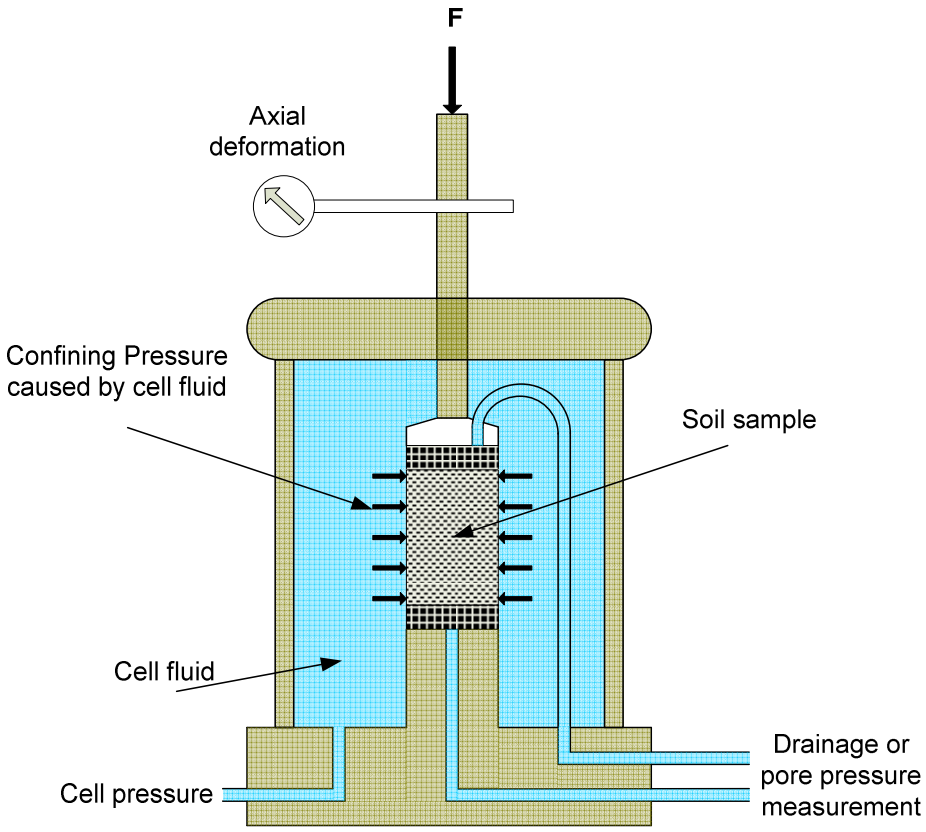

Figure 4.8: A schematic diagram of a triaxial apparatus

For triaxial loading conditions, due to the axisymmetric nature of the problem, equations 4.46 - 4.49 can be simplified as:

$$\acute{p} = \frac{\acute{\sigma}_a + 2\acute{\sigma}_r}{3} \tag{4.50}$$

$$q = \acute{\sigma}_a - \acute{\sigma}_r \tag{4.51}$$

$$\varepsilon_v = \varepsilon_a + 2\varepsilon_r \tag{4.52}$$

$$\varepsilon_q = \frac{2(\varepsilon_a - \varepsilon_r)}{3} \tag{4.53}$$

Where ε_a is axial strain, $\acute{\sigma}_a$ effective axial stress, ε_r is radial strain and $\acute{\sigma}_r$ is effective axial stress in the triaxial apparatus. Usually during a standard triaxial test a confining pressure is imposed on the sample to represent its in-situ condition in the ground. In order to identify the characteristics and different parameters of soil, a number of tests with different confining pressures are performed on samples of the same soil. The tests

conducted by Cekerevac & Laloui, (2004) were performed with similar conditions. The results of these tests are presented in the following figures.

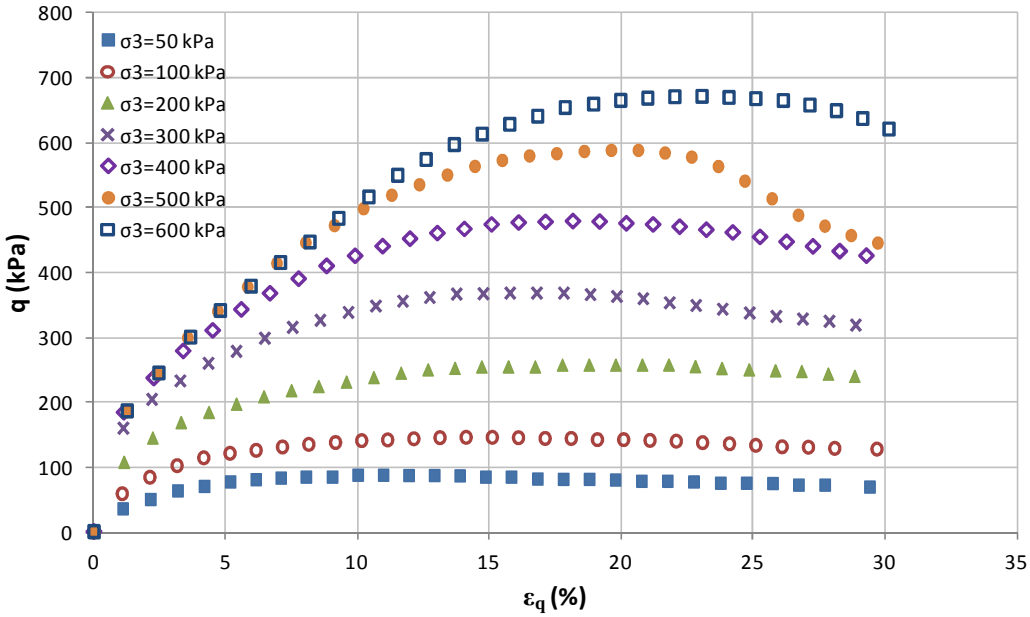

(a) Deviator stress vs. shear strain

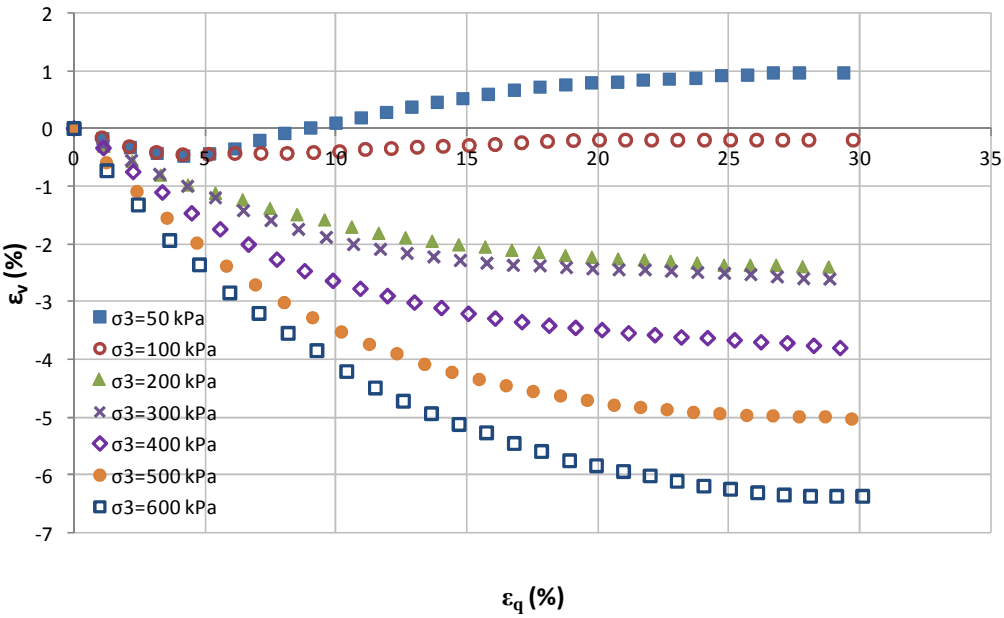

(b) Volumetric strain vs. shear strain

Figure 4.9: Drained triaxial test results (Cekerevac & Laloui, 2004)

The results from 5 tests conducted at confining pressures 50, 100, 300, 400, 600 kPa were used for training of the EPR models while those for the sixth and seventh tests at confining pressures of 200, and 500 kPa were used for validation of the trained models.

The maximum number of terms was set to 15 for the first model (deviator stress) and 5 for the 2nd model (volumetric strain) which was found to be adequate after a number of trial and error runs; the exponents were limited to $[0,\ 1,\ 2,\ 3]$. No function was chosen for EPR equations. After training, the best EPR models for both deviator stress and volumetric strain representing the behaviour of soil were selected. These equations are:

$$\begin{aligned} q^{i+1} = {} & 4.9186\varepsilon_q - 0.2521\varepsilon_q^2 + 3.7739\times10^{-3}\varepsilon_q^3 - 4.9147\varepsilon_v^i \\ & + 0.2220q^i - 0.1169q^i\Delta\varepsilon_q + 1.4363\times10^{-3}\left(q^i\right)^2 \\ & - 1.1096\times10^{-6}\left(q^i\right)^3 + 0.4485\acute{p} + 0.1355\acute{p}\Delta\varepsilon_q \\ & - 2.0212\times10^{-3}\acute{p}\varepsilon_q\Delta\varepsilon_q - 5.1741\times10^{-4}\acute{p}^2 \\ & + 3.6161\times10^{-10}\acute{p}^3q^i \end{aligned} \quad [*] \qquad 4.54$$

$$\begin{aligned} \varepsilon_v^{i+1} = {} & \varepsilon_v^i + 1.1251\times10^{-3}q\Delta\varepsilon_q - 1.0948\times10^{-3}\,\acute{p}\Delta\varepsilon_q + 1.7425 \\ & \times10^{-14}p^2q\,\varepsilon_q^3\Delta\varepsilon_q \end{aligned} \qquad 4.55$$

Figure 4.10 shows the stress-strain curves predicted by the EPR model, (equations 4.54 and 4.55) against those expected and used as training data. From these figures it is clearly seen that, the EPR models were able to capture the non-linear stress-strain relationship for the soil with very good accuracy.

The generalisation capability of the EPR models is shown in Figure 4.11. The data from the tests conducted at the confining pressures of 200 and 500 kPa (which did not form a part of the training data) were used to test the trained EPR models. The predicted output values of the EPR models are compared with experimentally measured values in Figure 4.11. Excellent agreement is observed between the model results and the laboratory experimental data which demonstrates excellent capability of the EPR-based material models in generalising the constitutive relationship for unseen cases.

[*] Units: $\acute{p}, q\ (kN/m^2)$

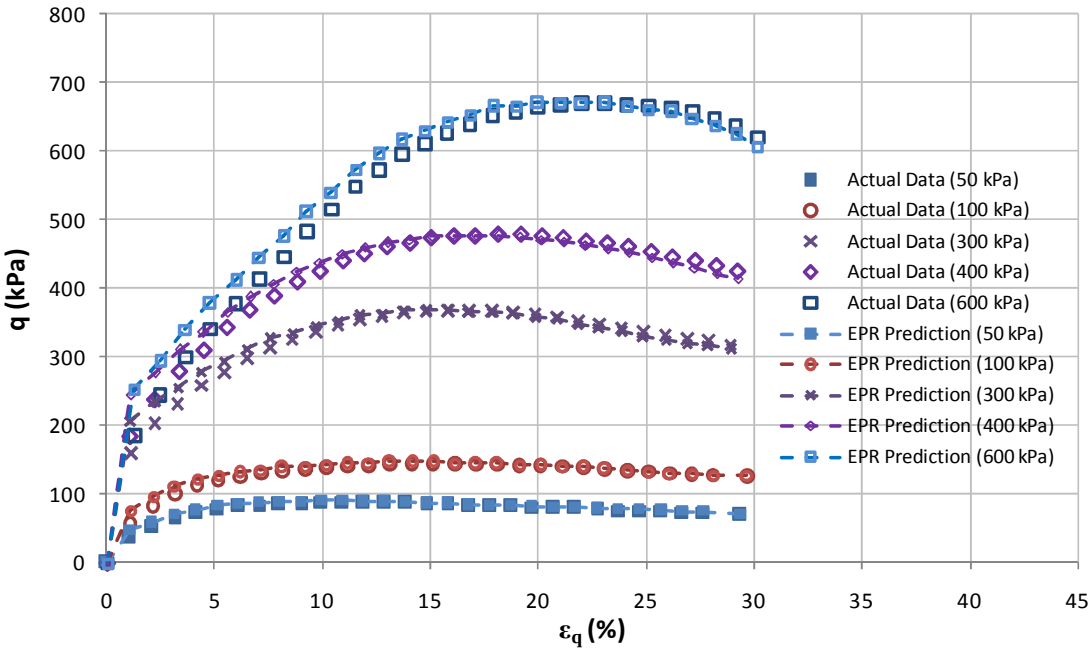

(a) Deviator stress vs. shear strain

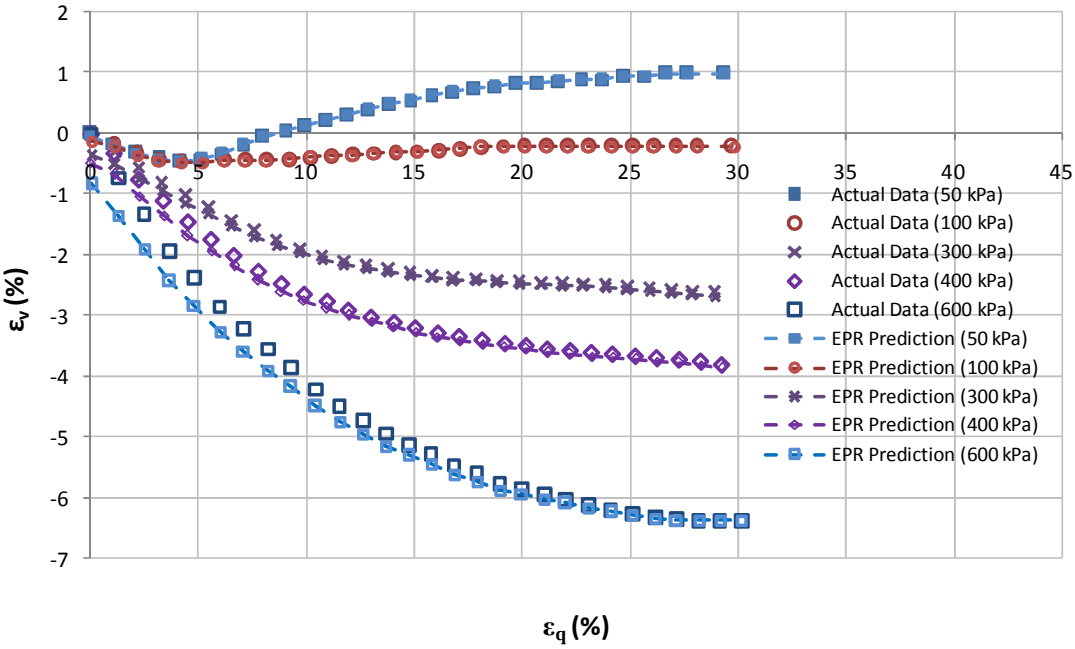

(b) Volumetric strain vs. shear strain

Figure 4.10: Results of training of the EPR

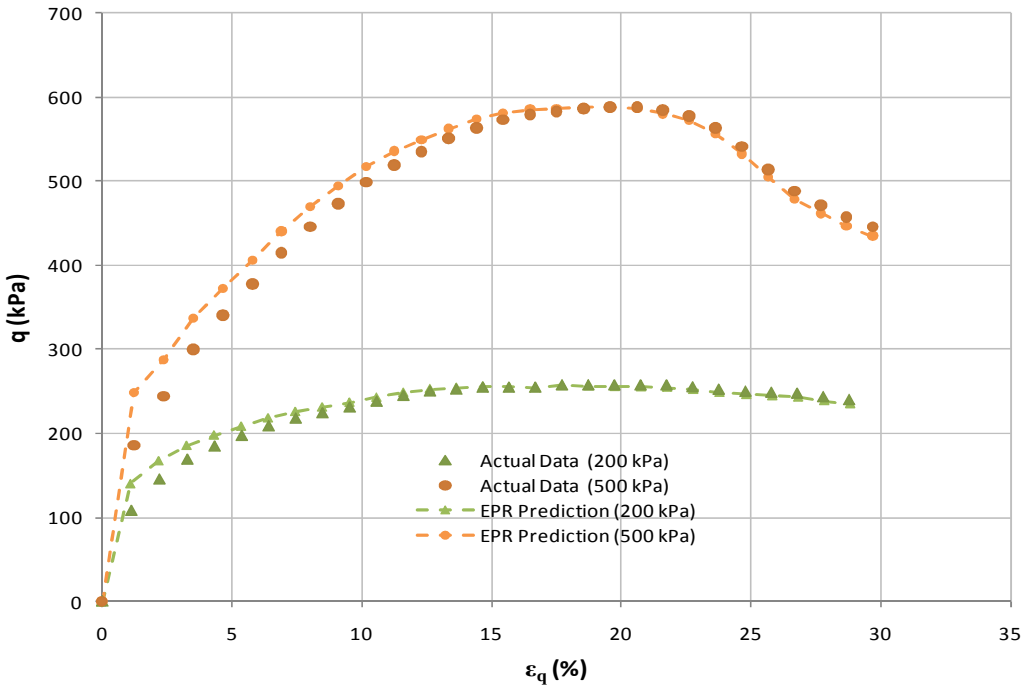

(a) Deviator stress vs. shear strain

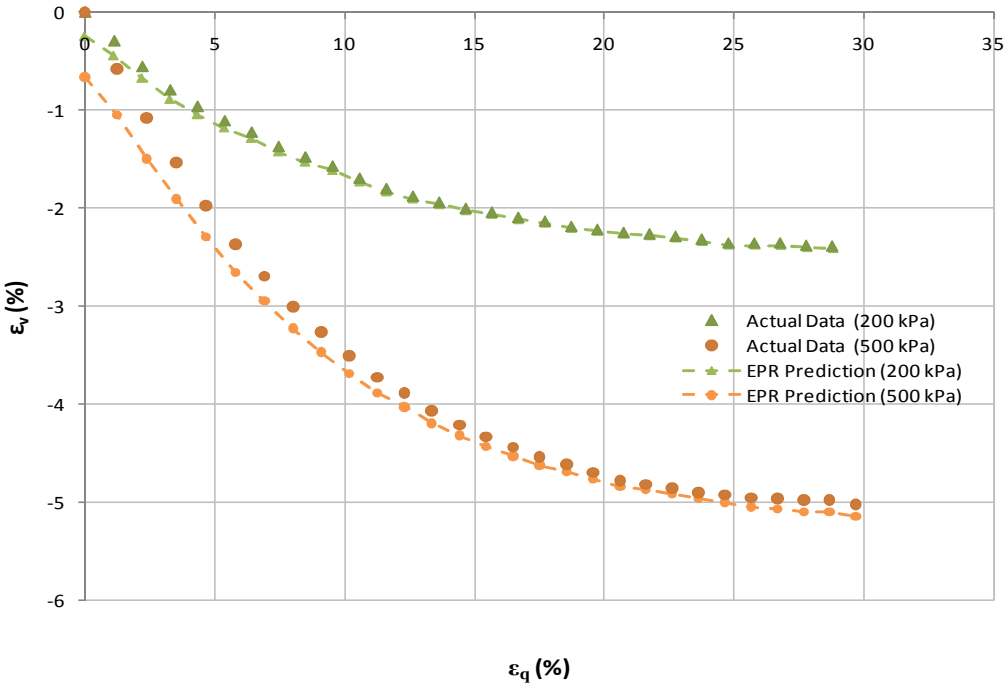

(b) Volumetric strain vs. shear strain

Figure 4.11: Results of validation of the EPR

4.3.3 Incremental (point by point) prediction of the entire stress paths

In addition to the validation that was presented in the previous section, the EPR models (equations 4.54 and 4.55) are used to predict the entire stress paths incrementally, point by point, in the $q:\varepsilon_q$ and $\varepsilon_v:\varepsilon_q$ spaces. This is used to evaluate the capability of the incremental EPR models to predict the behaviour of the soil during the entire stress paths. Figure 4.12 illustrates the procedure followed for updating the input parameters and building the entire stress path for the shearing stage of a triaxial test.

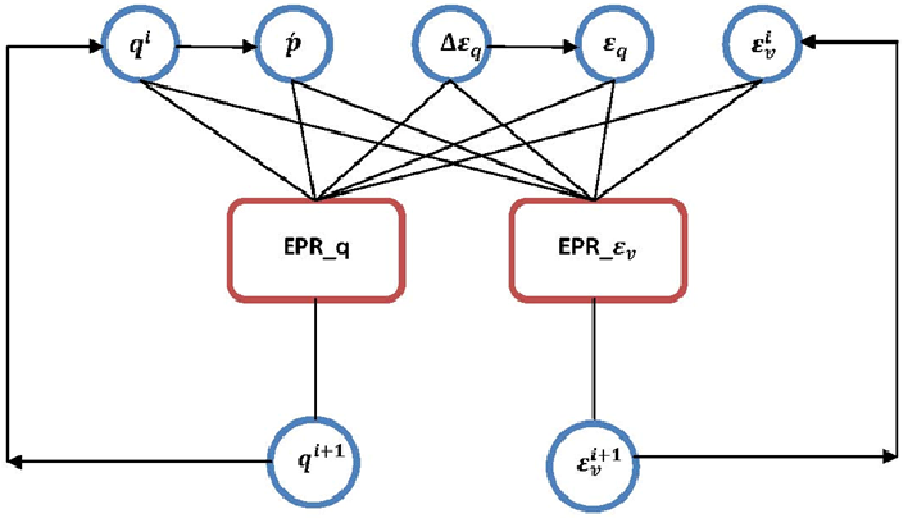

Figure 4.12: Procedure followed for updating the input parameters and building the entire stress path for a shearing stage of a triaxial test

At the start of the shearing stage in a conventional triaxial experiment, the values of all parameters are known. For example in a test on a sample of a saturated soil, the values of effective mean stress $\acute{p}^i$, deviator stress q^i, shear strain ε_q^i, and volumetric strain ε_v^i, are known from values of applied cell pressure, back pressure and volume change at the end of the previous stage (e.g., at the start of shearing stage $\varepsilon_q^0 = 0, \varepsilon_v^0 = 0$, and $q^0 = 0$). Then for a given increment of shear strain, $\Delta\varepsilon_q$, the values of q^{i+1} and ε_v^{i+1} are calculated from the EPR models (equations 4.54 and 4.55 respectively). For the next increment, the values of $\acute{p}^i, \varepsilon_q^i, \varepsilon_v^i$, and q^i are updated as:

$$q^i = q^{i+1} \tag{4.56}$$

$$\varepsilon_v^i = \varepsilon_v^{i+1} \tag{4.57}$$

$$\acute{p}^i = \acute{p}^i + \left(\frac{q^{i+1} - q^i}{3}\right) \tag{4.58}$$

$$\varepsilon_q^i = \varepsilon_q^i + \Delta\varepsilon_q \tag{4.59}$$

In these equations the current state of shear and mean stress as well as shear and volumetric strain are updated using the next state of these parameters and the next points on the curves are predicted using the EPR models. The incremental procedure is continued until all the points on the curves are predicted. Figure 4.13 shows the comparison between two complete sets of curves predicted using the EPR models following the above incremental procedure and the experimental results. The predicted results are in good agreement with the experimental results and the facts that (i) the entire curves have been predicted point by point; (ii) the errors of prediction of the individual points are accumulated in this process, and still the EPR models are able to predict the complete stress paths with a good degree of accuracy. These are testaments to the robustness of the developed EPR framework for modelling of soils.

These figures show that the EPR has been able to capture the general trend of the nonlinear relationship of stresses and strains with a good accuracy. It also shows that the EPR model was trained sufficiently to adequately model the stress-strain behaviour of the soil.

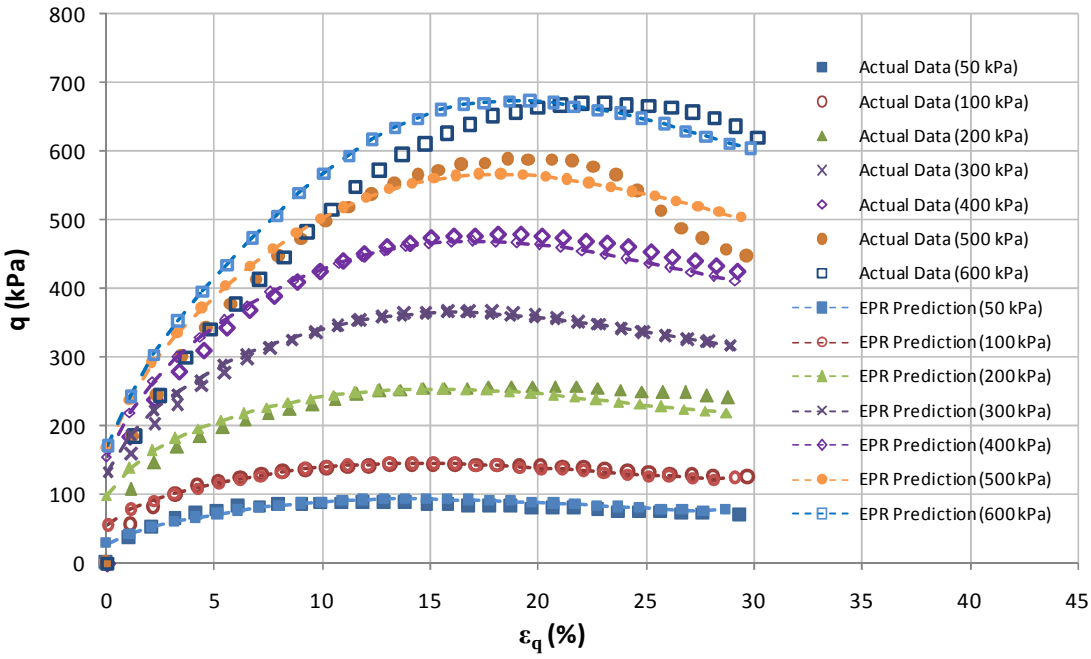

(a) $q: \varepsilon_v$

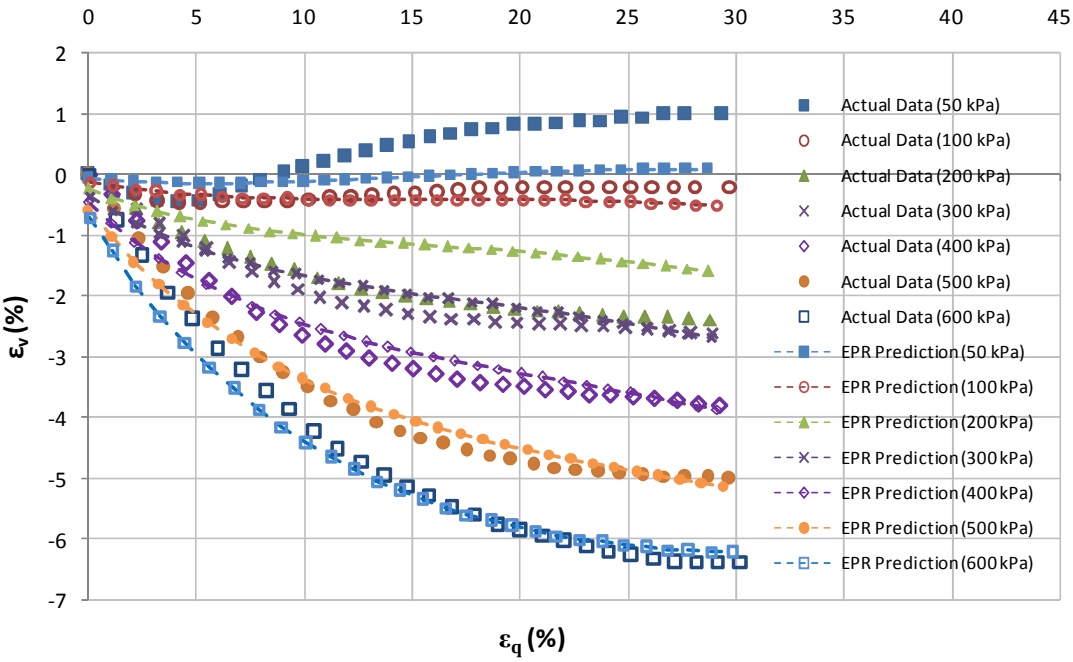

(b) $\varepsilon_v: \varepsilon_q$

Figure 4.13: Comparison of EPR incremental simulation with the actual data

4.3.4 Comparing the EPR-based models with conventional models

In this section the performance of the developed EPR-based models is compared with some of the well known existing constitutive models. Mohr-Coulomb (MC) and Modified Cam Clay (MCC) are two constitutive models that are widely used by engineers to analyse different boundary value problems in geotechnical engineering. A brief description of these two models is presented in the following.

(i) Mohr-Coulomb Model

Mohr-Coulomb elastic-perfectly plastic model is a constitutive model that describes the behaviour of soil linearly in the elastic range using two parameters E (Elastic modulus), and ν (Poisson's ratio). The failure in Mohr-Coulomb (MC) is defined by two parameters C and ϕ. The Mohr-Coulomb failure criterion states that failure of a soil mass will occur if the shear stress τ on any plane in the soil mass reaches a critical value. This can be written as:

$$\tau = \acute{C} + \acute{\sigma} \cdot \tan \acute{\phi} \qquad 4.60$$

This defines a straight line in the $\tau : \acute{\sigma}$ space as shown in the following figure.

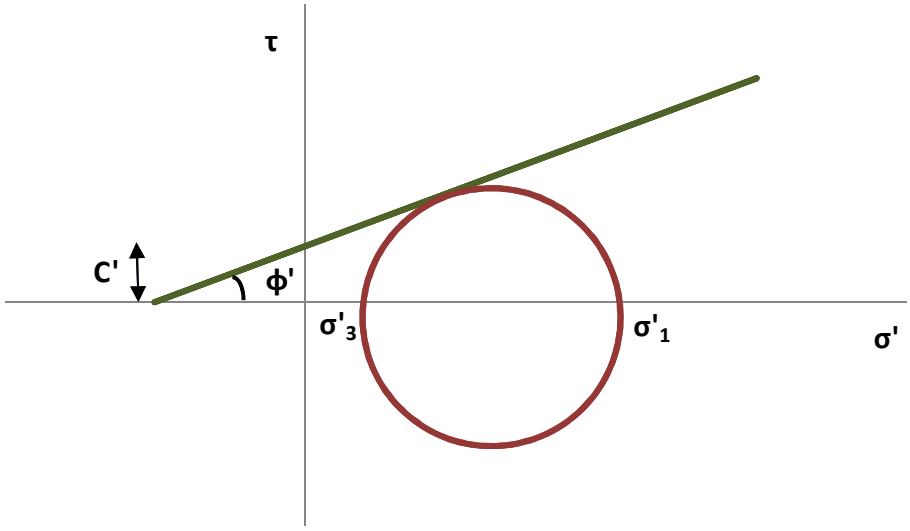

Figure 4.14: Mohr-Coulomb failure envelope

If Mohr's circle of effective stresses touches this line, then failure of the soil will occur. The intercept of this line, $\acute{C}$, is called cohesion intercept or apparent cohesion, and the

slope of the line corresponds to $\acute{\phi}$, friction angle. These parameters can be identified from a set of triaxial tests. Mohr-Coulomb failure can also be defined in terms of stress invariants. Equation 4.60 can be rewritten in terms of triaxial stress invariants $\acute{p}, q$ as following:

$$q = \frac{-6\sin\acute{\phi}}{3+\sin\acute{\phi}} \cdot p' + \acute{C}.\cot\acute{\phi} \qquad 4.61$$

(ii) Modified Cam Clay Model

Modified Cam Clay (MCC) is an elasto-plastic strain hardening model in which the non-linear behaviour is modelled using hardening plasticity. The MCC model assumes that the soil is fully saturated and there is a logarithmic relationship between the mean effective stress $\acute{p}$ and void ratio v (Roscoe & Burland, 1968).

A typical yield curve of MCC model in the space of $\acute{p}: q$ is illustrated in Figure 4.15. This figure shows that the yield curve has an elliptical shape in this space.

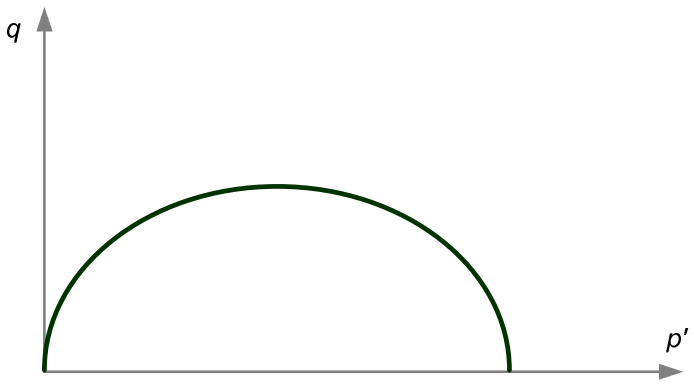

Figure 4.15: Elliptical yield curve for MCC model in p':q space

The model is based on critical state theory. This means that the MCC model assumes an ultimate condition in which plastic shearing could continue indefinitely without changes in volume or effective stresses. This condition of perfect plasticity is known as a critical state. A series of MCC yield curves which create a state boundary surface, and the critical state line are presented in $\acute{p}: q: e$ space in Figure 4.16.

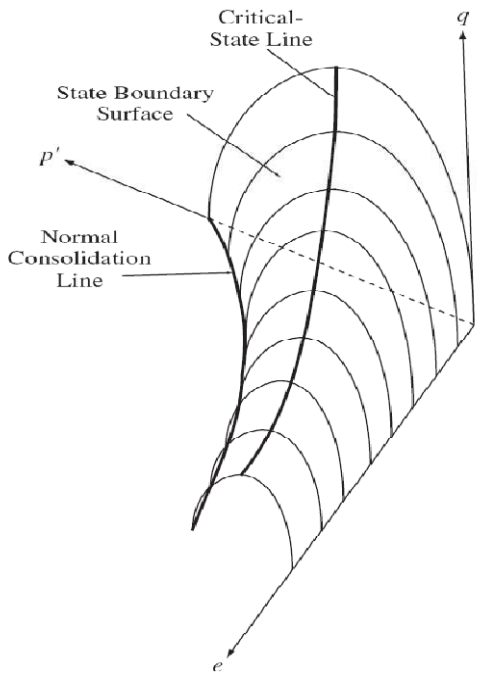

Figure 4.16: State boundary surface and critical state line of MCC model (Helwany, 2007)

The MCC model can be summarised in the following equations. The elastic stress-strain response in the matrix form describes the elastic behaviour as following:

$$\begin{bmatrix} \delta\varepsilon_v^e \\ \delta\varepsilon_q^e \end{bmatrix} = \begin{bmatrix} \kappa/\nu\acute{p} & 0 \\ 0 & 1/3G \end{bmatrix} \begin{bmatrix} \delta\acute{p} \\ \delta q \end{bmatrix} \qquad 4.62$$

and the plastic stress-strain response in the following form:

$$\begin{bmatrix} \delta\varepsilon_v^p \\ \delta\varepsilon_q^p \end{bmatrix} = \frac{(\lambda-\kappa)}{\nu\acute{p}\,(M^2+\eta^2)} \begin{bmatrix} (M^2-\eta^2) & 2\eta \\ 2\eta & 4\eta^2/(M^2-\eta^2) \end{bmatrix} \begin{bmatrix} \delta\acute{p} \\ \delta q \end{bmatrix} \qquad 4.63$$

In the above equations λ and κ are the slope of the normal consolidation line and unloading-reloading line in the $e - \ln\acute{p}$ plane respectively. M is the slope of the critical state line in the $\acute{p} - q$ plane and η is $q/\acute{p}$. It should be mentioned that M and $\acute{\phi}$ (friction angle in Mohr-Coulomb model) are related through the following equation.

$$M = \frac{6\sin\acute{\phi}}{3-\sin\acute{\phi}} \qquad 4.64$$

The parameters for both MC and MCC models can be obtained from a set of triaxial tests. The results of the triaxial test presented in section 4.3.2 are used to derive the material parameters. These parameters together with other characteristics of the soil presented in Cekerevac & Laloui (2004) are given in Table 4.3.

Table 4.3: Material parameters for Modified Cam Clay and Mohr-Coulomb models

$\acute{C}$ (kPa)	$\acute{\phi}$ (°)	M	κ	e_0	ν	γ (kN/m^3)	λ
11.7	21	0.8	0.00715	0.921	0.3	17	0.091

It should be noted that identifying the material parameters from material tests can be a difficult and subjective process. This presents another disadvantage of conventional material models in comparison to EPR-based material model where there are no material parameters to determine.

In order to compare the results of the EPR-based model with other conventional material models, the parameters in Table 4.3 are used to produce the stress-strain curves of this soil predicted by both Mohr-Coulomb and Modified Cam Clay models. These curves are plotted together with the actual (experimental) stress-strain curves obtained from the triaxial tests and those predicted by the EPR-based models (equations 4.54 and 4.55) for comparison. From seven different tests presented in Figure 4.9, three stress-strain curves corresponding to confining pressures of 50 kPa, 300 kPa, and 600 kPa are chosen for comparison. These confining pressures represent heavily over-consolidated, over-consolidated and normally consolidated samples of the soil respectively. The comparison is made between deviator stress and axial strain and the results are presented in Figure 4.17. From the figure it can be seen that the EPR-based model has been able to predict the entire stress-strain path for the triaxial test with a better accuracy in comparison with the MC and MCC models. The modified cam clay model has particularly presented a poor prediction for heavily over-consolidated sample (graph (a) of Figure 4.17). This is one of the recognised issues and drawbacks of the MCC model which has been the subject of some research and some suggestions have been offered to overcome this problem and other problems connected with this constitutive model (Gens & Potts, 1988; YU, 1998; Mita et al., 2004). However both EPR-based

model and MCC model have provided reasonably accurate results for normally consolidated samples (graph (c)).

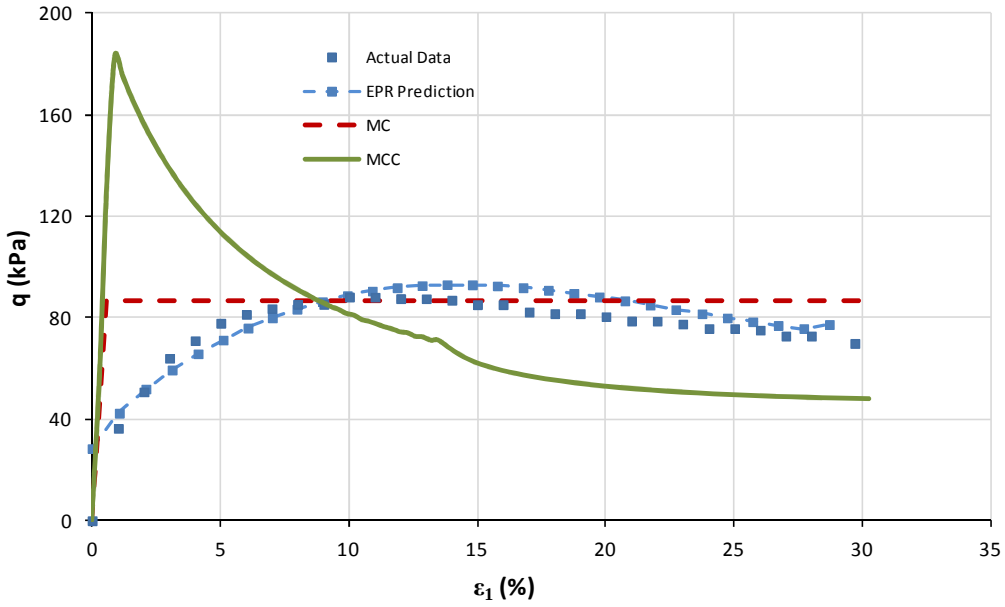

(a) $\acute{\sigma}_3 = 50\ kPa$

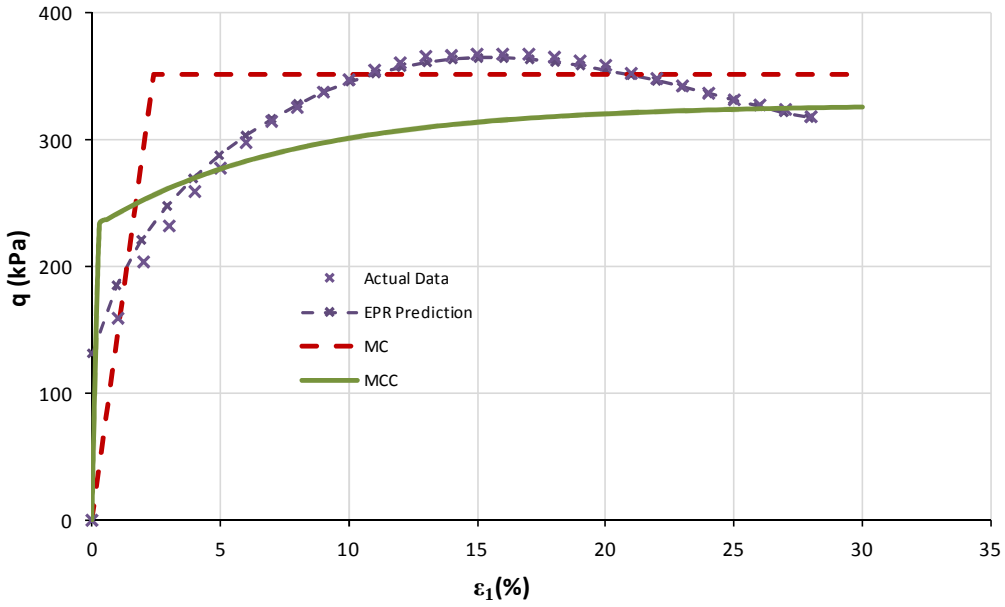

(b) $\acute{\sigma}_3 = 300\ kPa$

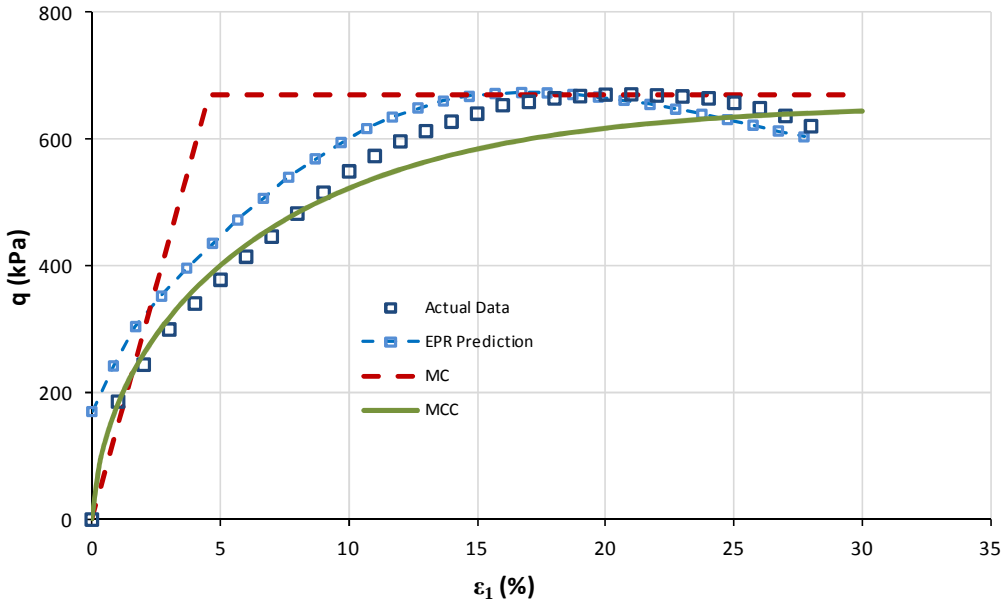

(c) $\acute{\sigma}_3 = 600\ kPa$

Figure 4.17: Comparison of stress-strain curve predicted by EPR-based, MC and MCC models versus the actual data

Specific volume is a parameter that is used as a measure of the ratio of the total volume (volume of voids plus volume of soil particles) and soil particles. This parameter is related to the volumetric strain, ε_v, through the following equation.

$$\Delta\varepsilon_v = \frac{-\Delta v}{v} \qquad 4.65$$

If the specific volume (or void ratio) is known at the initial stage of loading then using the above equation and the EPR model developed for volumetric strain (Equation 4.55) specific volume at any stage of loading can be determined.

In the following figure the specific volume versus natural logarithm of mean effective stress ($v - \ln p'$) is plotted for three different confining pressures using actual data, MCC model and predictions provided by the EPR model. For confining pressure 400, graph (a), EPR has clearly presented a better prediction than MCC model. The EPR model has given almost the same results as the actual data in both graphs (a), and (b). This figure shows that EPR model has captured the volumetric behaviour of the soil, and is also capable to predict the changes of specific volume against effective mean stress correctly.

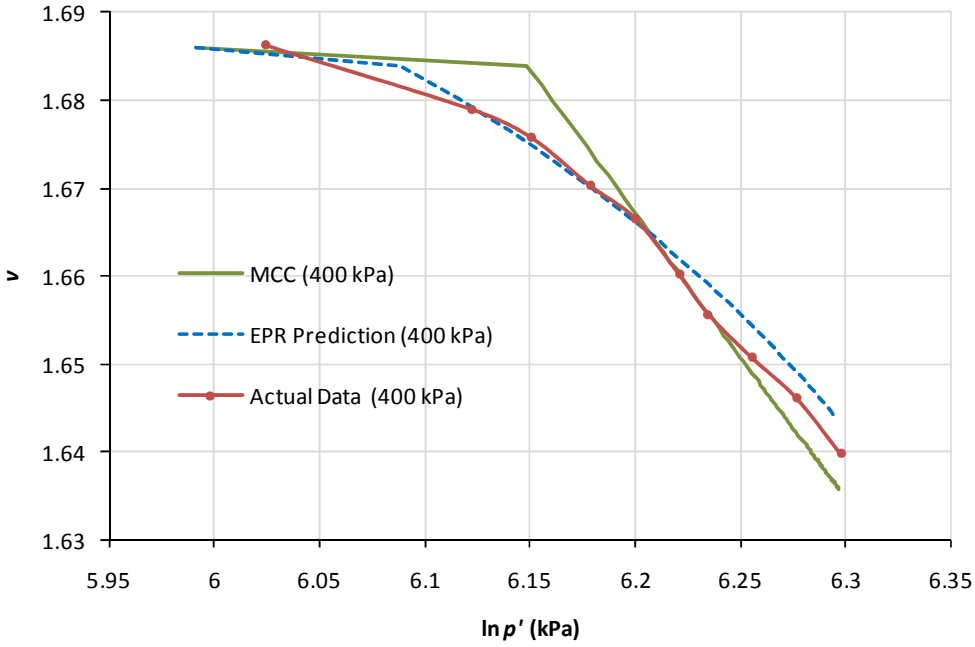

(a)

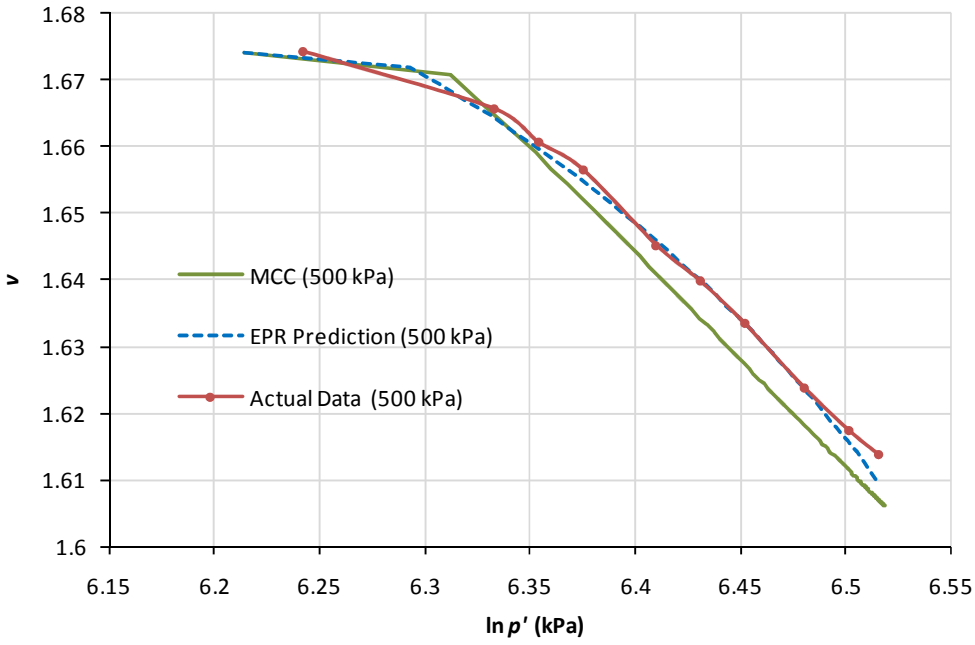

(b)

Figure 4.18: Comparison of v-ln(p') curve predicted by EPR-based, MC and MCC models versus the actual data

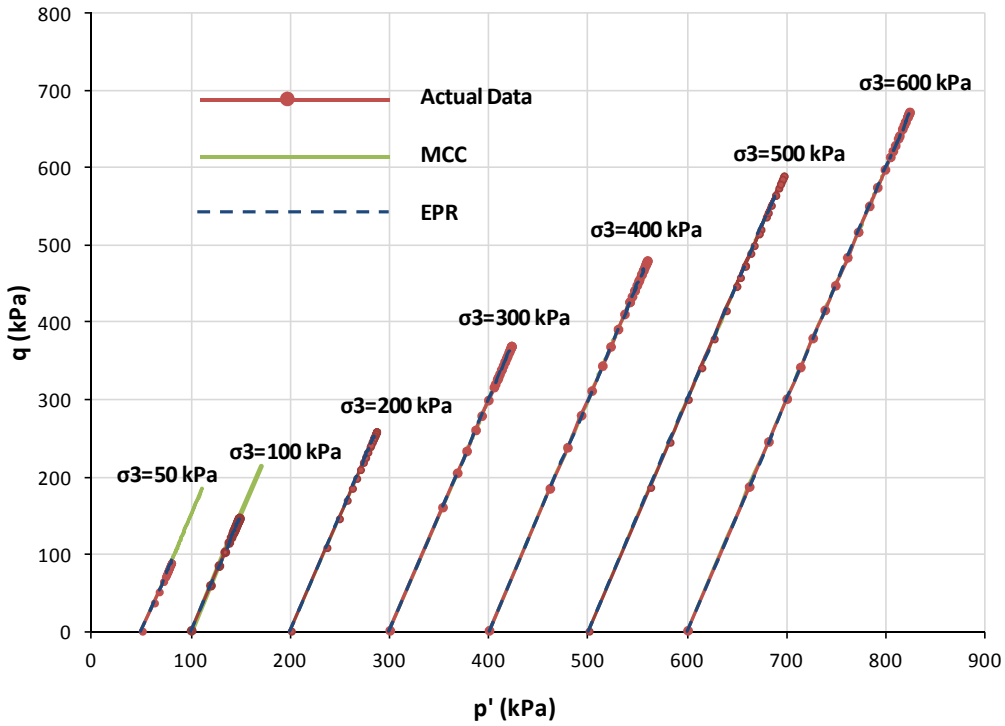

Figure 4.19: Comparison of p'-q curve predicted by EPR-based, MC and MCC models versus the actual data

In addition to the figures presented above, the deviator stress versus mean effective stress (stress path) for MCC and EPR models together with the actual data is depicted in Figure 4.19. The figure shows that the EPR model is in excellent agreement with the actual data. However, it can be noticed that the MCC model has over-predicted the deviator stress in the first two confining pressures (50 kPa, 100 kPa). These two confining pressures are representing heavily over-consolidated samples.

The performance and capabilities of the developed EPR-based models have been shown in the previous sections for monotonic loading conditions. In the next section the capability of EPR-based models to predict cyclic behaviour of materials (soil in particular) is presented.

4.3.5 EPR-based material model of soils under cyclic loading

In this section, the behaviour of a soil is studied in triaxial tests under cyclic axial loading. The test data for this example were generated by numerical simulation of triaxial experiments. In general, generating data by numerical simulation has advantages including: (i) it is more economic (ii) it is far less time demanding, (iii) it can simulate loading paths and test conditions that can not be easily achieved in physical testing due to physical constraints of the testing equipment. The data for training and validation of the EPR models were created by finite element simulation of triaxial cyclic loading tests at constant cell pressure using the *Modified Cam Clay Model*. The material parameters assumed for the soil are:

$\lambda = 0.174$ (Slope of the virgin consolidation line),
$\kappa = 0.026$ (Slope of the unloading-reloading lines in $e - \ln \acute{p}$ plane),
$M = 1$ (Slope of the critical state line in the $q - \acute{p}$ plane),
$p_0 = 100\ kPa$ (Isotropic pre-consolidation pressure),

The simulated tests were conducted at five different confining pressures on triaxial samples. The data generated by numerical simulation of the cyclic loading along axial direction at confining pressures of 100, 150, 200, 250 and 300 kPa are shown in Figure 4.20.

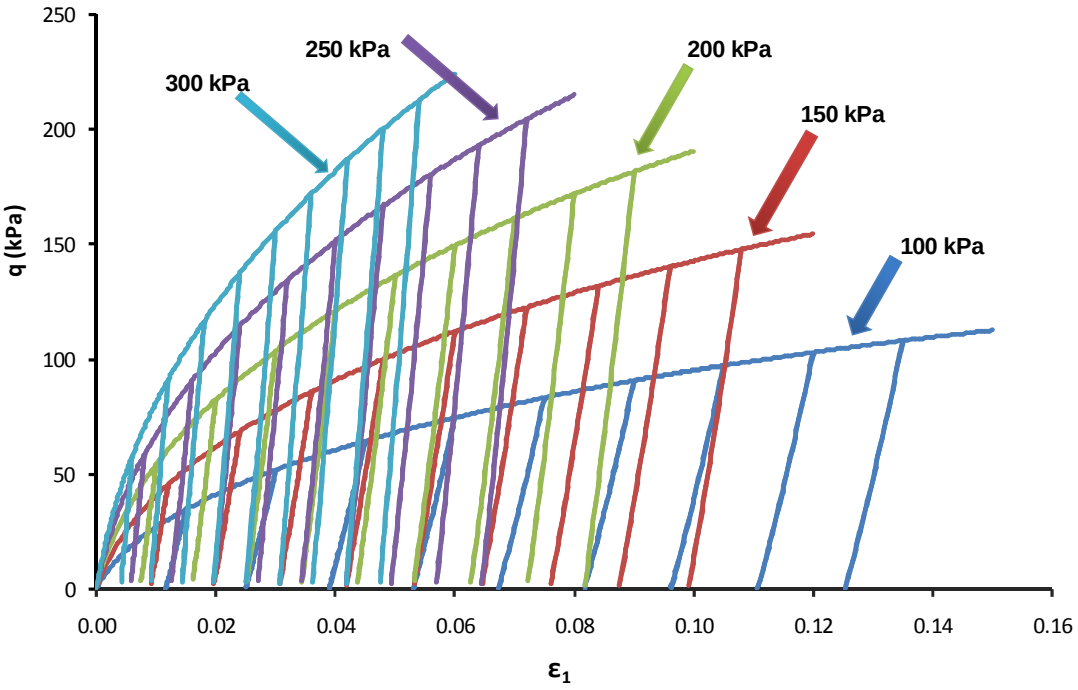

(a)

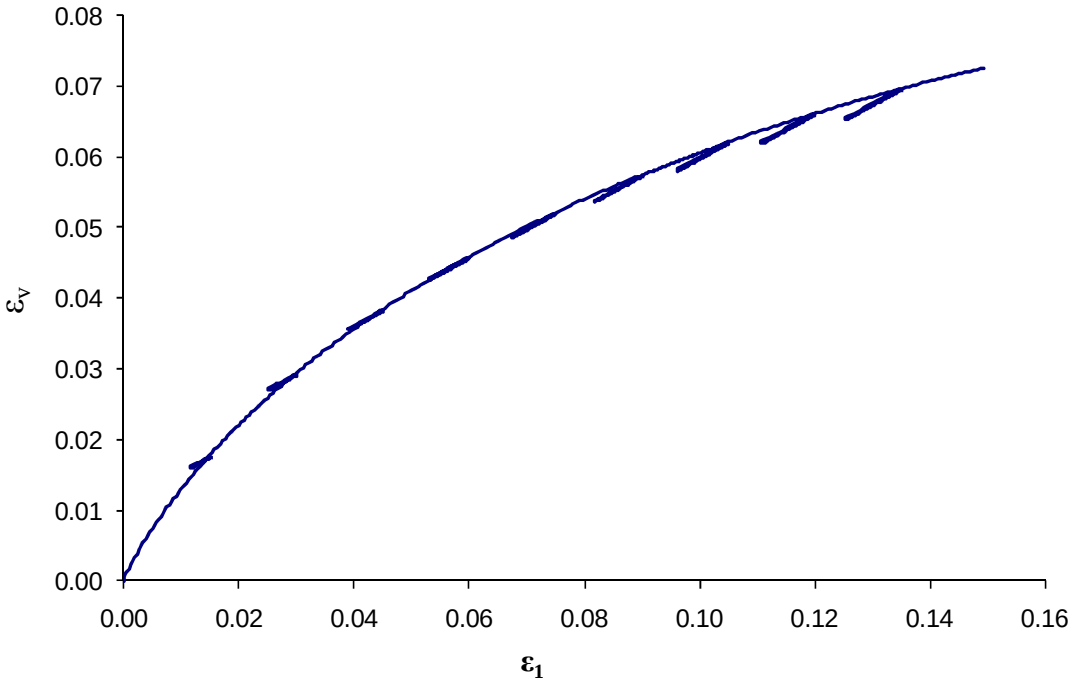

(b)

Figure 4.20: Cyclic loading test data used for training and validation of EPR-based model (a) Deviator stress (b) Volumetric strain

In order to introduce a level of noise that inevitably exists in real triaxial test data, numerical simulation for each confining pressure was repeated by changing the total number of load increments in the simulation and the obtained data were combined and used in training of the EPR models. Figure 4.21 shows typical results of the tests conducted at confining pressure of 150 kPa with four different load increments.

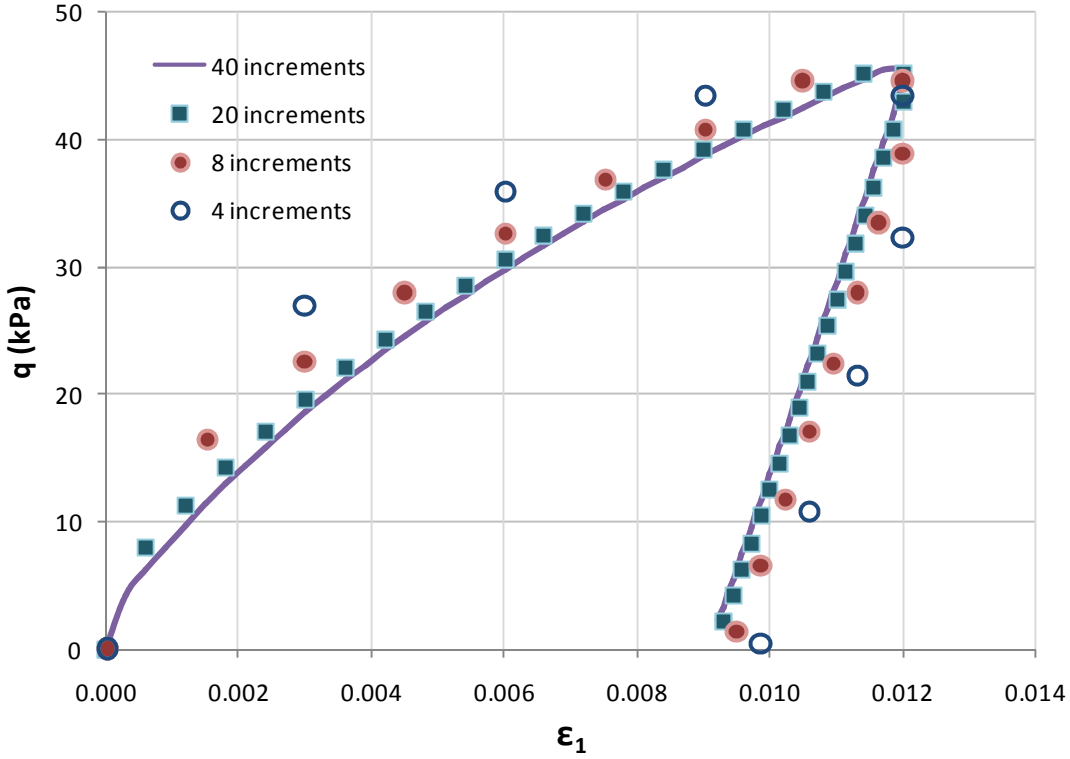

Figure 4.21: Typical cyclic loading test results with different load increments at confining pressure of 150 kPa

The data from the tests at confining pressures of 100, 150, 200 and 300 kPa were used for the training of the two EPR models. The trained EPR models were validated using the data from the test at confining pressure of 250 kPa.

The first model was developed to predict the deviator stress q^{i+1} and the second one to predict the volumetric strain ε_v^{i+1}. In the input parameters of the developed EPR models for cyclic loading, the distortional strain ε_q and increment of distortional strain $\Delta\varepsilon_q$ is replaced with axial strain ε_1 and increment of axial strain $\Delta\varepsilon_1$ respectively but the other parameters were kept the same as those used for monotonic loading. It should be

mentioned that in triaxial testing conditions ε_q can be calculated from the following equation at any stage of the loading:

$$\varepsilon_q = \varepsilon_1 - \frac{\varepsilon_v}{3} \tag{4.66}$$

The selected EPR models for q and ε_v are:

$$\begin{aligned} q^{i+1} = & -\frac{0.0084\ (q^i)^3}{\acute{p}^2\ \varepsilon_v^i} - \frac{2667.247 (q^i)^2 (\Delta\varepsilon_1)^2}{\acute{p}\ \varepsilon_1} \\ & - \frac{0.060714\ (q^i)^3 \Delta\varepsilon_1}{\acute{p}\ \varepsilon_v^i} + \frac{1.8866\ \varepsilon_v \Delta\varepsilon_1}{q^i} \\ & - \frac{1.9676\ q^i \Delta\varepsilon_1}{\varepsilon_v^i} + \frac{888.4\ (q^i)^2 (\Delta\varepsilon_1)^3}{\varepsilon_v^i} \\ & + 104.4964\ \acute{p}\Delta\varepsilon_1 - 1.4 \times 10^{-5}\acute{p}^2 \\ & + 0.018826\ \acute{p}^2 q^i\ \varepsilon_v^i\ \Delta\varepsilon_1 + 1.0525 q^i - 0.71525 \end{aligned} \tag{4.67}$$

$$\begin{aligned} \varepsilon_v^{i+1} = & \frac{0.02369 q^i \Delta\varepsilon_1}{\acute{p}\ \varepsilon_1} - \frac{0.4217 q^i\ \Delta\varepsilon_1}{\acute{p}} + \frac{9.3 \times 10^{-6}\ \varepsilon_1}{q^i} \\ & + 0.45727\ \Delta\varepsilon_1 + 0.99\ \varepsilon_v^i + 0.000041535 \end{aligned} \tag{4.68}$$

Figure 4.22 shows the curves predicted by equations 4.67 and 4.68 for the training data set. In this figure, the actual (numerically simulated) data are plotted together with results of the EPR models predictions. It can be seen from the figures that EPR models were capable of learning, with a very good accuracy the constitutive relationships of the soil under cyclic loading paths.

* Units: $p', q\ (N/m^2)$

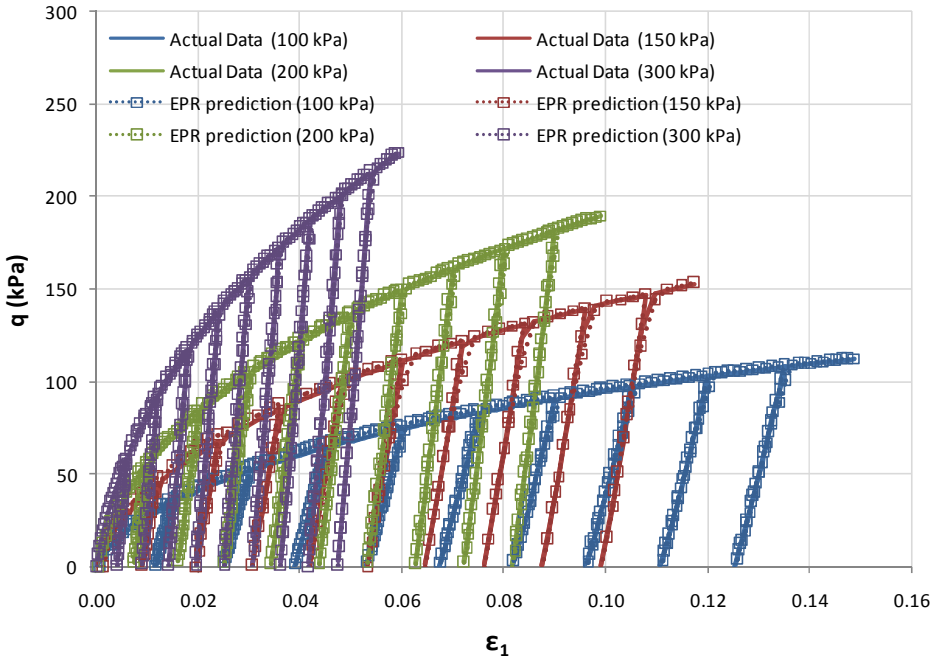

(a)

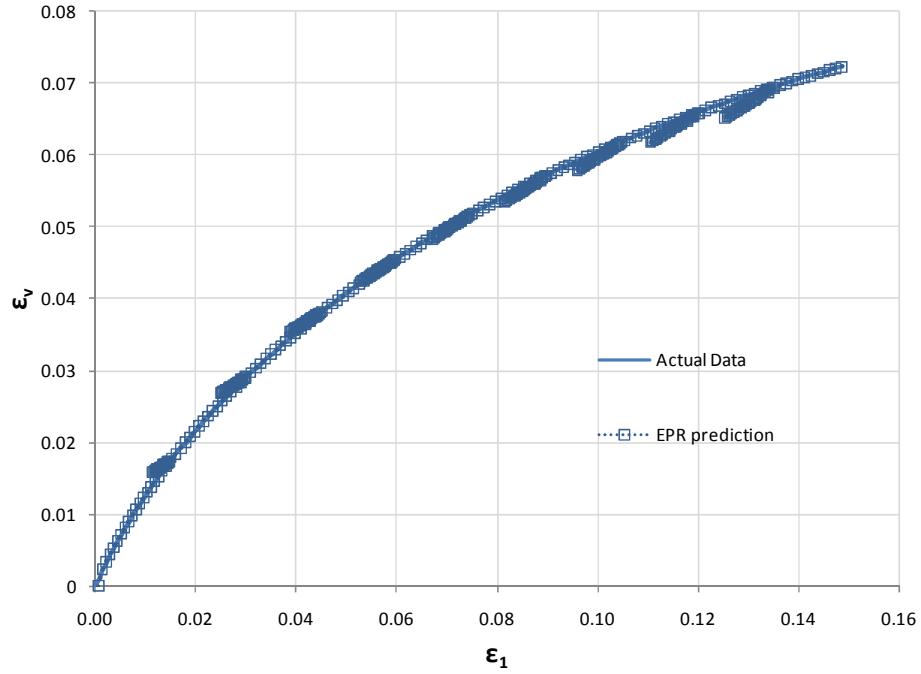

(b)

Figure 4.22: EPR prediction for cyclic loading versus actual data

The trained EPR models were validated using a data set corresponding to the confining pressure of 250 kPa. The results of the validation tests are shown in Figure 4.23. It is shown that the trained EPR models were able to generalise the training to loading cases that were not introduced to the EPR during training.

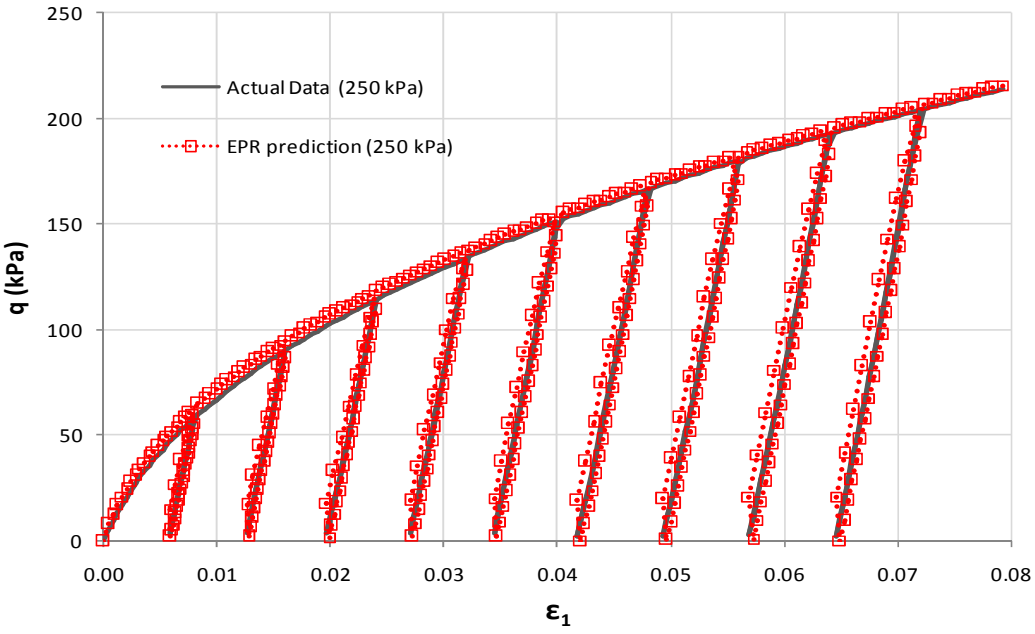

(a)

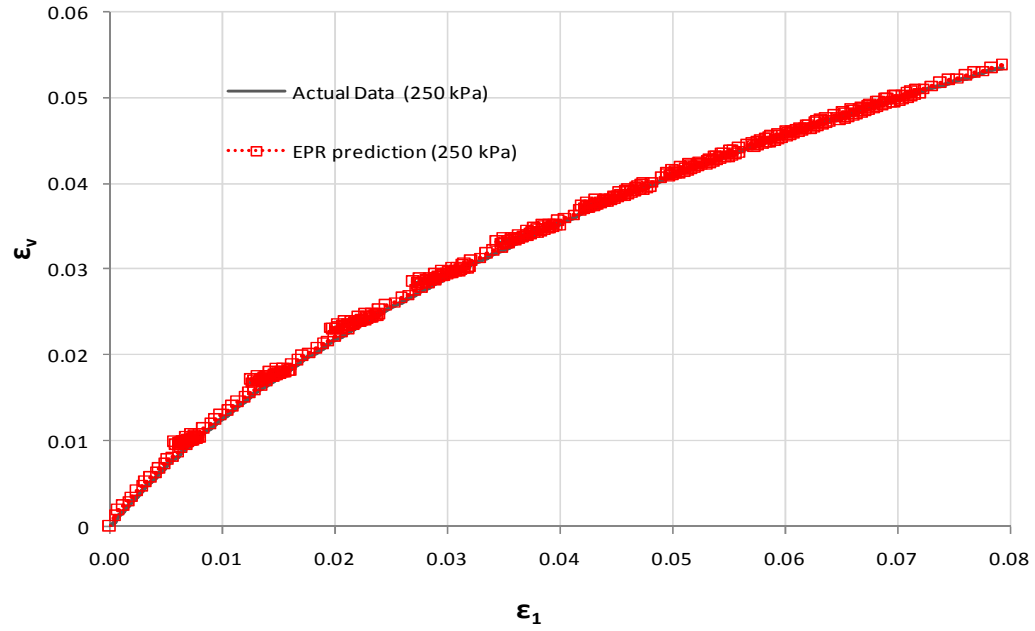

(b)

Figure 4.23: Results of the validation of the trained EPR models: comparison between the actual (numerically simulated) data and the EPR predictions for confining pressure of 250 kPa (a) deviator stress (b) volumetric strain

Moreover the incremental prediction capability (described in section 4.3.3) of the developed EPR models is examined and presented in Figure 4.24 where the point by point prediction of EPR models are compared to the actual data.

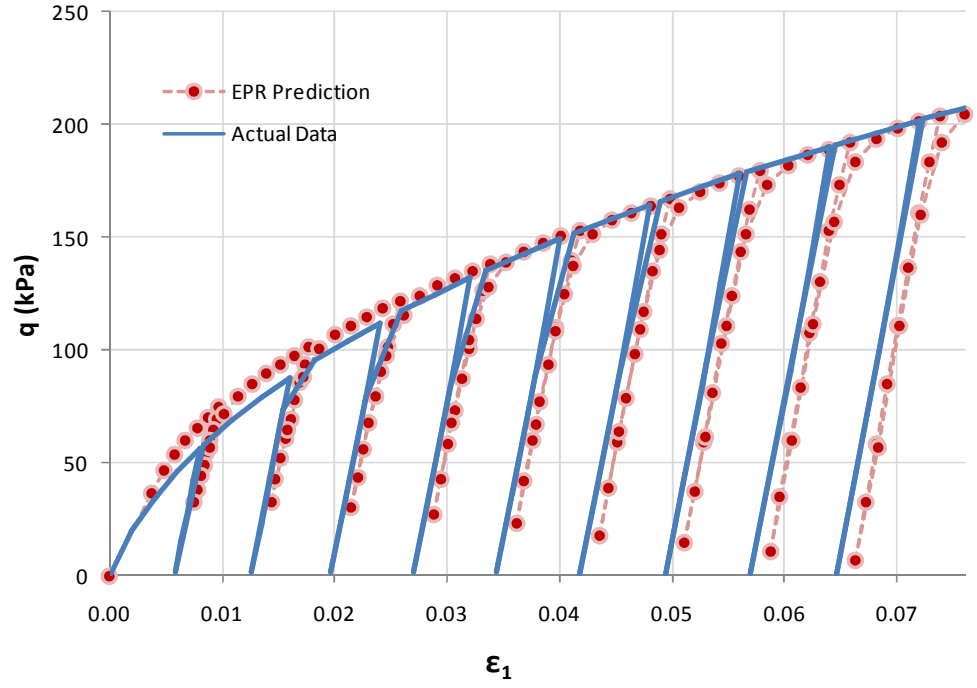

(a)

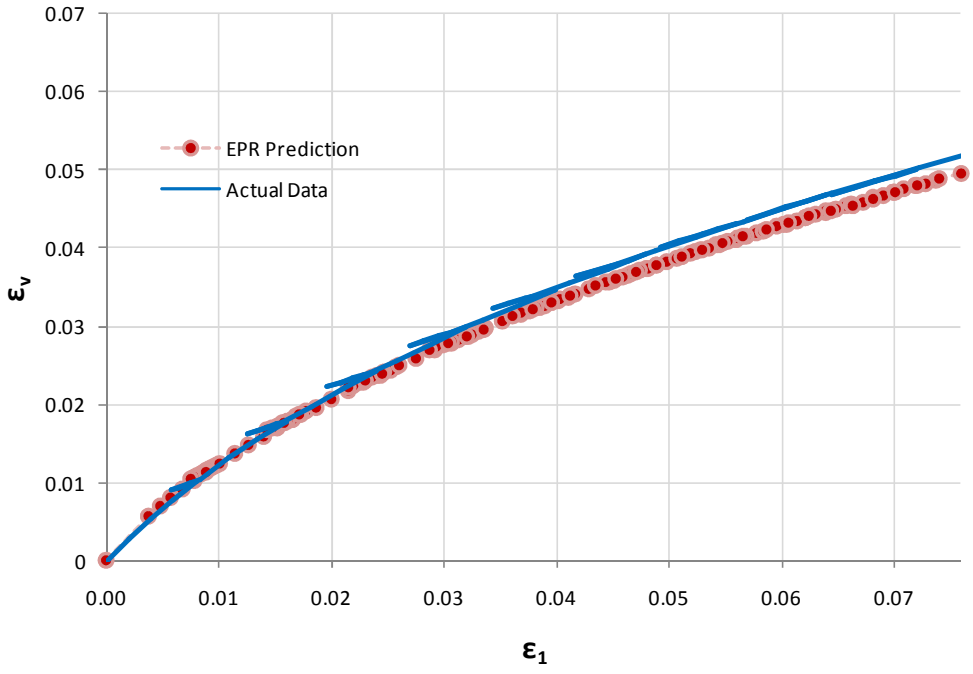

(b)

Figure 4.24: Comparison of EPR (incremental) predictions with the actual data for confining pressure of 250 kPa (a) $q - \varepsilon_1$ (b) $\varepsilon_v - \varepsilon_1$

It should be mentioned that, for practical problems, the data used for training EPR, should cover the range of stresses and strains that are likely to be encountered in practice. This is due to the fact that EPR models are good at interpolation but not so good at extrapolation. Therefore, any attempt to use EPR-based FE method for loading conditions that may lead to stresses or strains outside the range of the stresses and strains used in training of the EPR may lead to unacceptable errors. The following table is provided to show the acceptable ranges of stresses and strains in the developed equations.

Table 4.4: Range of stresses and strains for developed EPR models

Equations 4.54, 4.55					
Parameters	ṕ (kPa)	q (kPa)	ε_v(%)	ε_q(%)	$\Delta\varepsilon_q$(%)
Max	823	670.0	0.9	31.8	1.48
Min	50	0.0	-6.3	0.0	0.08
Equations 4.67, 4.68					
Parameters	ṕ (kPa)	q (kPa)	ε_v(%)	ε_1(%)	$\Delta\varepsilon_q$(%)
Max	375	223	7	14	0.6
Min	100	0	0	0	-0.2

In this chapter it was shown that EPR can be employed to construct material models using both synthetic and experimental data gathered from material tests. Two different approaches were presented, total and incremental strategies, in order to obtain EPR-based material models. It was shown that EPR can produce mathematical expressions that can accurately predict the material behaviour in both cases. Different materials (including soil that is known for having a complex behaviour) with different behaviour (e.g. linear, elasto-plastic) under different loading conditions (monotonic and cyclic loading) were examined to asses the capability of EPR-based models in predicting material behaviour. In the next chapter EPR-based models will be incorporated in a finite element model and will be used to analyse different engineering problems. The advantages of the developed EPR-based finite element method will be highlighted.

Chapter 5

EPR Based Finite Element Method

5.1 Introduction

As it was mentioned in chapter 2, the finite element method (FEM) has been used successfully in modelling and analysing a wide range of engineering problems in different fields including aerospace, automotive, biomechanical, chemical process, geotechnical engineering and many others. It was also shown that neural network based constitutive models (NNCM) have been implemented successfully in the finite element procedure to analyse engineering systems, in particular structural and geotechnical engineering problems.

Two different strategies were introduced in chapter 4 to train EPR-based constitutive material models. In this chapter the EPR-based material models developed in the previous chapter will be incorporated in the finite element model for both strategies. Different examples will be presented to illustrate the capabilities of the proposed EPR-based finite element method.

5.2 EPR-based Jacobian Matrix

Any material model that is intended to be incorporated in finite element method must provide material stiffness matrix, also called Jacobian matrix, and can be defined as the following equation.

$$\mathbf{J} = \frac{\partial(d\boldsymbol{\sigma})}{\partial(d\boldsymbol{\varepsilon})} \tag{5.1}$$

where, $\boldsymbol{\sigma}$ and $\boldsymbol{\varepsilon}$ are the vectors of stresses and strains respectively. This matrix is defined explicitly for different material models. For instance the stiffness matrix **(D)** for a linear elastic material model obeying the Hook's law in plane strain geometrical conditions is defined as follow (Stasa, 1986):

$$\mathbf{D} = \frac{E}{(1+\nu)(1-2\nu)}\begin{bmatrix} 1-\nu & \nu & \nu & 0 \\ \nu & 1-\nu & \nu & 0 \\ \nu & \nu & 1-\nu & 0 \\ 0 & 0 & 0 & \frac{(1-2\nu)}{2} \end{bmatrix} \tag{5.2}$$

where E represents elastic modulus and ν is the Poisson's ratio.

Hashash et al. (2004) recommended to use consistent Jacobian matrix (Equation 5.3) and proposed a method to estimate partial derivation of NNCM to form the Jacobian matrix.

$$\mathbf{J} = \frac{\partial \Delta\boldsymbol{\sigma}^{\mathbf{i+1}}}{\partial \Delta\boldsymbol{\varepsilon}^{\mathbf{i+1}}} \tag{5.3}$$

where $\boldsymbol{\sigma}$ and $\boldsymbol{\varepsilon}$ are the vectors of stresses and strains respectively and i+1 denotes the next state of stresses and strains. Clearly this formulation of Jacobian matrix needs the constitutive model to be constructed in an incremental form.

On the other hand Shin (2001) and Shin and Pande (2003) used direct derivation of NNCM (Equation 5.4) and proposed a procedure to calculate the first order partial derivation of NNCM.

$$\mathbf{D}_{\mathrm{NN}} = \frac{\partial \boldsymbol{\sigma}}{\partial \boldsymbol{\varepsilon}} \tag{5.4}$$

In this study direct derivation of EPR-based material models is used to construct the Jacobian matrix for materials.

5.2.1 Partial derivatives of EPR models

Differentiation of the models developed by data mining techniques has been studied by a number of researchers. In particular derivation of neural networks models developed for constitutive modelling of materials has been discussed by Shin, (2001); Hashash et al., (2004); and Shin & Pande, (2000). Due to the nature of EPR models which are in the form of mathematical expressions, differentiation of them seems to be a straightforward task. However it should be mentioned that the accuracy of derivative of the developed EPR models depends on the accuracy of the EPR model.

Consider an objective function $\mathbb{F}(X_1, X_2, \dots, X_n)$ that is intended to be estimated by an EPR model $\mathbb{G}(X_1, X_2, \dots, X_n)$ where $X_1, X_2, \dots, X_n$ are all effective parameters that influence the objective function. It is known that in any regression model an error term exists which captures all other factors that influence the objective function (following equation).

$$\mathbb{F}(X_1, X_2, \dots, X_n) = \mathbb{G}(X_1, X_2, \dots, X_n) + err \qquad 5.5$$

The relationship between the error term and input parameters is a crucial matter in modelling a phenomenon. If the partial derivative of equation 5.5 with respect to an arbitrary input X_i is performed, the following equation is obtained.

$$\frac{\partial \mathbb{F}(X_1, X_2, \dots, X_n)}{\partial X_i} = \frac{\partial \mathbb{G}(X_1, X_2, \dots, X_n)}{\partial X_i} + \frac{\partial err}{\partial X_i} \qquad 5.6$$

Obviously if the error term err is a constant value and not a function of other input parameters, its derivative is zero and can be omitted from equation 5.6. In this case the error term has no influence on the differentiation of the EPR models. On the other hand if the error term is correlated with other input parameters and varies with them the error term plays an important role in both EPR model and its derivatives.

There could be different reasons for the error term being non-constant and significant in an EPR model. For instance, incorrect or insufficient training data, not having all the

input parameters, user mistakes in setup of control parameters, improper choice of the solutions provided by EPR, etc. or a combination of the above. Among these reasons, two of them which have the most effect on the quality of the EPR models are described here.

One of the reasons could be that one or more input parameters which influence the phenomenon are not included in the EPR model and therefore the obtained EPR model is not a proper representative of the phenomenon. This raises the importance of the fact that the physics behind the event must be studied thoroughly before construction of EPR models. Mechanics of the event and literature are two most important sources of information that must be considered and studied prior to modelling by EPR in order to include all the effective parameters in the model. It should be mentioned when modelling a phenomenon using EPR, if the user has doubt about including a parameter, it is advised to involve that parameter since EPR has the capability to disregard the parameters that have negligible or no influence on the model (Doglioni, 2004).

Another main reason for having an error term with a correlation with other input parameters could be the fact that the right model is not chosen from the solutions provided by EPR. This emphasises the importance of model selection in the modelling process using EPR. As it was described in chapter 3, EPR offers a range of solutions in the form of a pareto-front surface (or curve) which helps the user to choose the right mathematical expression to describe the phenomenon. EPR can control the number of input parameters, and the number of terms versus the coefficient of determination (CoD) using a multi-objective strategy. Moreover the wide range of available functions and EPR types assist the user to explore among these available options to select the suitable mathematical expression. In what follows a number of examples will be presented to evaluate the accuracy of the partial derivatives of the EPR models.

5.2.1.1 Illustrative examples

A number of different mathematical functions are considered and the values of functions are determined for different input values in order to generate the required data points. These data points are then used to train and obtain EPR models. The derivatives

of the EPR models are determined and comparisons are made between the EPR models and the original mathematical functions as well as their derivatives.

(i) Example 1

For the first example a polynomial equation is chosen as following:

$$f(x_1, x_2) = x_1 x_2^2 + x_1 x_2 + x_1^2 + x_2^2 \qquad 5.7$$

The surface (red mesh) and the generated data points (blue dots) from this surface are plotted in the following figure.

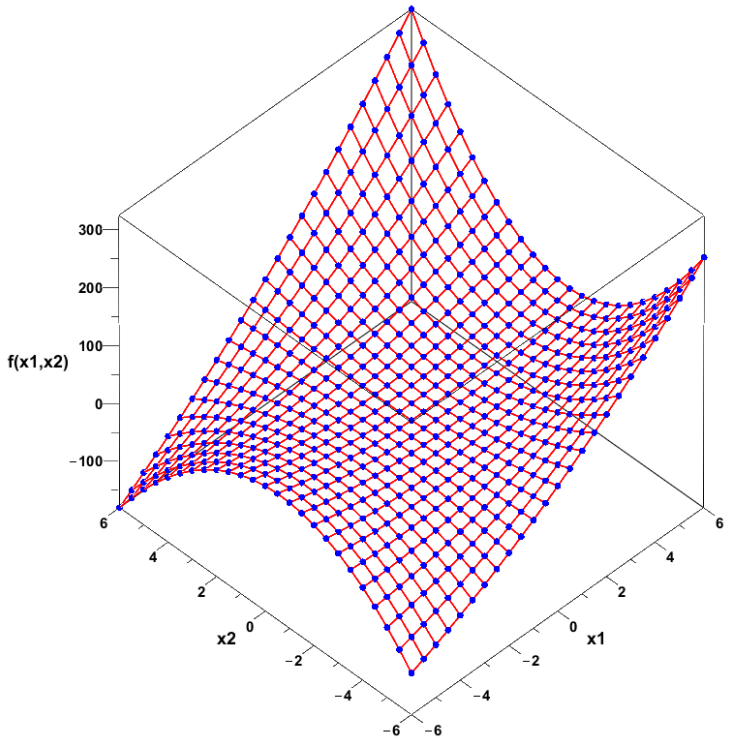

Figure 5.1: Polynomial function and training data

These data points are fed into EPR to obtain an EPR model. Since it is supposed that the objective function is not known a priori, the exponents range is limited to integer numbers between -4 to 4 including 0 and the number of terms is limited to 20. The results of training of EPR are presented in the following equations.

Equations	CoD	
$g(x_1, x_2) = 26$	0.0 %	5.8
$g(x_1, x_2) = x_1 x_2^2 + 26$	89.95 %	5.9
$g(x_1, x_2) = x_1 x_2^2 + 0.055 x_1^2 x_2^2 + 16.7$	94.38 %	5.10
$g(x_1, x_2) = x_1 x_2 + x_1 x_2^2 + 0.055 x_1^2 x_2^2 + 16.7$	98.23 %	5.11
$g(x_1, x_2) = x_1 x_2^2 + x_1 x_2 + x_1^2 + x_2^2 + 4.1 \times 10^{-15}$	100 %	5.12

In these equations $g(x_1, x_2)$ is the estimated EPR model. From these equations it can be seen that although the maximum number of terms was set to 20 and the range of exponents was $-4: +4$ however, the maximum number of terms achieved by EPR in the final stage of the evolutionary steps is 5. This shows the strength of EPR to avoid the problem of over-fitting by using different strategies as described in detail in chapter 3.

The accuracy of equation 5.12 is 100% and by comparing it to the function $f(x_1, x_2)$ it can be seen that it exactly matches the original function except for the constant term 4.1×10^{-15} which is negligible. As it was mentioned earlier this constant term has no influence in differentiation of the function and clearly the partial derivative of the estimated function is equal to that of the objective function.

(ii) Example 2

A trigonometric function (equation 5.13) is chosen for the second example to illustrate how well the derivatives of the EPR model can approximate the derivatives of the function.

$$f(x_1, x_2) = \text{sech}\,(x_1) \cdot \tanh(x_2) \qquad 5.13$$

This function is used to generate data points and train EPR models to find the best EPR function that can approximate this function. Before training the EPR model, the number of terms was set to 20, the range of exponents to [-4:+4], and no function was chosen. After training, the best EPR model representing equation 5.13 was as follow:

$$\begin{aligned} g(x_1, x_2) \;=\; & -1.15 \times 10^{-5} x_1^4 x_2^3 \; + 5.41 \times 10^{-4} x_1^2 x_2^3 \; + 6.05 \\ & \times 10^{-4} x_1^4 x_2 - 0.03 x_1^2 x_2 - 5.55 \times 10^{-3} x_2^3 + 0.29 x_2 \\ & + 7.58 \times 10^{-17} \end{aligned} \qquad 5.14$$

The coefficient of determination of this equation was 85.16% which shows the EPR model is not a perfect representative of the original function. The original function and EPR prediction (points) are depicted in the following figure.

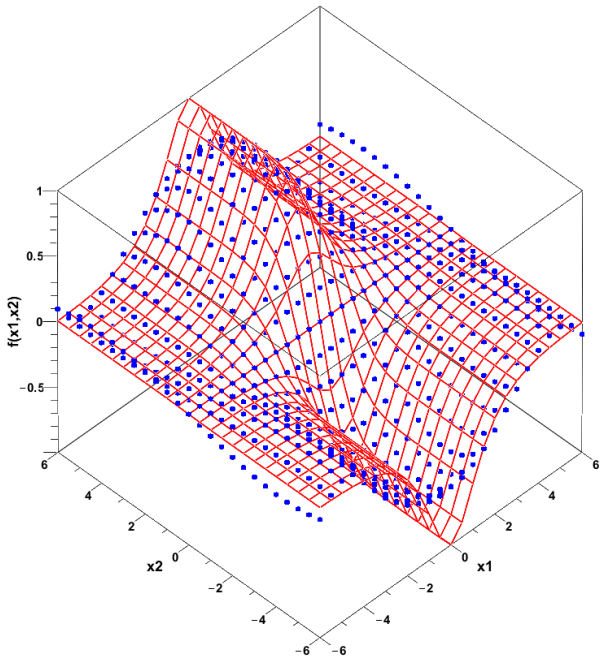

Figure 5.2: Trigonometric function (red mesh) and EPR prediction (blue dots)

Differentiation of the trigonometric function and the EPR model with respect to x_1 is compared in Figure 5.3. It can be seen that the accuracy of the differentiation is not

acceptable and therefore the selected polynomial function is not good enough to represent the original function.

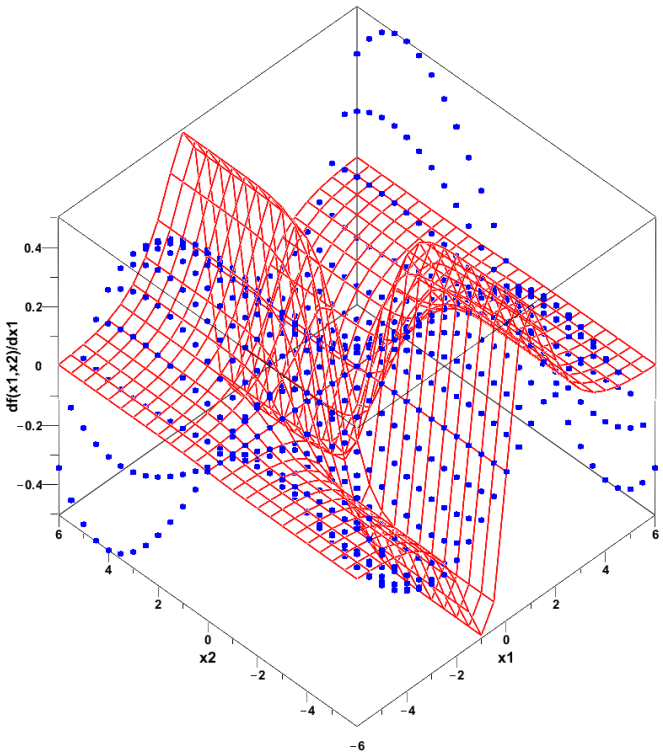

Figure 5.3: EPR prediction for partial derivatives of the trigonometric function with respect to x_1 versus the differentiation of original function

In order to find a better EPR model, different available functions in EPR and various EPR types with different exponent ranges and number of terms were tried and eventually it was found that the accuracy of the EPR models will only get better if tangent hyperbolic or secant hyperbolic is used as the function to train EPR. After training the EPR using tangent hyperbolic function, the following equation was chosen to compare the EPR model and its derivative with the original function.

$$\begin{aligned} g(x_1, x_2) = & -0.49\, x_1^2 \tanh^2(x_1) \tanh(x_2) \\ & - 0.93 \tanh^2(x_1) \tanh(x_2) + 0.49 x_1^2 \tanh(x_2) \\ & + 0.99 \tanh(x_2) \end{aligned} \qquad 5.15$$

The CoD of this equation is 99.98 % and it is compared with original function in Figure 5.4. The derivatives of this equation with respect to x_1 and x_2 are determined and presented in equations 5.16 and 5.17 respectively. A good agreement between the

partial derivatives of the EPR model and partial derivatives of the original function with respect to x_1 and x_2 can be seen in Figure 5.5 and Figure 5.6.

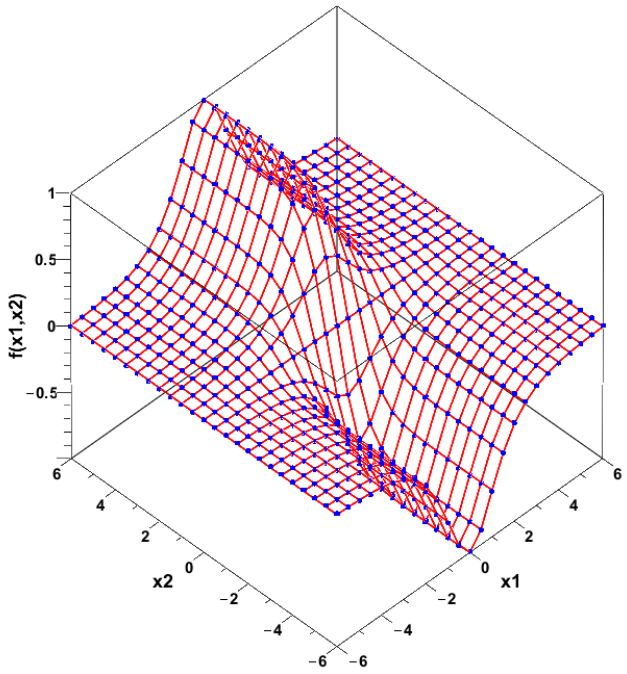

Figure 5.4: Trigonometric function (red mesh) and EPR prediction using tanh function (blue dots)

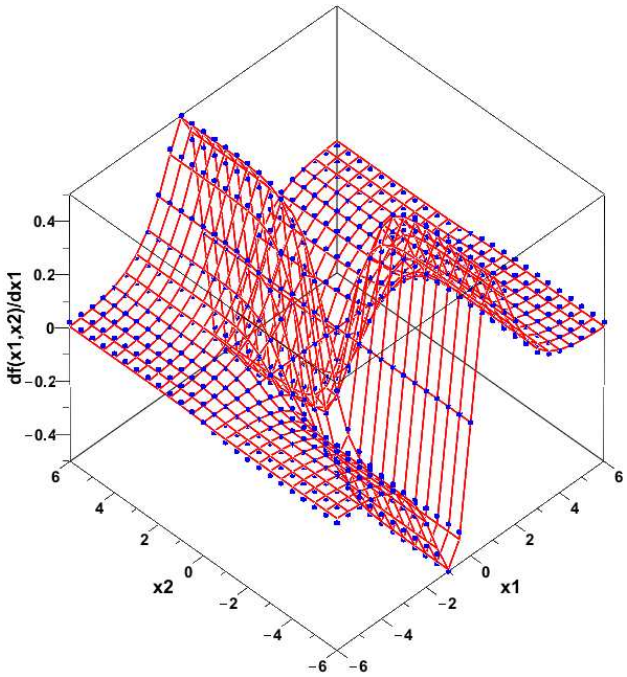

Figure 5.5: EPR prediction using tanh function for partial derivatives of the trigonometric function with respect to x_1 versus the differentiation of the original function

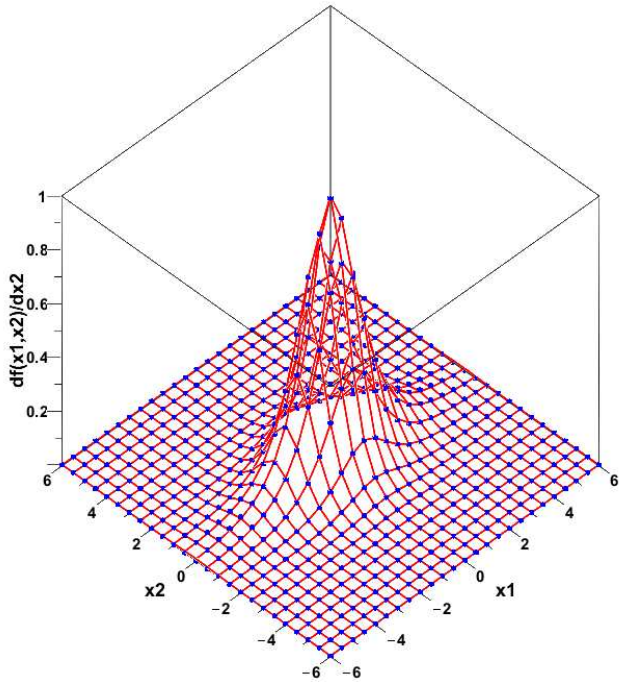

Figure 5.6: EPR prediction using tanh function for partial derivatives of the trigonometric function with respect to x_2 versus the differentiation of the original function

$$\frac{\partial g(x_1,x_2)}{\partial x_1} = -1.86\tanh(x_1)\tanh(x_2)\left(1-\tanh^2(x_1)\right) + 0.98x_1\tanh(x_2) - 0.98x_1\tanh^2(x_1)\tanh(x_2) - 0.98x_1^2\tanh(x_1)\tanh(x_2)\left(1-\tanh^2(x_1)\right) \quad 5.16$$

$$\frac{\partial g(x_1,x_2)}{\partial x_2} = 0.99\left(1-\tanh^2(x_2)\right) + 0.49x_1^2\left(1-\tanh^2(x_2)\right) - 0.93\tanh^2(x_1)\left(1-\tanh^2(x_2)\right) - 0.49x_1^2\tanh^2(x_1)\left(1-\tanh^2(x_2)\right) \quad 5.17$$

The presented examples show that if the right model is chosen from the results of EPR, the selected model and its partial derivatives provide a good approximation to the phenomenon being studied.

5.3 Incorporation of EPR models (total stress-strain strategy) in FEM

The developed EPR-based material models in chapter 4 are implemented in a widely used general-purpose finite element code ABAQUS through its user defined material module (UMAT). UMAT updates the stresses and provides the material Jacobian matrix for every increment in every integration point (ABAQUS, 2007).

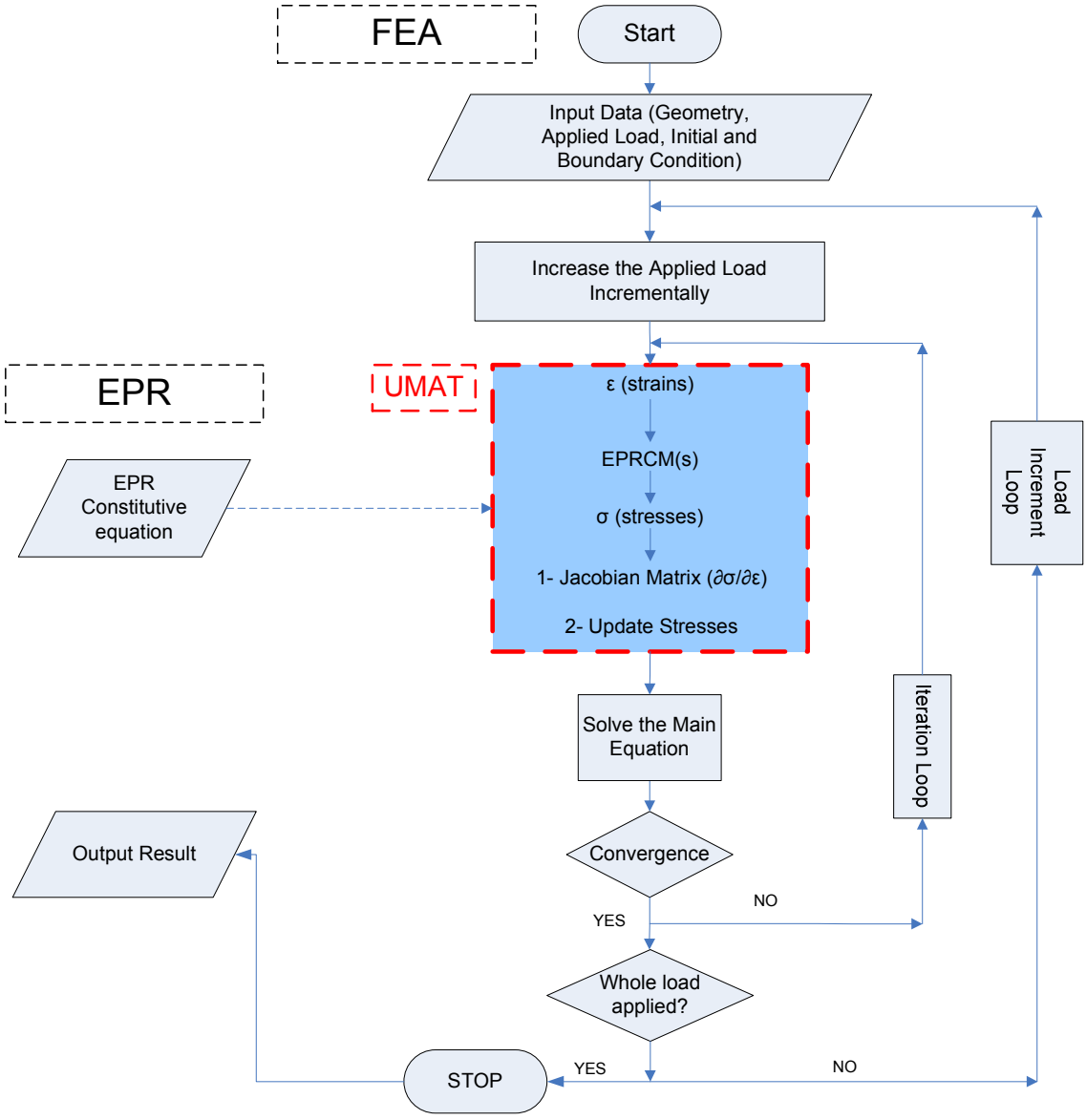

Figure 5.7: The incorporation of EPRCM in ABAQUS finite element software

The material Jacobian matrix can be derived using the developed EPR models using the total stress-strain strategy using the following equation:

$$\mathbf{J} = \frac{\partial \boldsymbol{\sigma}}{\partial \boldsymbol{\varepsilon}} \qquad 5.18$$

Equation 5.18 can be applied in both elastic and inelastic regions because an EPR constitutive model (EPRCM) does not require the definition of a transition between elastic and inelastic regions (i.e. yield points). The Jacobian matrix resulting from the EPRCM can be directly incorporated in a conventional FE code instead of the conventional elasto-plastic constitutive matrix. The way in which EPRCM is incorporated in the finite element method, is shown in Figure 5.7.

5.3.1 Numerical Examples

To illustrate the developed computational methodology described in the previous section, five examples of application of the developed EPR-based finite element method to boundary value problems are presented. In the first two examples, the application of the methodology to a simple case of linear elastic behaviour is examined. The constitutive equations for this material were developed in the previous chapter (section 4.2.1.3). For the third example a finite element model of the material test in section 4.2.2, chapter 4 is considered in order to choose the best EPR model among those presented in that section. In the fourth and fifth examples, the method is applied to a problem with the same geometries as the first and second one but with a non-linear material behaviour chosen from the results of the third example.

5.3.1.1 Example 1: Plate with a circular hole (linear elastic)

This example involves a plane stress plate with a circular hole in its centre. The plate is assumed to be made of a linear elastic material with elastic modulus $\mathrm{E} = 500$ Pa and Poisson's ratio $\nu = 0.3$. An EPRCM was developed for this linear elastic material in section 4.2.1.3 in chapter 4 and the developed constitutive equations are repeated here.

$$\sigma_x = 549.4505\varepsilon_x + 164.8352\varepsilon_y - 5.1338 \times 10^{-12} \qquad 5.19$$

$$\sigma_y = 164.8352\varepsilon_x + 549.4505\varepsilon_y - 1.2134 \times 10^{-11} \qquad 5.20$$

$$\tau_{xy} = 192.3077\gamma_{xy} + 3.2319 \times 10^{-12} \qquad 5.21$$

Figure 5.8 shows the geometry, boundary conditions and loading of the plate. Due to the symmetry in the geometry of the plate only a quarter of the plate is modelled and therefore appropriate boundary conditions are provided on the bottom and left sides of the model. The model is made of 100 isoparametric 8-node elements and is stretched along Y direction by applying of a uniform pressure of 10 Pa.

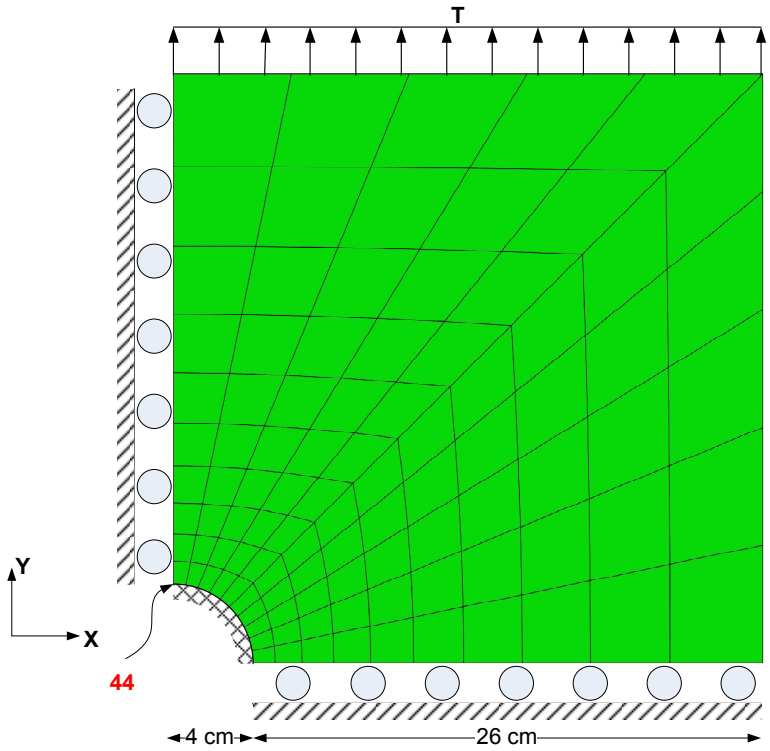

Figure 5.8: A plate with circular hole at its centre under tension loading along Y direction

Using equations 5.18 and 5.19-5.21 the EPR-based material Jacobian matrix for this example is computed and presented in the following equation.

$$\mathbf{J} = \begin{bmatrix} \frac{\partial \sigma_x}{\partial \varepsilon_x} & \frac{\partial \sigma_x}{\partial \varepsilon_y} & \frac{\partial \sigma_x}{\partial \varepsilon_{xy}} \\ \frac{\partial \sigma_y}{\partial \varepsilon_x} & \frac{\partial \sigma_y}{\partial \varepsilon_y} & \frac{\partial \sigma_y}{\partial \varepsilon_{xy}} \\ \frac{\partial \sigma_{xy}}{\partial \varepsilon_x} & \frac{\partial \sigma_{xy}}{\partial \varepsilon_y} & \frac{\partial \sigma_{xy}}{\partial \varepsilon_{xy}} \end{bmatrix} = \begin{bmatrix} 549.45 & 164.83 & 0.00 \\ 164.83 & 549.45 & 0.00 \\ 0.00 & 0.00 & 192.31 \end{bmatrix} \quad 5.22$$

On the other hand the conventional stiffness matrix for an isotropic, elastic material for plane stress conditions in terms of Young's modulus and Poisson ratio is given as follow (Stasa, 1986):

$$\mathbf{D} = \frac{E}{1-\nu^2}\begin{bmatrix} 1 & \nu & 0 \\ \nu & 1 & 0 \\ 0 & 0 & (1-\nu)/2 \end{bmatrix} \qquad 5.23$$

If the values of $\mathrm{E} = 500\,\mathrm{Pa}$ and $\nu = 0.3$ are substituted in the above equation the following matrix will be obtained:

$$\mathbf{D} = \begin{bmatrix} 549.45 & 164.83 & 0 \\ 164.83 & 549.45 & 0 \\ 0 & 0 & 192.31 \end{bmatrix} \qquad 5.24$$

By comparing the equation 5.22 and 5.24 it can be seen that the Jacobian matrix obtained from EPR models is in an excellent agreement with the conventional elastic plane stress stiffness matrix.

The EPR Jacobian matrix is implemented in UMAT and the above structure is analysed under the given loading and boundary conditions. The problem is also analysed using the elastic material model provided by ABAQUS which requires elastic modulus and Poisson's ratio. The vertical displacement of the crown of the hole versus the applied tension is compared between standard finite element analysis and EPR-based finite element method and the results are depicted in Figure 5.9.

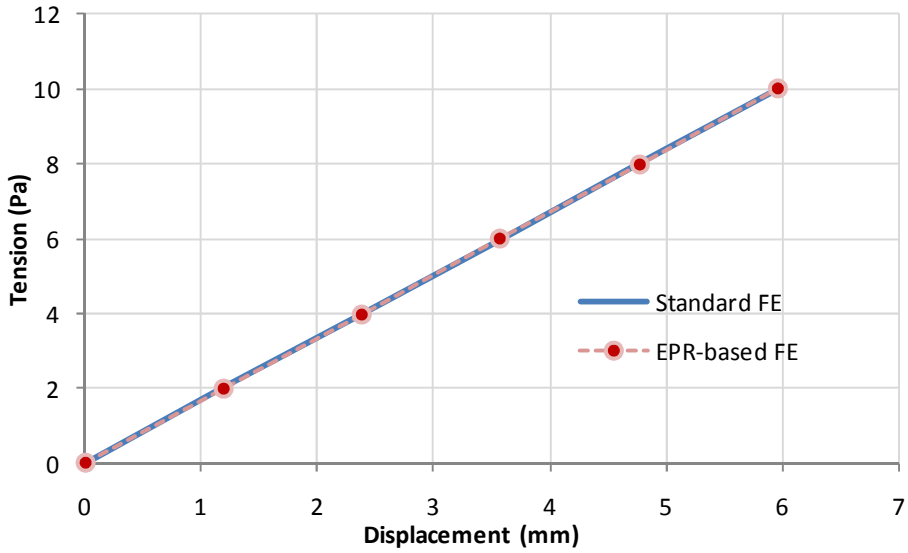

Figure 5.9: Tension-displacement curve of node 44 for Standard FE and EPR-based FE

An excellent agreement can be seen from this figure between the displacement of node 44 using standard FE and EPR-based FE analyses. This shows that the EPR-based material Jacobian matrix has been successfully implemented in the finite element analysis and the methodology can be used to predict the behaviour of a linear elastic material.

5.3.1.2 Example 2: Plate subjected to an in-plane load (linear elastic)

A 2D plane stress panel subjected to an in-plane compression is set up to evaluate further, the potential of the proposed EPR-based FE method. The model of the panel with applied load and its surrounding boundary conditions is shown in Figure 5.10. It is assumed that the plate is made of the same material as the one introduced in section 4.2.1.3 in chapter 4. It is also assumed that the EPR models developed for this material in chapter 4 are valid and will be used here.

The FE analysis of the panel is first carried out using a standard FE model with 270 isoparametric elements. The elastic parameters used for the panel are; Young's modulus $E = 500$ Pa and Poisson's ratio $\nu = 0.3$. On the other hand the EPR-based FE analysis was performed using the Jacobian matrix presented in equation 5.22. The results of these two analyses are compared in terms of vertical stresses and strains in Figure 5.11 and Figure 5.12.

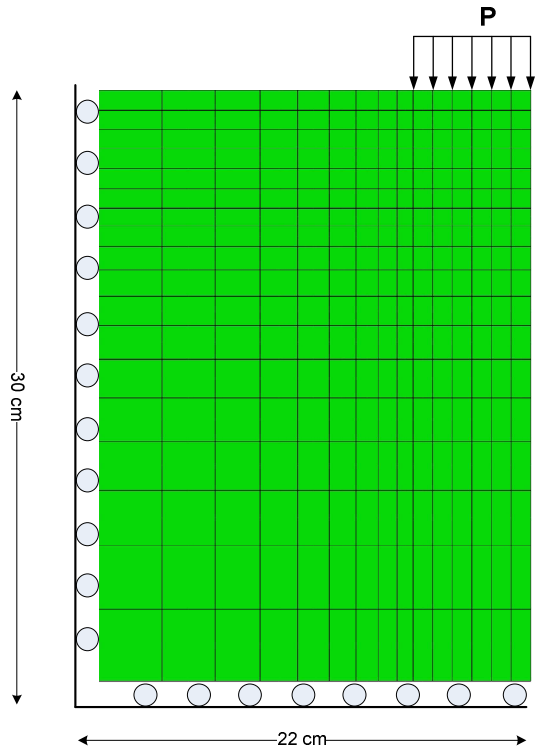

Figure 5.10: The FE mesh and geometry of plane stress panel and its boundary conditions and loading

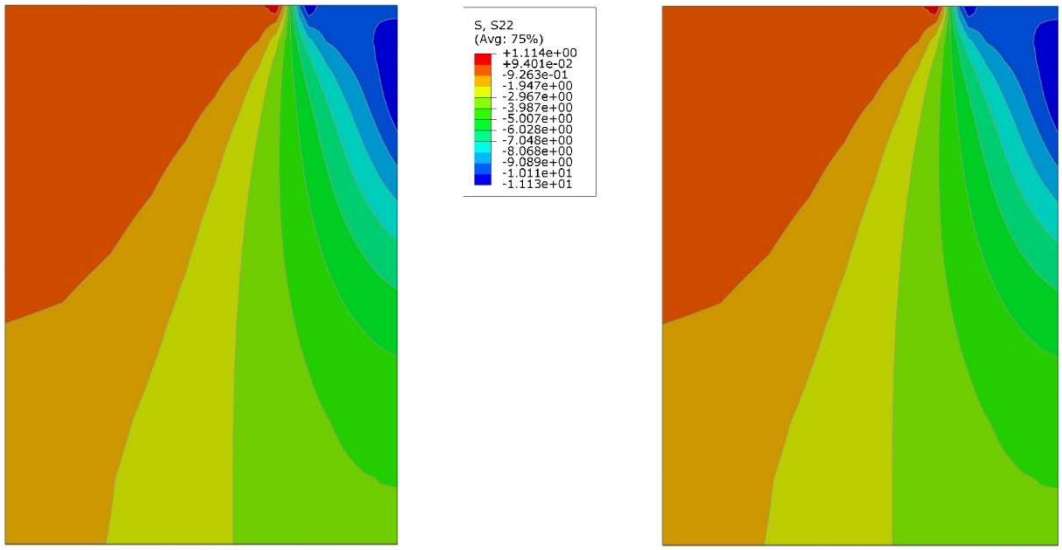

(a) (b)

Figure 5.11: Comparison between vertical stress contours in (a) standard FEM (b) EPR-FEM

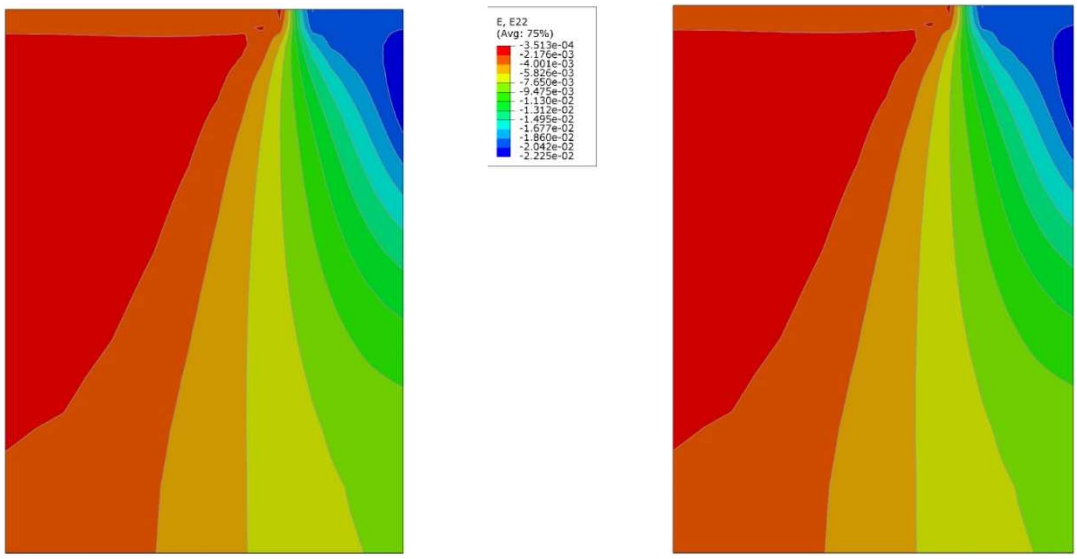

(a) (b)

Figure 5.12: Comparison between vertical strain contours in (a) standard FEM (b) EPR-FEM

From the above figures it can be seen that the results of the EPR-based FE analysis are in a very good agreement with the standard FEM results.

5.3.1.3 Example 3: A plate under biaxial tension (non-linear elastic)

A finite element model of the hypothetical test conducted in section 4.2.2, chapter 4, is employed here in order to find the best EPR model representing the nonlinear material behaviour. In section 4.2.2, it was shown that EPR has returned one equation for each stress (three in total) at every evolutionary step. Using these equations, the Jacobian matrix corresponding to each evolutionary step (10 in total) is constructed. For instance, the Jacobian matrix for the 2nd evolutionary step of EPR is as follow:

$$\mathbf{J} = \begin{bmatrix} 149.97 & 0.0 & 0.0 \\ 0.0 & 150.50 & 0.0 \\ 0.0 & 0.0 & 72.64 \end{bmatrix} \qquad 5.25$$

The calculated Jacobian matrix for each evolutionary step is implemented in finite element to analyse the model of the material test. The finite element mesh of the model is shown in Figure 5.13.

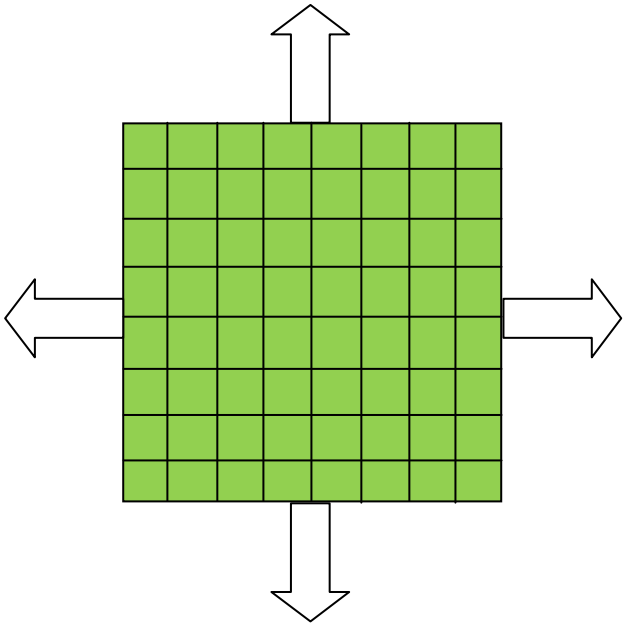

Figure 5.13: Finite element model of the material test conducted in section 4.2.2

After analysis, the stress-strain curve of each model is recorded to compare the stress-strain behaviour of the different evolutionary steps provided by EPR. These stress-strain curves are presented in the following figure.

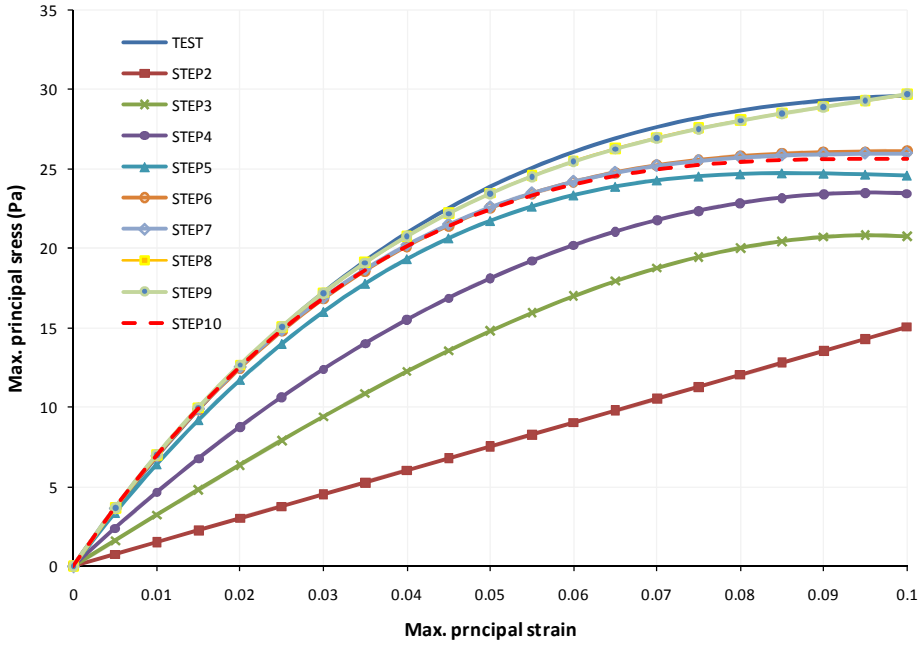

Figure 5.14: Stress-strain curve, obtained from different evolutionary steps

Since the EPR model corresponding to the first evolutionary step consisted of a constant value, its Jacobian matrix becomes zero and therefore it is not possible to perform an analysis for the 1st step. From the figure it can be seen that as the EPR steps increase, the predictions provided by EPR models become closer to the test data. Once the EPR model from the 8th step is incorporated in the FE, it is seen that the results are in a very good agreement with the test data; this is also valid for the 9th step. However it can be seen that the 10th model (red dashed line) has provided less accurate results in compared to the 8th and 9th steps. One reason for this could be the over-fitting problem in the EPR equations of 10th model. From the results of this example it can be concluded that the best EPR model representing the material tested in section 4.2.2 is 8th model (equations 4.26, 4.36, 4.45). This model will be used to analyse the next two numerical examples.

5.3.1.4 Example 4: Plate with a circular hole (non-linear elastic)

The same plate used in example 1 (section 5.3.1.1) with same geometry and boundary conditions is used for the fourth example. This time the plate is under tension loading on both right and top sides. The EPRCM selected from the previous example is used to represent the material behaviour.

The EPR-based Jacobian matrix is then implemented in the finite element model to analyse the plate with the circular hole (Figure 5.15) under a biaxial tension which is applied through prescribed boundary conditions of 5 mm on each side.

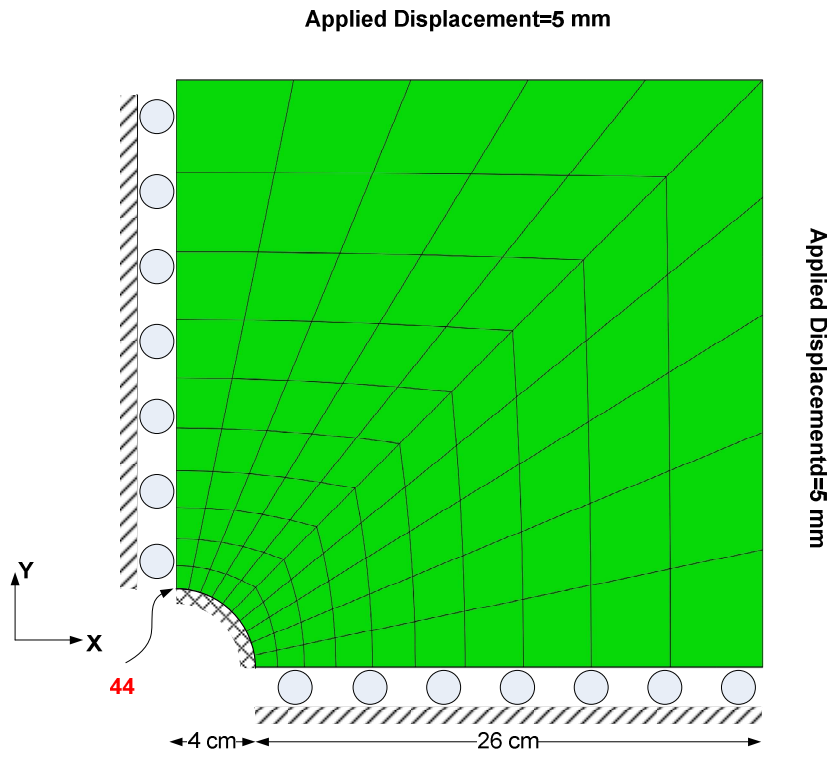

Figure 5.15: A plate with circular hole at its centre under tension loading along both X and Y direction

The plate was also analysed using a standard finite element model. For the standard finite element analysis an existing elasto-plastic material model in ABAQUS was chosen, in which for the elastic part the elastic modulus and Poisson's ratio were used and a tabulated stress-strain data was entered for the plastic part. The data for the Elastic properties and tabulated stress-strain were obtained from the hypothetical test discussed in chapter 4 (section 4.2.2). The results of the analysis of this problem using the two material models are compared in Figure 5.16 and Figure 5.17. In these figures major and minor principal stresses are shown for standard FE analysis and EPR-based finite element analysis. The maximum difference between the major principal stress from standard FEM and EPR-FEM is 4.2%. This value for the minor principal stress is 7.3%. The average difference between the major principal stress in standard FE and EPR-FE is 1.67% while the average difference for the minor principal stress is 4.48%. Small differences can be spotted between two results; however apart from that, the figures show that EPR has been able to predict the nonlinear behaviour of the material and provided a good estimation of the resulting stresses in the plate due to the biaxial tension loading.

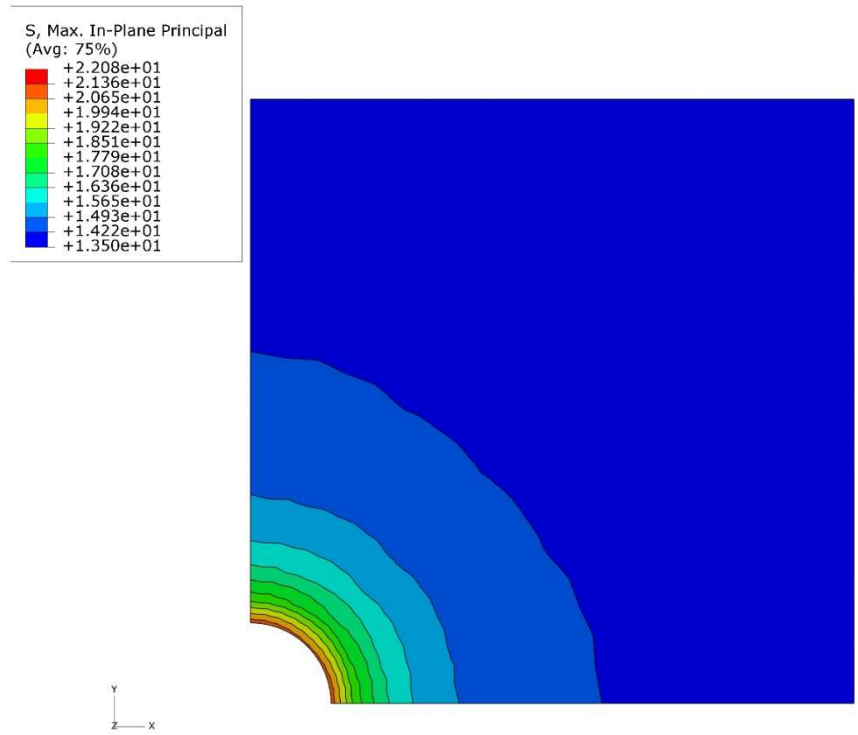

(a)

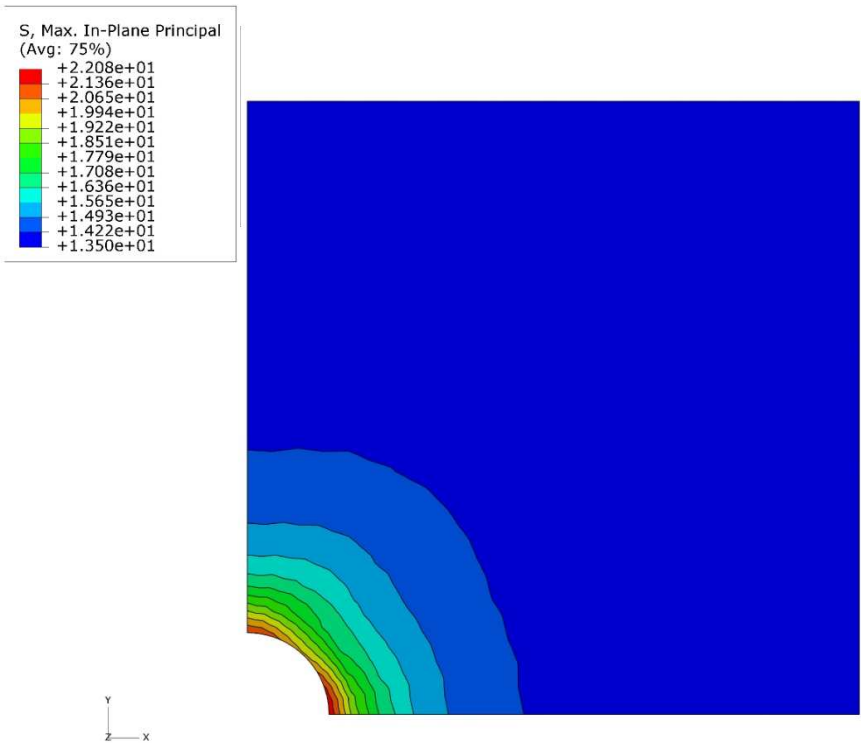

(b)

Figure 5.16: Comparison of max principal stress (a) results of the standard FE analysis (b) results of the EPR-based FE analysis

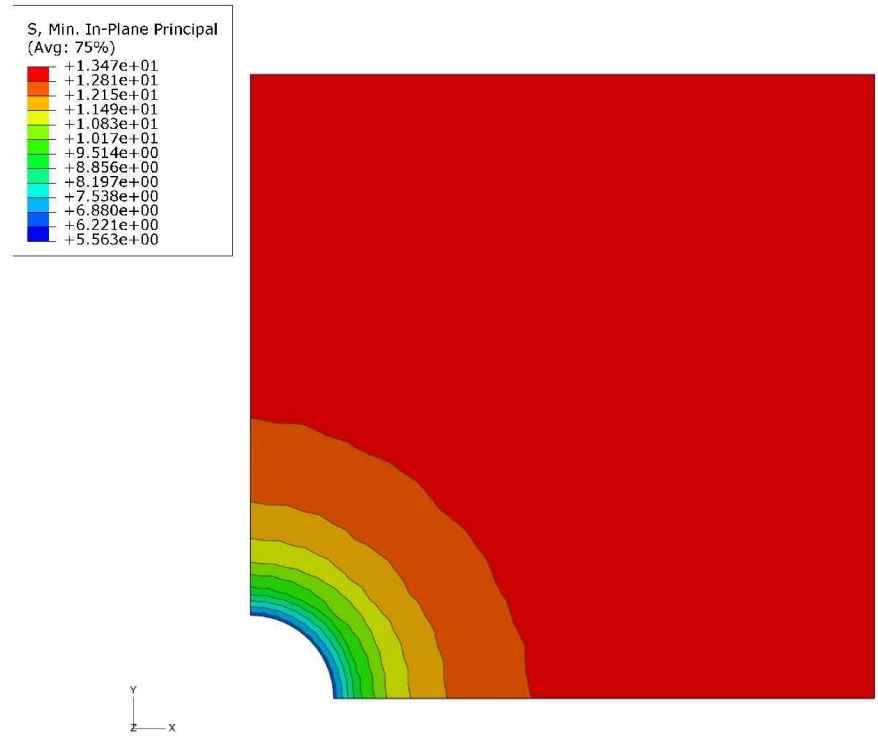

(a)

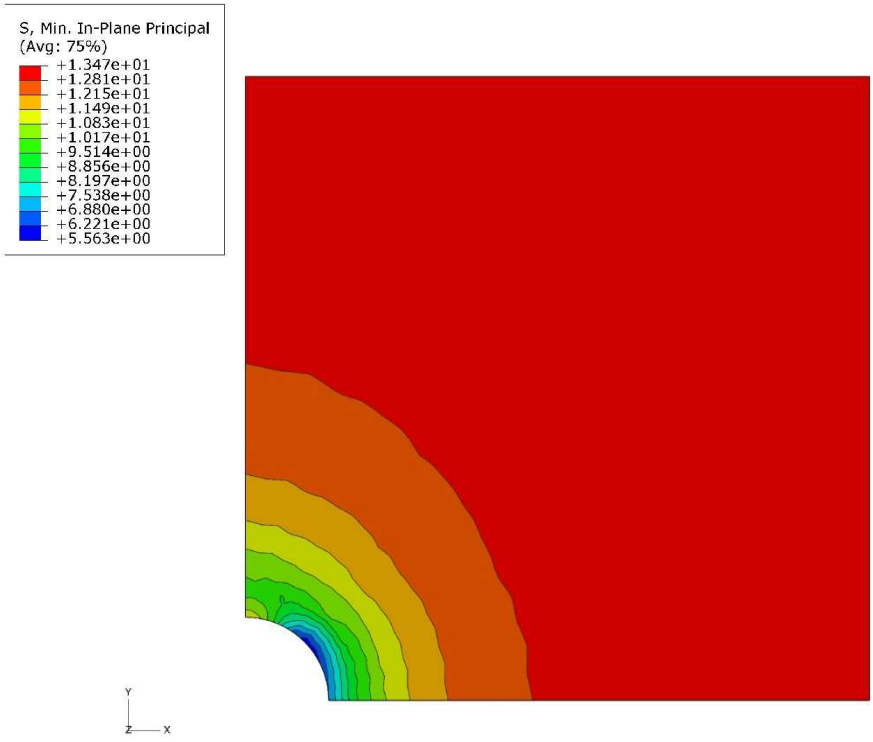

(b)

Figure 5.17: Comparison of min principal stress (a) results of standard FE analysis (b) results of the EPR-based FE analysis

5.3.1.5 Example 5: Plate subjected to an in-plane load (nonlinear elastic)

The same plate as the one presented in example 2 with same geometry and boundary conditions is employed here to compare the results of nonlinear FE analyses using standard FEM and EPR-FEM. It is assumed that the panel material is identical to the one used in example 4. For standard FE analysis elasto-plastic material model with Young's modulus and Poisson's ratio for elastic region and tabulated stress-strain data for plastic region are used. It is also assumed that the EPR equations developed for this material (discussed in example 3) are valid and can be used to establish the Jacobian matrix. The panel is loaded using two biaxial prescribed displacements of 1 cm as shown in Figure 5.18.

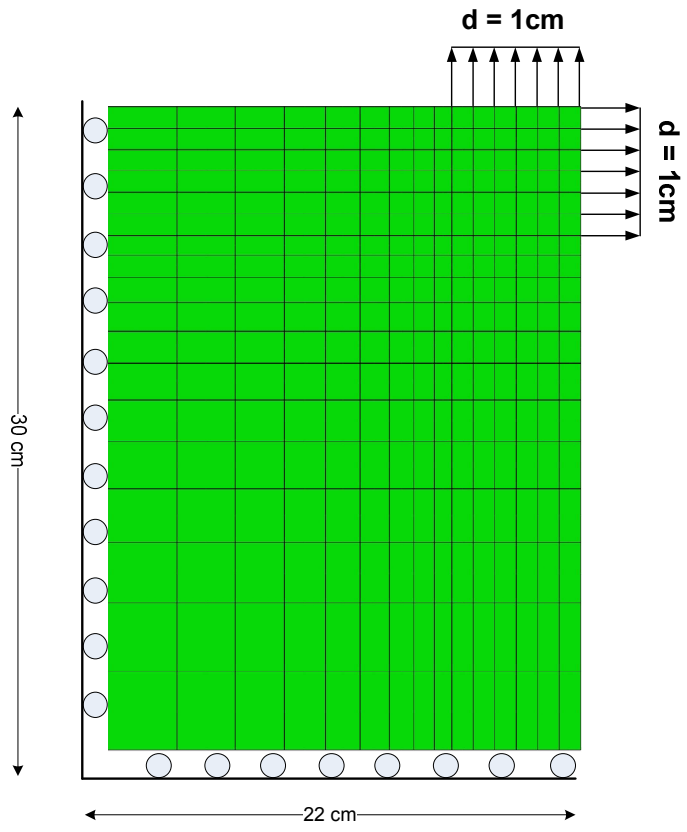

Figure 5.18: The FE mesh and geometry of plane stress panel under biaxial tension loading

The results of the two different analyses are compared in terms of maximum stresses and maximum strains. The results reveal that the EPR-FEM provides a very close (less than 2% difference for max principal stress and less than 0.7% for max principal strain) prediction to those of the standard FEM.

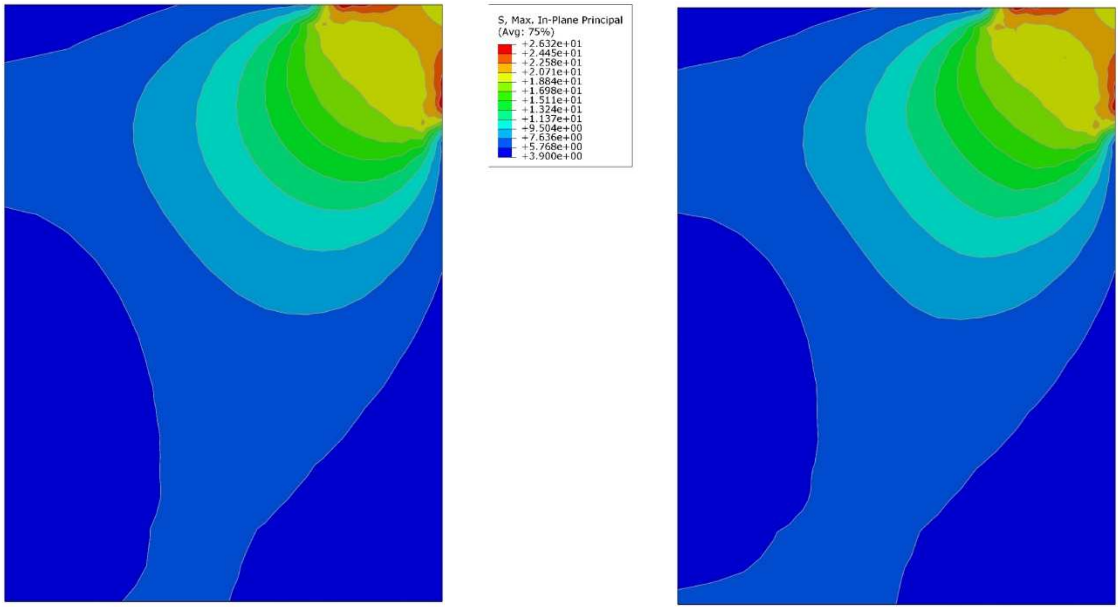

(a) (b)

Figure 5.19: Contours of max principal stress (a) standard FE (b) EPR-FEM

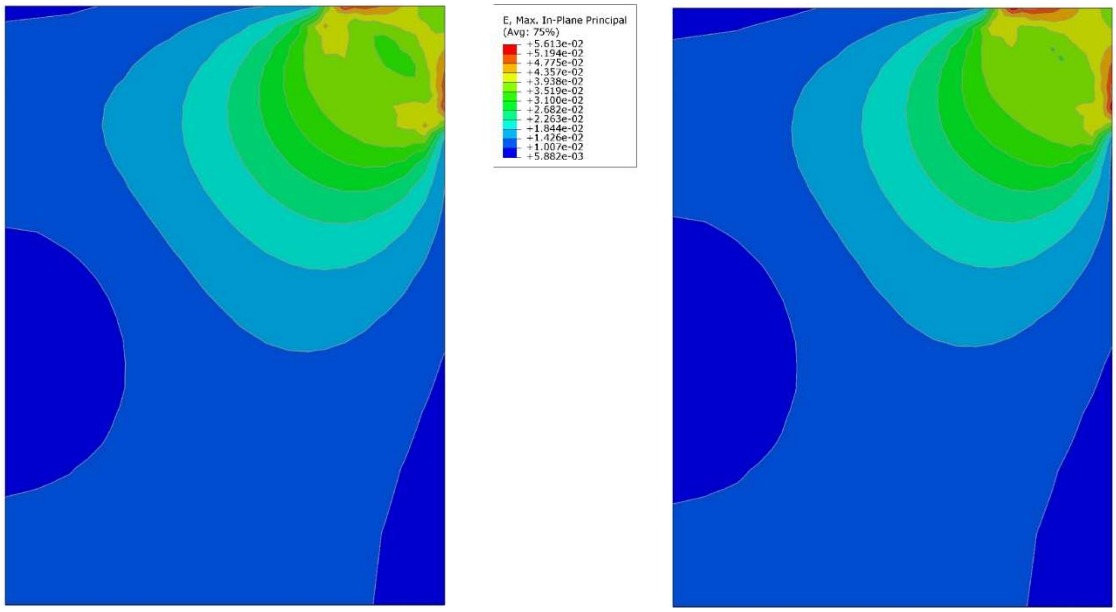

(a) (b)

Figure 5.20: Contours of max principal strains (a) standard FE (b) EPR-FEM

5.4 Incorporation of EPR models (incremental stress-strain strategy) in FEM

The developed EPR-based material models can also be implemented in the finite element method in a different manner from that presented in section 5.2. This strategy takes advantage of the definition of the elastic stiffness matrix which is usually described in terms of elastic parameters. The constitutive relationships are generally given in the following form (Owen & Hinton, 1980):

$$\delta\boldsymbol{\sigma} = \mathbf{D}\delta\boldsymbol{\varepsilon} \tag{5.26}$$

where **D** is material stiffness matrix, also known as the Jacobian matrix. For an isotropic and elastic material, matrix **D** can be expressed in terms of two elastic constants. Generally there are six different elastic constants E (Young Modulus), ν (Poisson's ratio), G (shear modulus), K (bulk modulus), λ (Lame's first parameters), and M (P-wave modulus) to describe elastic behaviour of materials (Timoshenko & Goodier, 1970). However for isotropic materials, only two of these parameters are required to form stiffness matrix since they are all related to each other through the following equations.

$$K = \frac{E}{3(1-2\nu)} \tag{5.27}$$

$$\lambda = \frac{E\nu}{(1-2\nu)(1+\nu)} \tag{5.28}$$

$$G = \frac{E}{3(1+\nu)} \tag{5.29}$$

$$M = \frac{E(1-\nu)}{(1+\nu)(1-2\nu)} \tag{5.30}$$

In order to construct the stiffness matrix in this section, the material constitutive models developed in section 4.3 are used. Therefore the function of EPR-based material model in a FE model (at every element's integration point) can be described as follows:

(I) For the i+1th load increment, the input pattern for the EPR-based material model contains (1) the values of $(\acute{p}^i, q^i, \varepsilon_v^i, \varepsilon_q^i)$ which have already been

calculated in the previous load increment and (2) value of $\Delta\varepsilon_q^i$. The new values of q^{i+1} and ε_v^{i+1} are then calculated for the next step.

(II) For each load increment the material Young's modulus, $\mathrm{E_{EPR}}$ and the Poisson's ratio, ν_{EPR} can be calculated from the relationship between the relevant stresses and strains. For example for axisymmetric condition:

$$\mathrm{E_{EPR}} = \frac{\Delta q^i}{\Delta\varepsilon_1^i} \tag{5.31}$$

$$\nu_{\mathrm{EPR}} = \left(\frac{1 - \frac{\Delta\varepsilon_v^i}{\Delta\varepsilon_1^i}}{2} \right) \tag{5.32}$$

Once the stiffness matrix is built it will be implemented in the finite element analysis in the same way described in the previous section. The EPR-based finite element method does not require yielding, plastic potential, failure functions, flow rules, etc. In this method the conventional elasto-plastic stiffness matrix will be replaced by the EPR stiffness matrix and the problem will be treated as a nonlinear problem from beginning to the end of analysis. This is more straightforward than conventional finite element method and can save lots of computational time since there is no need to check the yielding, compute gradients of the plastic potential curve, update the yield surface etc. A number of examples are provided in the next section to show the capabilities of this approach.

5.4.1 Numerical Examples

To illustrate the developed computational methodology, five numerical examples of application of the developed EPR-based finite element method to engineering problems are presented. In the first example, the application of the methodology to a simple case of linear elastic material behaviour is examined. In the second example, the method is applied to a boundary value problem involving the analysis of stresses and strains around a tunnel considering nonlinear and elasto-plastic material behaviour. In the third and fourth examples, the proposed method is applied to analyse the deformation of 2D and 3D foundation under vertical pressure. And finally in the fifth example the

application of the method to the analysis of the behaviour of soil under cyclic loading is presented.

5.4.1.1 Example 1: circular cylinder under internal pressure

This example involves a thick circular cylinder conforming to plane strain geometrical condition. Figure 5.21 shows the geometric dimensions and the element discretisation employed in the solution where 12 8-node isoparametric elements have been used. The cylinder is made of linear elastic material with Young's modulus of $E=2.1\times10^5$ N/mm^2 and a Poisson's ratio of 0.3 (Owen & Hinton, 1980). This example was deliberately kept simple in order to verify the computational methodology by comparing the results with those of a linear elastic finite element model. The compressibility of the material is assumed to be negligible and hence the EPR model for volumetric strain is not considered in this example. The loading considered involves an internal pressure of 80.0 MPa as shown in Figure 5.21.

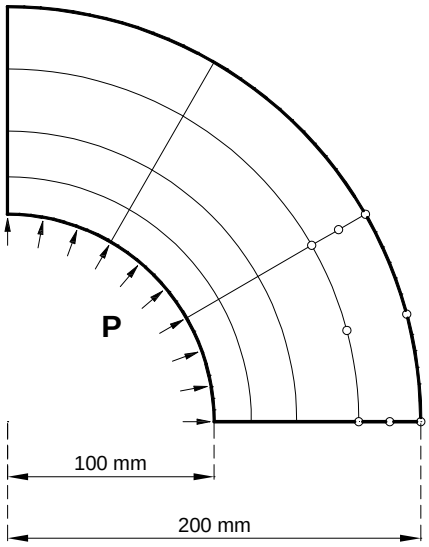

Figure 5.21: FE Mesh in symmetric quadrant of a thick cylinder

Figure 5.22 (a) shows a linear elastic stress-strain relationship with a gradient of 2.1×10^5. The slope of this line represents the elastic modulus, E, for the material. The data from this figure were used to train the EPR model in order to capture the linear stress-strain relationship for the material. After training, the selected EPR model is as follow:

$$q^{i+1} = -\frac{1.47 \times 10^{-8}}{\Delta\varepsilon} - 3.47 \times 10^{-6}\sqrt{q^i} + 2.42 \times 10^{11}(\Delta\varepsilon + \varepsilon) - 0.005\varepsilon\sqrt{q^i} + 0.012 \quad 5.33$$

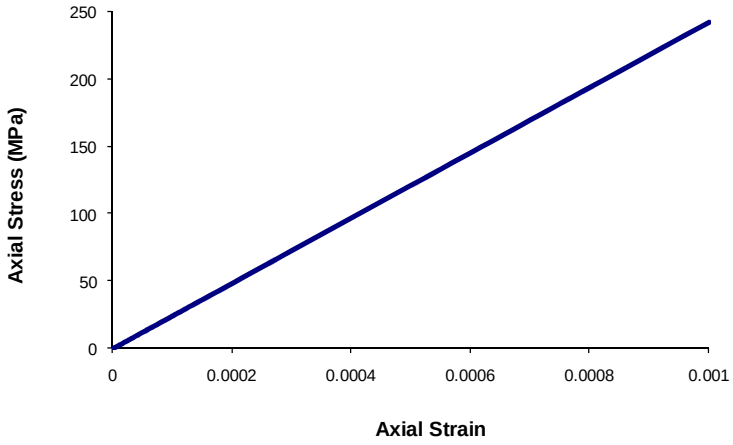

(a)

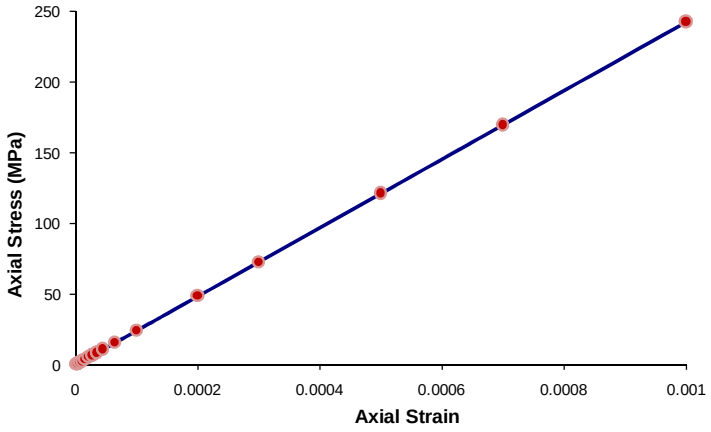

(b)

Figure 5.22: (a) Linear stress-strain relationship used for training, (b) the results of EPR predictions (red circles) for stress-strain value

Figure 5.22 (b) shows the stress-strain relationship predicted by the EPR model, together with the original one. It is seen that after training, the EPR model has successfully captured the stress-strain relationship with a precise accuracy.

The EPR-based finite element model incorporating the trained EPR model was used to analyse the behaviour of the cylinder under applied internal pressure. The results are compared with those obtained using a standard linear elastic finite element method.

Figure 5.23 shows the radial displacement and radial stresses predicted by the two methods. Comparison of the results shows that the results obtained using the EPR-based FEM are in excellent agreement with those obtained from the standard finite element analysis. This shows the potential of the developed EPR-based finite element method in deriving constitutive relationships from raw data using EPR and using these relationships to solve boundary value problems.

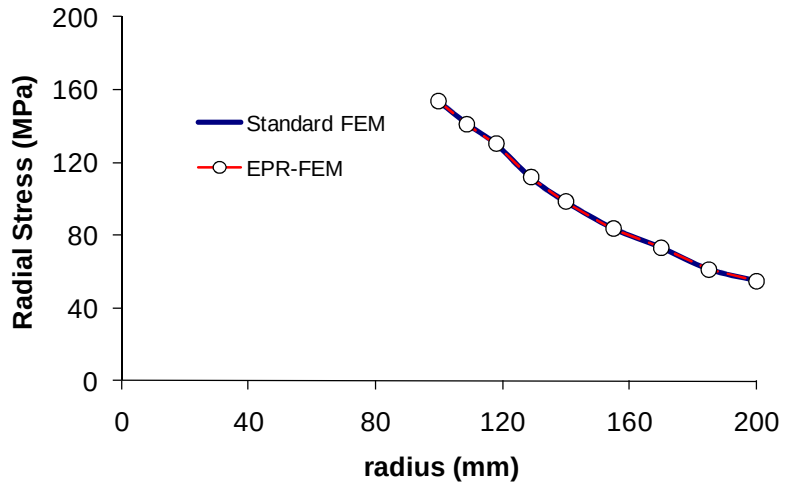

(a)

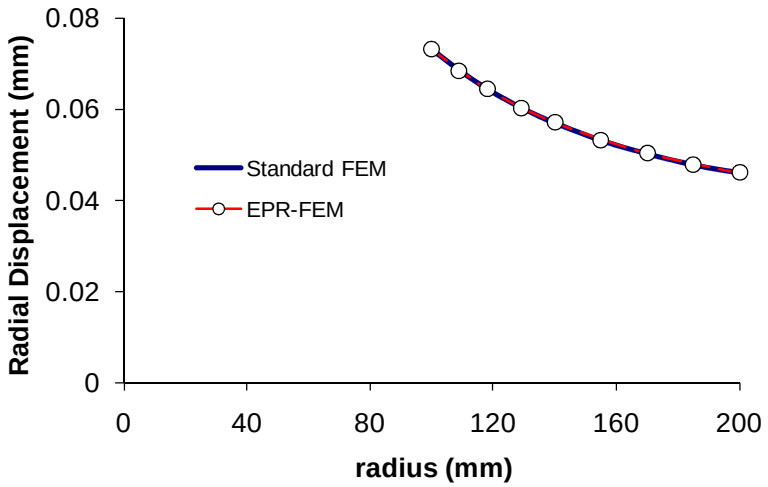

(b)

Figure 5.23: Comparison of the results of the EPR-FEM and standard FEM solution (a) radial stress, (b) radial displacement

5.4.1.2 Example 2: Tunnel subjected to gravity and excavation loading

This example involves the analysis of deformations around a tunnel subjected to excavation and gravity loadings. The geometry of the tunnel and the finite element mesh are shown in Figure 5.24.

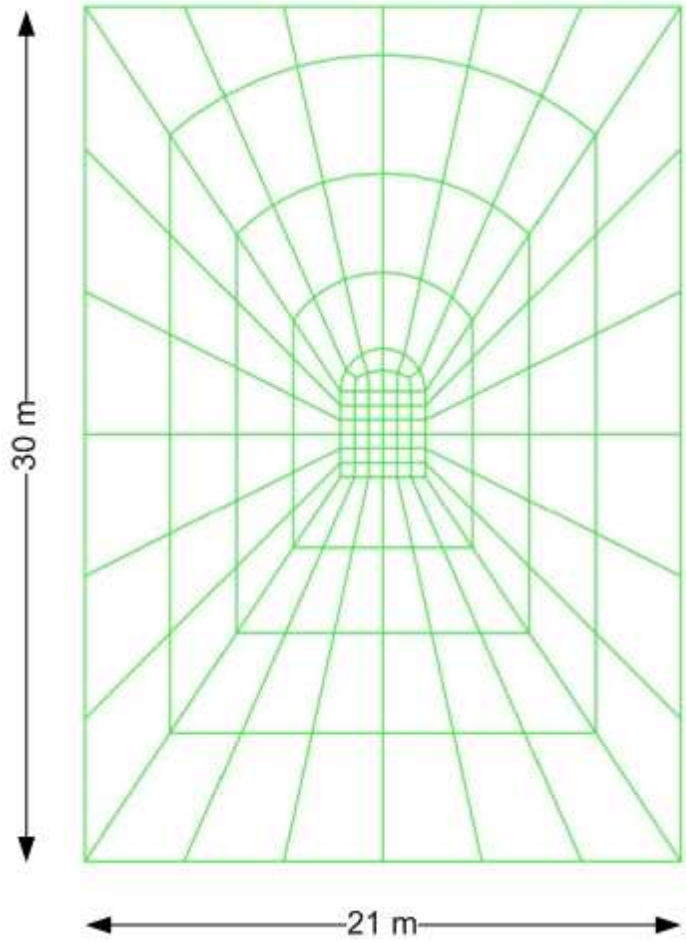

Figure 5.24: Geometry of the tunnel and the FE mesh

The finite element mesh includes 142 8-node isoparametric elements and 451 nodes. The depth of the tunnel crown from the ground surface is 12 meters. The analysis is done in two steps. The first step includes a geostatic analysis where all the elements are subjected to gravity loading. In the second step 46 elements representing the tunnel elements, are removed to simulate the excavation process. It was assumed that the soil tested in chapter 4 section 4.3.2, is representative of the soil material around the tunnel. The problem was analysed using three different constitutive models, (a) Mohr-Coulomb (MC), (b) Modified Cam Clay (MCC), and (c) EPR-based material model. For the first two methods the material parameters presented in chapter 4, Table 4.3 were entered in

finite element software (ABAQUS) and the tunnel was analysed under gravity and excavation loading. For the EPR-based material model, the models developed in chapter 4, section 4.3.2 (equations 4.56 and 4.57), were used to construct the stiffness matrix. Then the obtained stiffness matrix was implemented in user material subroutine (UMAT) in ABAQUS. The FE model incorporating the EPR models was then used to simulate the behaviour of the tunnel under gravity and excavation loadings.

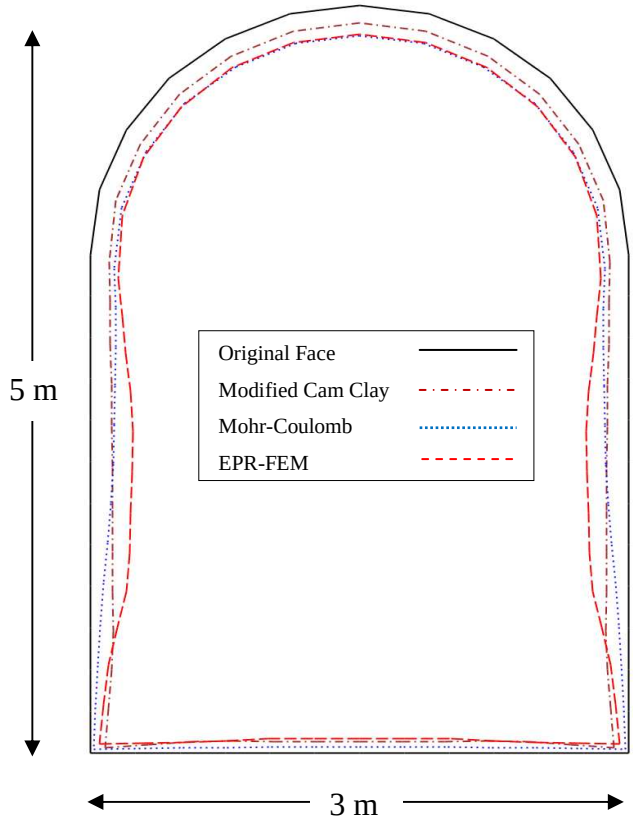

Figure 5.25: Comparison between the results of the EPR-FEM and conventional FE using Mohr-Coulomb and Modified Cam Clay models

Figure 5.25 shows the comparison between the displacements in the tunnel predicted by standard finite element analyses using MCC and MC constitutive models as well as the EPR-based finite element method where the raw data from the triaxial tests were directly used in deriving the EPR-based constitutive model (chapter 4, section 4.3.2). In this figure deformation of the tunnel face is magnified by a factor of 5 in order to show the difference between the three different approaches. The pattern of deformations is similar in all 3 analyses. Despite the relatively small difference between the results from the different analyses, it can be argued that the EPR-based FE results are more reliable, as this method used the original raw experimental data to learn the constitutive

relationships for the material and it did not assume any particular constitutive relationships, yield conditions, etc. in priori.

The results show that the developed EPR-FEM can offer very realistic prediction for the behaviour of complex structures.

5.4.1.3 Example 3: Settlement of a 2D shallow foundation

This example presents finite element analysis of a strip foundation using the EPR-based FEM. Settlement and stress distribution of the foundation is obtained using standard finite element method and EPR-FEM. The results of these two methods are compared to show the capability of the EPR-FEM. Plane strain geometrical condition is considered for modelling the foundation and due to the symmetry only half of the foundation is modelled. The finite element mesh of the foundation has 304 isoparametric 8-node element and 340 nodes. The geometry and finite element mesh of the foundation are presented in Figure 5.26. The density of the FE mesh is increased in the vicinity of the foundation since it is the zone of stress concentration. The footing is made of concrete but it's not modelled here to simplify the model. The foundation is constructed 2.5 meters beneath the surface and to simulate the foundation depth, the 2.5 meters layer of soil is replaced by an overburden pressure equivalent to the weight of soil.

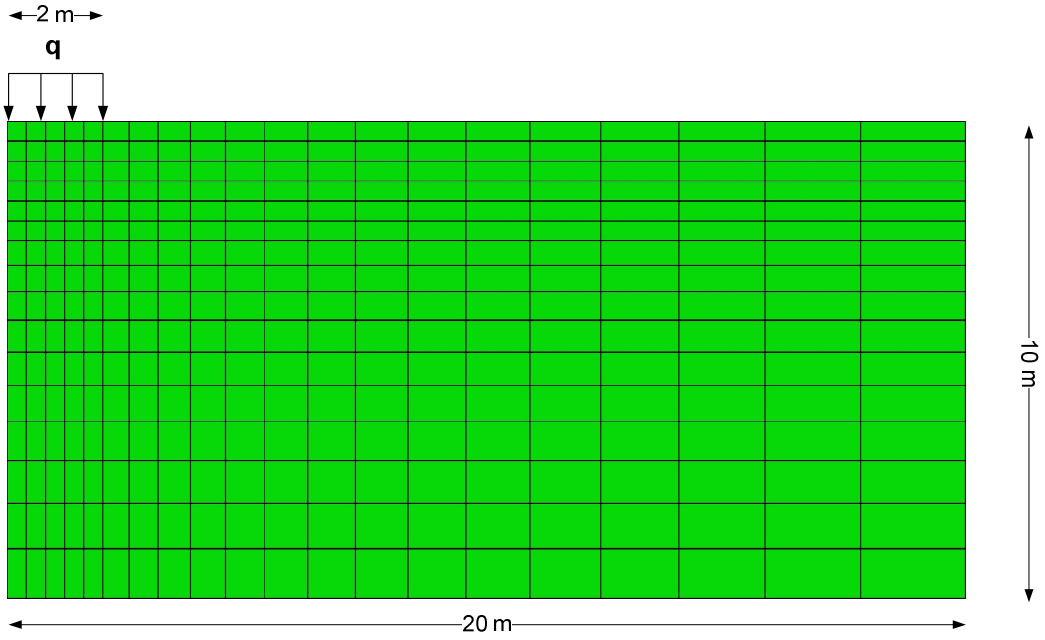

Figure 5.26: FE mesh and geometry of foundation

The soil material is same as the one introduced in chapter 4 section 4.3.2. The foundation was analysed under its weight as well as footing pressure of 150 kPa. For the standard finite element analysis, the Mohr-Coulomb and modified cam clay material constitutive models are employed, using material parameters presented in chapter 4, Table 4.3. Figure 5.27 shows the resulting max principal stress contours obtained from (a) standard FE using MCC constitutive model, and (b) EPR-based FEM.

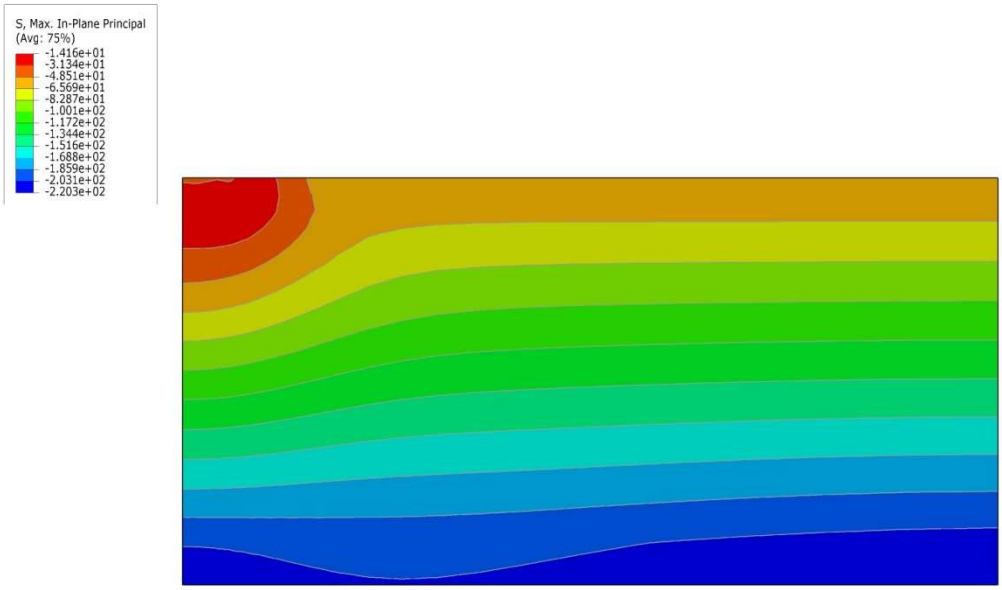

(a)

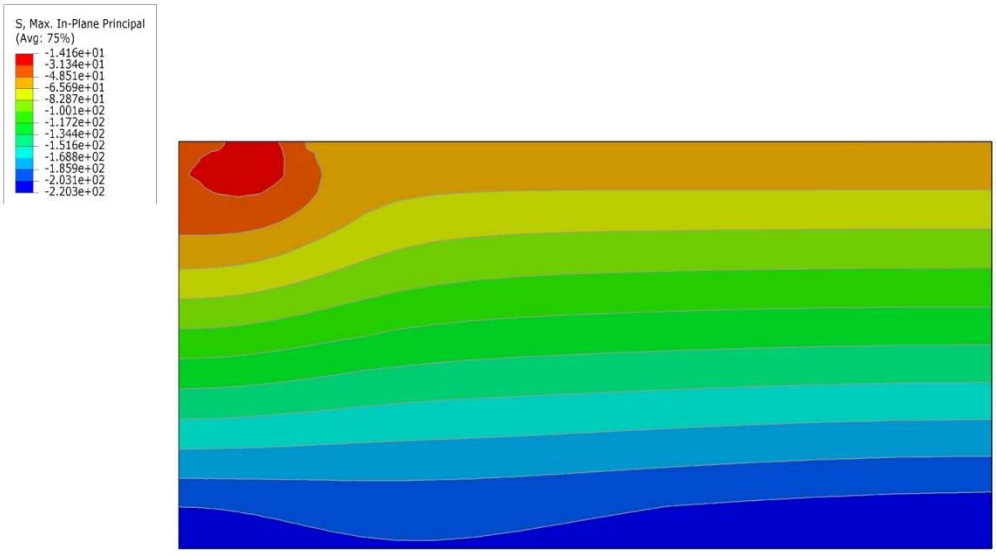

(b)

Figure 5.27: Distribution of max principal stress obtained from

(a) MCC-FEM (b) EPR-FEM

In addition, the settlement of the footing at its centre is presented in Figure 5.28. In this figure the surface settlements obtained from the standard FEM using MC and MCC models are compared with those obtained from the EPR-FEM. The settlement due to the gravity load is not considered in this graph. The EPR-FEM has predicted a larger settlement compared with the other two methods and MCC has especially provided a small deformation. This can be explained by the fact that MCC model underestimates the deformation for heavily over-consolidated soils (Gens & Potts, 1988; Mita et al., 2004) while EPR material model is providing a more realistic prediction (see chapter 4 section 4.3.4). For this reason it can be claimed that the results of EPR-FEM are more reliable than MCC-FEM especially for heavily over-consolidated soils as the EPR models are trained directly with raw data.

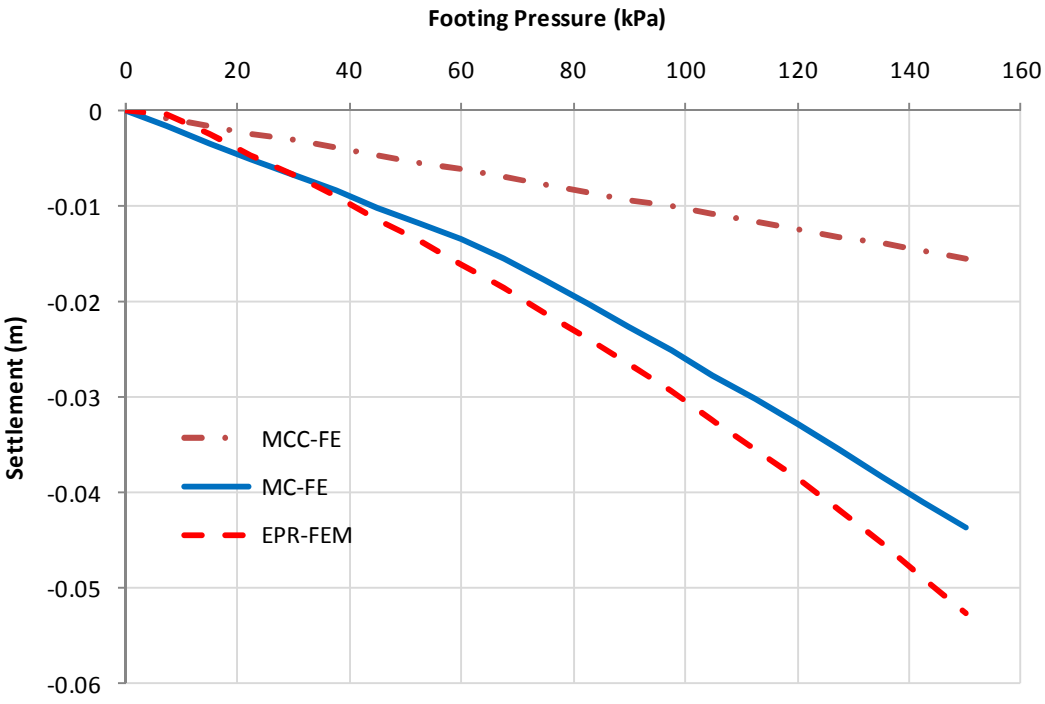

Figure 5.28: Comparison of the settlement of the footing obtained from standard finite element and EPR-FEM

5.4.1.4 Example 4: Settlement of a 3D shallow foundation

This example involves analysis of a square shallow foundation subjected to applied pressure of 150 kPa. Due to symmetry only a quarter of the domain is modelled and analysed. The geometry of the foundation and the finite element mesh are shown in Figure 5.29.

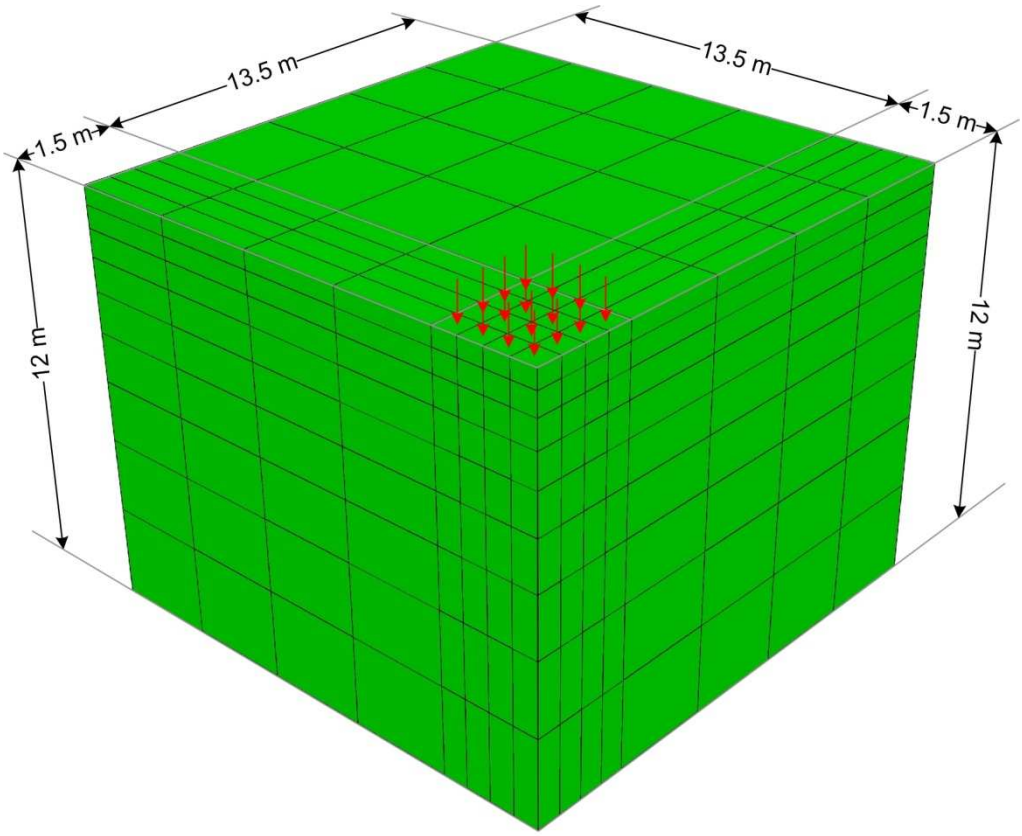

Figure 5.29: Dimension and finite element mesh of a quarter of the square shallow foundation

The finite element mesh includes 576 eight-node elements and 810 nodes. The aim of the analysis is to calculate settlement of the 3m×3m foundation on a 12m thick homogeneous layer of a soil, using Mohr-Coulomb and EPRCM based finite element method. The foundation is situated at a depth of 2.5m from ground level. It is assumed that the soil material is same as the one used in the 2D shallow foundation example.

Figure 5.30 shows the pressure-settlement curves for the centre of the foundation predicted by standard finite element analysis using the Mohr-Coulomb elasto-plastic

model as well as the EPR-based finite element method. In the initial elastic zone, the predictions of the two models are almost the same. As loading progresses, inelastic deformations start and differences appear in the prediction of pressure-settlement behaviour of the foundation.

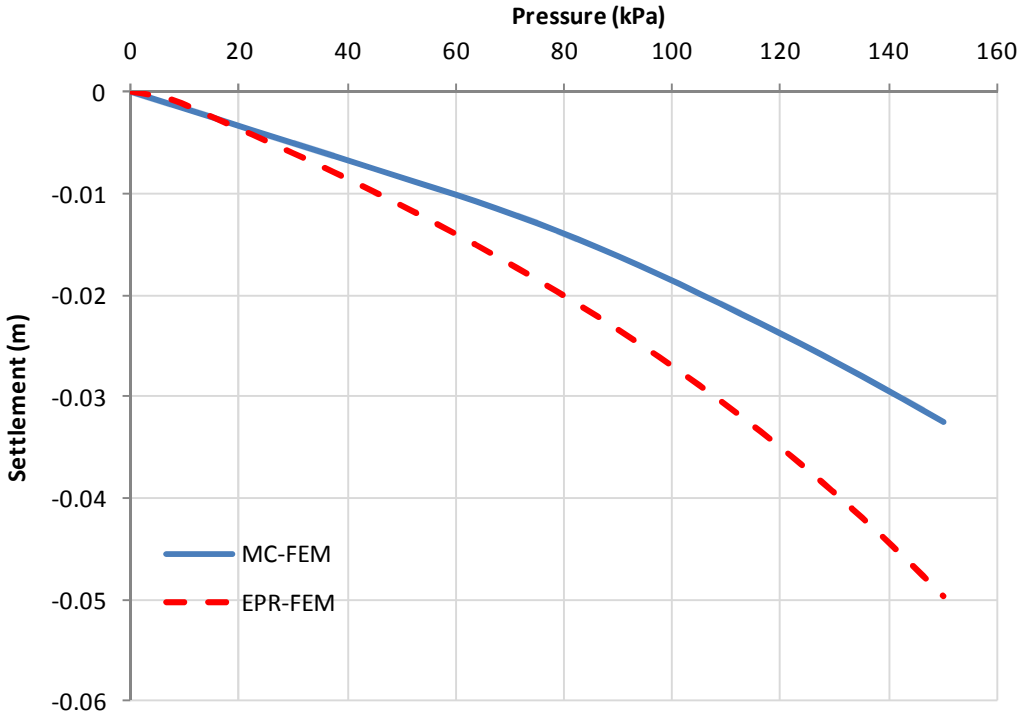

Figure 5.30: Comparison of the results for foundation settlement obtained from MC-FEM and EPR-FEM

In addition the contours of vertical stresses are plotted for both MC-FE and EPR-FE in Figure 5.31. Despite the difference between the results of the two different methods, their pattern is similar. It can be concluded that the developed EPR-model can be used to analyse three dimensional problems despite the fact that they have been constructed using data from a triaxial apparatus. It shows that the results of the EPR-based FEM are reliable and provide reasonable predictions (close to conventional methods) for 3D boundary value problems.

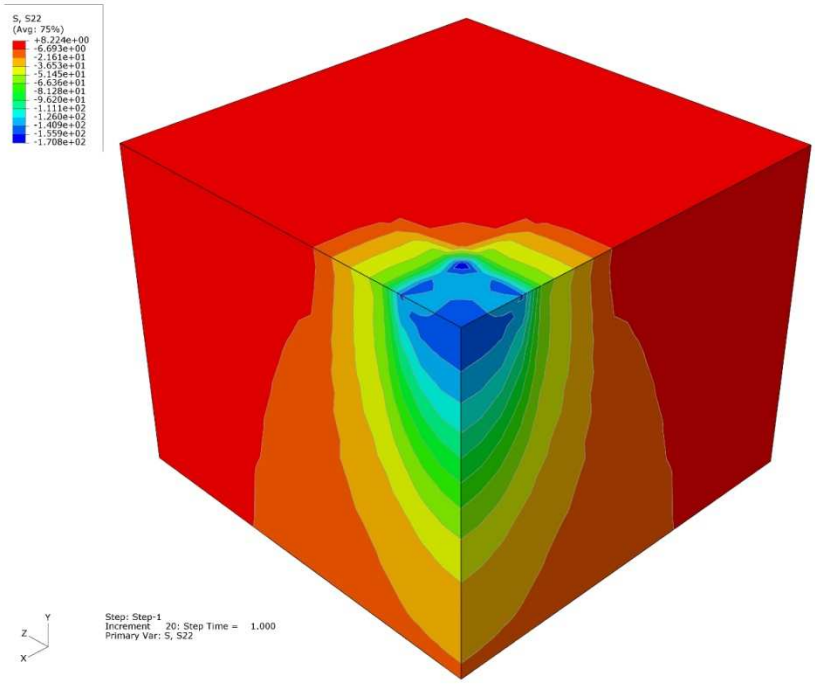

(a)

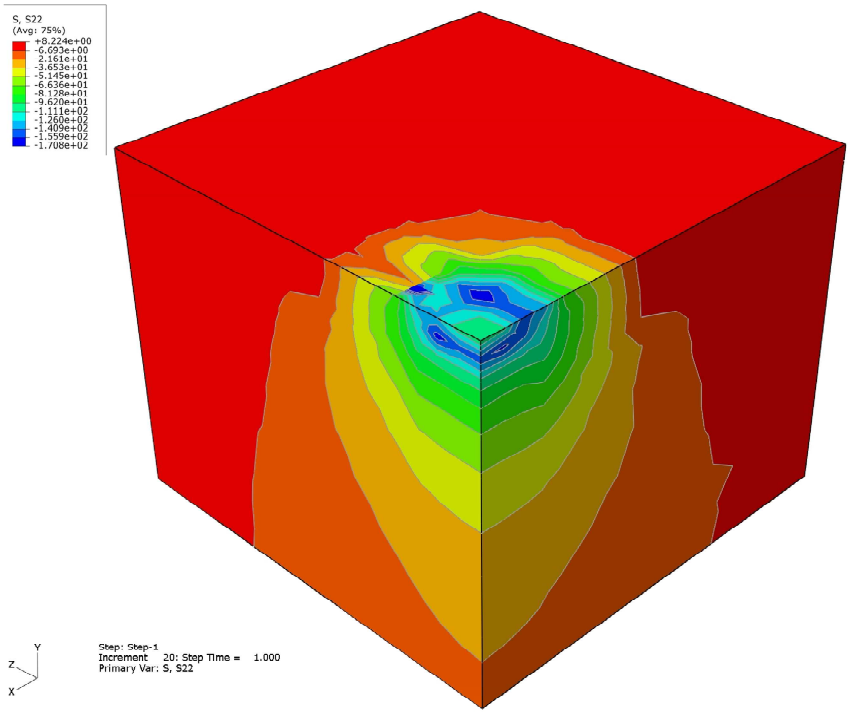

(b)

Figure 5.31: Vertical stress distribution in (a) MC-FEM (b) EPR-FEM

5.4.1.5 Example 5: Behaviour of soil under cyclic loading

In this example, the behaviour of soil is studied in triaxial tests under cyclic axial loading. The test data for this example were generated in chapter 4 section 4.3.5 by numerical simulation of triaxial experiments. The generated data were used to train, validate and develop EPR-based material models (equations 4.68 and 4.69). The developed models are incorporated in the EPR-based finite element model to represent the soil behaviour under cyclic loading. The results of the EPR-based FE analyses are compared with those attained using conventional finite element method. The performance of the EPR-FEM is evaluated for two separate cases of loading where the soil is subjected to (i) regular and (ii) irregular cyclic loading and unloading conditions.

(i) Multiple regular cycles

In the first case, the EPR-based FE model was used to simulate a triaxial test on a sample of the soil subjected to multiple and regular cycles at a confining pressure of 250 kPa which was an unseen case for EPR during its training (chapter 4, section 4.3.5). The loading cycles involved the application of a total axial strain of 8% in ten loading and unloading cycles.

The results of the EPR-FEM are compared with those attained using the conventional FE simulation in Figure 5.32. It is seen that the results of the EPR-FEM are in close agreement with those of the conventional FE simulation. It can be seen from the figure that, the EPR-based FE model is capable of solving boundary value problems involving cyclic loading with a good accuracy.

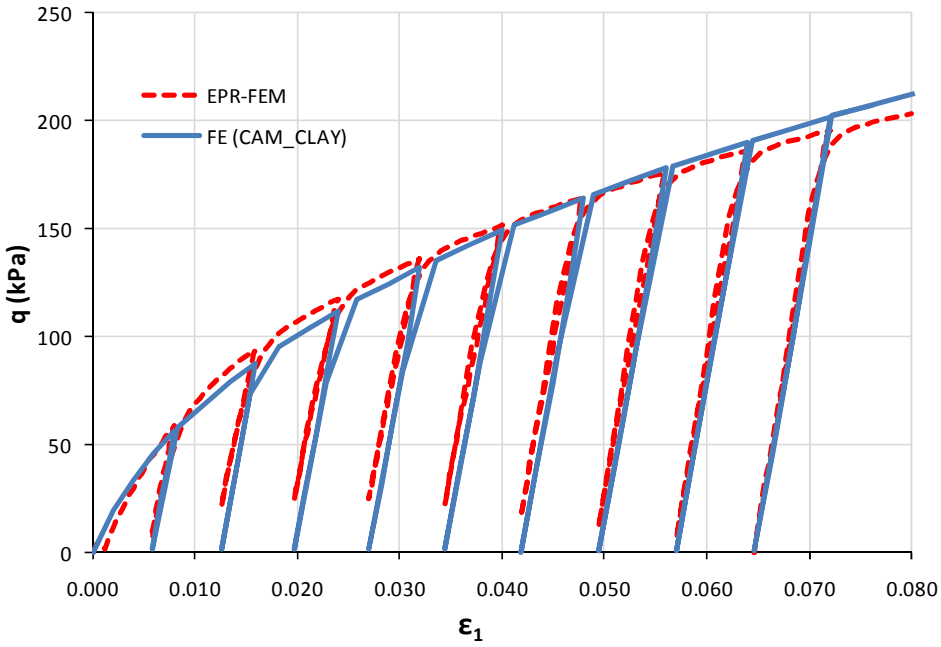

(a)

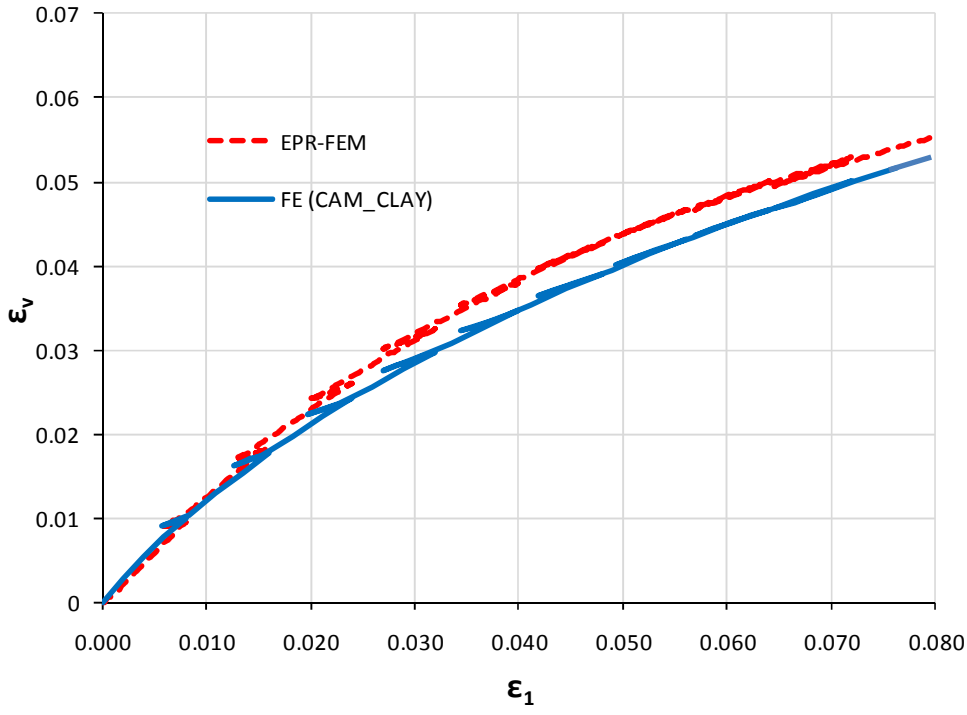

(b)

Figure 5.32: Comparison between the results of the EPR-FEM and conventional FE for multiple regular loading cycles (a) deviator stress (b) volumetric strain

(ii) Irregular loading cycles

In the first case, all the simulations (including those used for training and testing of the EPR) were performed with a regular loading pattern involving regular induced displacements in the cycles. This case is set out to examine if the EPR-based FE model, trained with regular cyclic loading data, would be able to generalise the training to predict the behaviour of the soil for irregular loading patterns that are different from those used for training of the EPR model. Although the loading pattern was different from that used for training of the EPR, the imposed strains (and loads) used in the simulation were kept within the ranges of values used for training so as to avoid extrapolation.

In this case, the EPR-FEM was used to simulate the behaviour of the soil with an irregular cyclic loading pattern as shown in Figure 5.33. The test was simulated at confining pressure of 250 kPa that was not introduced to the EPR during training. The test involved the application (and removal) of total axial strains of 1.6% and 4% in the first and second cycles respectively.

In Figure 5.33, the results of the EPR-FEM are compared with those obtained using the conventional FE simulation (using MCC model) of the same irregular pattern. From the figure, it can be seen that the results of the EPR-based FE simulation are in a very good agreement with those obtained using the conventional FE. The results are also compared with those obtained for a regular 5-cycle pattern with imposed strains of 0.8, 1.6, 2.4, 3.2, and 4 percent in cycles 1 to 5 respectively and has been depicted in Figure 5.34. Comparison of the results shows that, although the EPR was only trained with data from regular cyclic loading tests, the EPR-FEM was able to predict the behaviour of the soil under irregular loading patterns. It can be concluded that the EPR-FEM is also capable of generalising the behaviour of the soil for cyclic loading with different loading and unloading patterns. This further illustrates the robustness of the proposed EPR-FEM and shows the excellent capability of the method in capturing the underlying constitutive relationships for the material from raw data and generalising it to predict different conditions not introduced to the EPR during training.

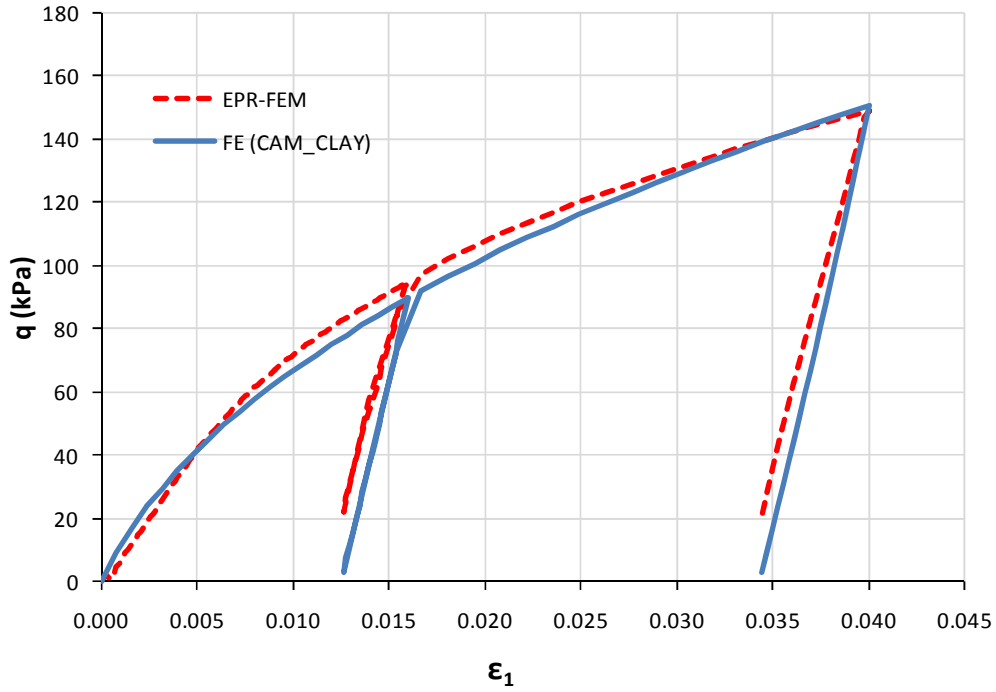

(a)

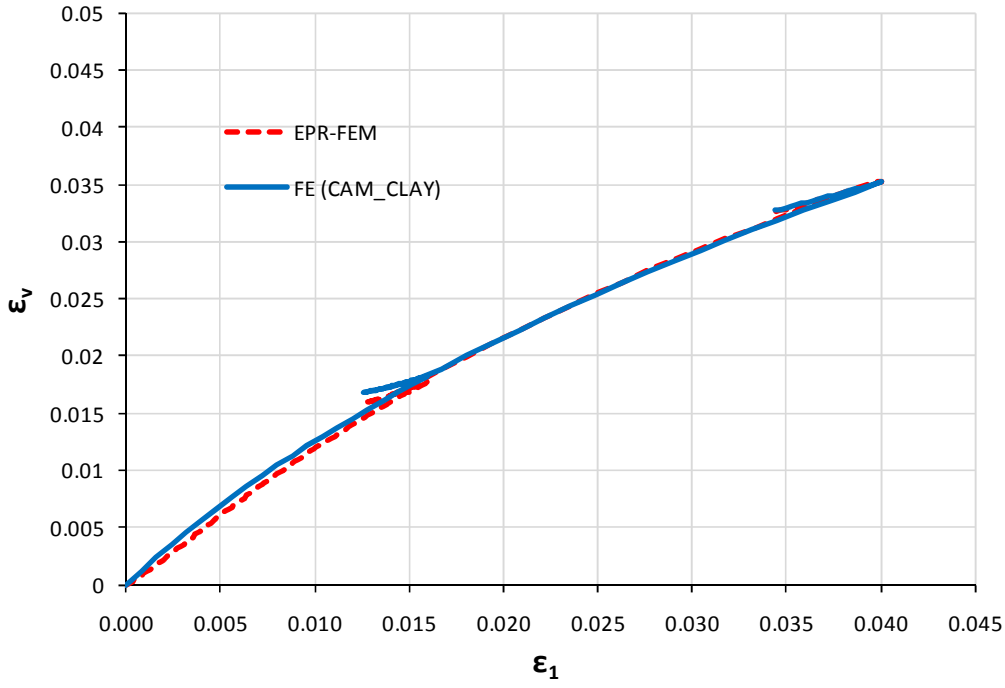

(b)

Figure 5.33: Comparison between the results of the EPR-FEM and conventional FE for two irregular loading cycles (a) deviator stress (b) volumetric strain

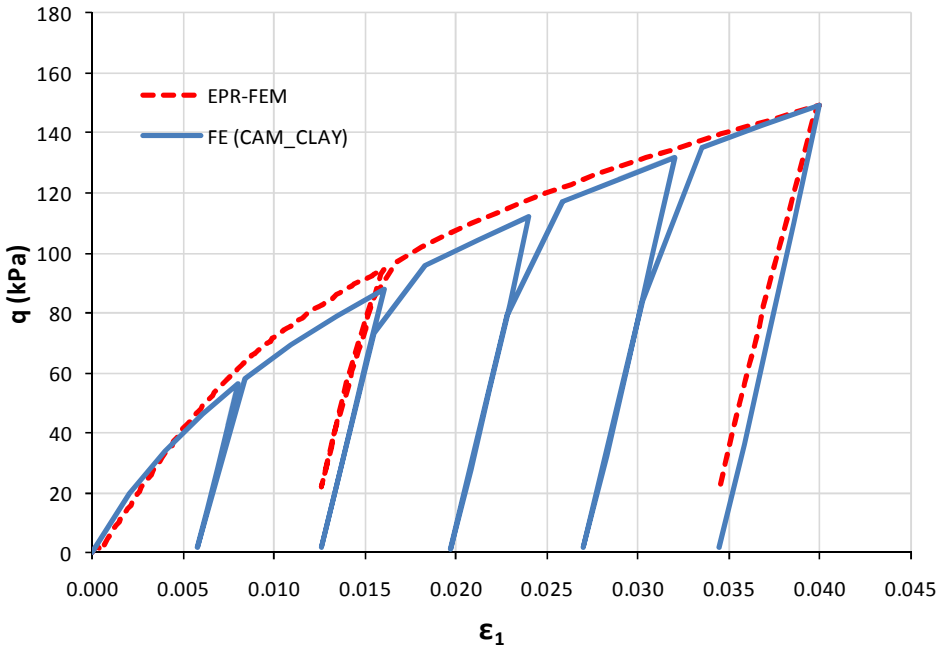

(a)

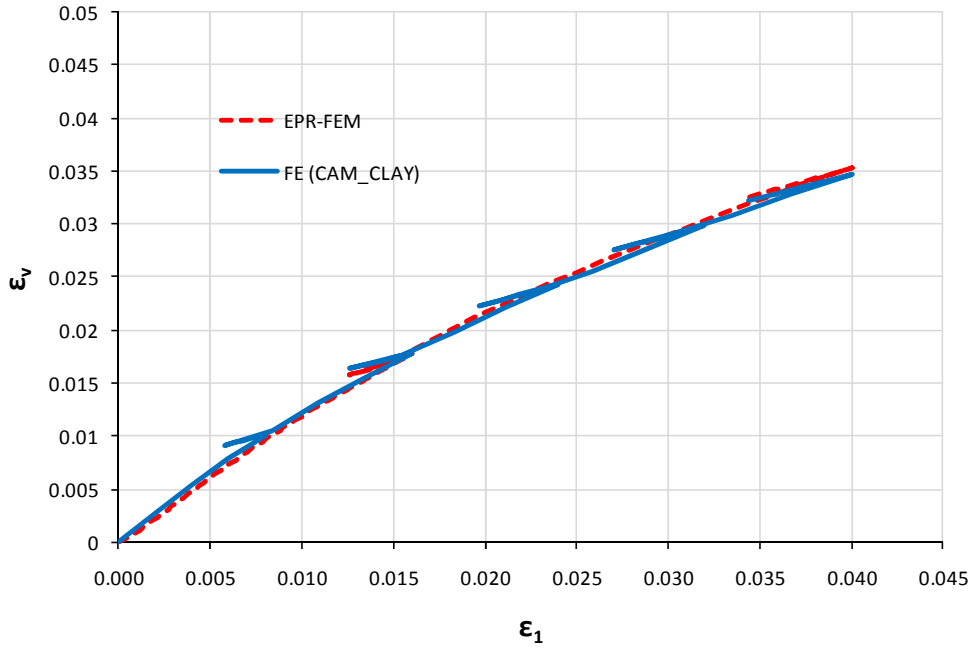

(b)

Figure 5.34: Comparison between the results of the EPR-FEM for 2 irregular loading cycles and the original cycle loading data used for training (a) deviator stress (b) volumetric strain.

Chapter 6

CONCLUDING REMARKS

6.1 Summary

In this thesis a novel approach is presented for material modelling in general and modelling the behaviour of soils in particular, using evolutionary polynomial regression (EPR). EPR is a hybrid data mining technique that searches for symbolic structures using a genetic algorithm and estimates the constant values by the least squares method. Stress-strain data from experiments were employed to train EPR and develop EPR-based material models. The developed models were compared to the existing conventional constitutive material models and their advantages were highlighted. It was also shown that the developed EPR-based material models can be incorporated in finite element (FE) analysis. Different examples were used to verify the developed EPR-based FEM. The results of the EPR-FEM were compared with standard FEM where conventional constitutive models were used to model the behaviour of materials. These results showed that EPR-FEM can be successfully employed to analyse different

structural and geotechnical engineering problems. The following are the achievements of this research in presenting a new framework for constitutive modelling in FEA:

- A total stress-strain strategy was introduced for developing EPR-based material models and a procedure was described to expand the data from a single experimental test on isotropic materials.
- Also an incremental strategy was presented and a set of actual experimental data on samples of a soil from a triaxial apparatus was considered to develop EPR models to predict the soil behaviour using this strategy.
- Volume change was modelled using EPR in order to predict volumetric behaviour of soils.
- A strategy was introduced to examine the developed EPR models using a point by point prediction of the entire stress paths.
- The implementation of the developed EPR models in commercial finite element software (ABAQUS) was presented.
- A model for simulating the behaviour of soil under cyclic loading was developed using EPR. It was shown that EPR can learn the behaviour of the material under complex and cyclic loading conditions taking into account the stress history of the soil.
- A methodology was introduced to incorporate the developed EPR models in FEM. It was shown that it is possible to construct the material stiffness matrix (also known as Jacobian) using partial derivatives of the developed EPR models. The EPR-based Jacobian matrix was implemented in FEM and a number of boundary value problems (including 2D and 3D problems as well as monotonic and cyclic loading conditions) were used to verify the methodology.

6.2 Conclusions

The following conclusions are drawn from the results of this thesis:

- The EPR has all the advantages of ANN and in addition it provides the user with transparent and practical mathematical equations.

- When modelling using EPR it should be noted that different EPR types and functions and their combinations should be explored to find the best model.

- The main benefits of using EPR-based material models are that it provides a unified approach to constitutive modelling of all materials (i.e., all aspects of material behaviour can be implemented within a unified environment of an EPR model); it does not require any arbitrary choice of the constitutive (mathematical) models.

- In EPR-based material models there are no material parameters to be identified and the model is trained directly from experimental data. It should be noted that identifying the material parameters from material tests can be a difficult and subjective process. This presents another disadvantage of conventional material models in comparison to EPR-based material models where there are no material parameters to determine. EPR is capable of learning the material behaviour directly from raw experimental data; therefore, EPR-based material models are the shortest route from experimental research (data) to numerical modelling.

- Another advantage of EPR based constitutive model is that as more experimental data become available, the quality of the EPR prediction can be improved by learning from the additional data, and therefore, the EPR model can become more effective and robust.

- A trained EPR-based model can be incorporated in a FE code in the same way as a conventional constitutive model. It can be incorporated either as incremental or total stress-strain strategies. An EPR-based FE method can be used for solving boundary value problems in the same way as the conventional FEM.

- The incorporation of an EPR-based constitutive model in FE procedure avoids the need for complex yielding/plastic potential/failure functions, flow rules, etc.; there is no need to check yielding, to compute the gradients of the plastic potential curve or to update the yield surface.

- It should be noted that, for practical problems, the data used for training EPR, should cover the range of stresses and strains that are likely to be encountered in practice. This is due to the fact that EPR models are good at interpolation but not so good at extrapolation. Therefore, any attempt to use EPR-based FE method for loading conditions that may lead to stresses or strains outside the range of the stresses and strains used in training of the EPR may lead to unacceptable errors.

- EPRCMs are especially useful for materials that their constitutive models are not well developed (e.g., biomaterials).

6.3 Recommendations for future research

- Although it was shown that it is possible to develop constitutive models for materials in general and in particular soils with both linear and non-linear behaviour using EPR; its application to materials with more complex behaviour (e.g., unsaturated soils) can be the subject of future works.

- In chapter 4 a strategy was introduced to extend and enrich data from a single laboratory experiment. However as it was mentioned there, the strategy was only applicable if the material under consideration was isotropic. The strategy should be extended to non-isotropic materials, as some materials like wood or some composites demonstrate orthotropic or non-isotropic behaviour.

- All the examples presented in chapter 5 are static and dynamic problems are not studied in this thesis. The capability of EPR to capture the behaviour of material under dynamic (e.g., earthquake) loading can be investigated. Appropriate boundary value examples that involve dynamic analysis should be used to validate the EPR-based FEM.

References

ABAQUS, 2007. *User Subroutine Reference Manual*. 683rd ed. Dassault Systems.

Ahangar-Asr, A., Faramarzi, A. & Javadi, A., 2010. A New Approach for Prediction of the Stability of Soil and Rock Slopes. *Engineering Computations*, 27(7), pp.878-93.

Ahangar-Asr, A., Faramarzi, A., Javadi, A. & Giustolisi, O., 2011. Modelling Mechanical Behaviour of Rubber Concrete Using Evolutionary Polynomial Regression. *Engineering Computations*, 28(4), pp.492-507.

Aquino, W. & Brigham, J.C., 2006. Self-learning finite elements for inverse estimation of thermal constitutive models. *International Journal of Heat and Mass Transfer*, 49(15-16), p.2466–2478.

Berardi, L. & Kapelan, Z., 2007. Multi-Case EPR Strategy for the Development of Sewer Failure Performance Indicators. In *Proceedings of the World Environmental and Water Resources Congress*. Tampa, Florida, USA, 2007.

Calado, L., De Matteis, G. & Landolfo, R., 2000. Experimental response of top and seat angle semi-rigid steel frame connections. *Materials and Structures*, 33(8), p.499–510.

Doglioni, A., 2004. *A Novel Hybrid Evolutionary Technique for Environmental Hydraulic Modelling*. PhD Thesis. Technical University of Bari, Italy.

Doglioni, A., Giustolisi, O., Savic, D. & Webb, B.W., 2008. An investigation on stream temperature analysis based on evolutionary computing. *HYDROLOGICAL PROCESSES*, 22(3), pp.315-26.

Drucker, D.C. & Prager, W., 1952. Soil mechanics and plastic analysis or limit design. *Q. Applied Mathematics*, 10(2), pp.157-75.

Ellis, G., Yao, C. & Zhao, R., 1992. Neural network modelling of mechanical behaviour of sand. In *Proceeding of the 9th ASCE Conference on Engineering Mechanics*. Texas, 1992.

Faramarzi, A., Mehravar, M., Veladi, H. & Javadi, A., 2011. A Hysteretic Model for Steel Plate Shear Walls. In *Proceedings of the 19th ACME Conference, 5-6 April*. Edinburgh, Heriot-Watt University, 2011.

Feng, X. & Yang, C., 2004. Coupling recognition of the structure and parameters of non-linear constitutive material models using hybrid evolutionary algorithms. *International Journal for Numerical Methods in Engineering*, 59(9), p.1227–1250.

Fu, Q., Hashash, Y.M.A., Jung, S. & Ghaboussi, J., 2007. Integration of laboratory testing and constitutive modeling of soils. *Computers and Geotechnics*, 34(5), p.330–345.

Furukawa, T. & Hoffman, M., 2004. Accurate cyclic plastic analysis using a neural network material model. *Engineering Analysis with Boundary Elements*, 28(3), p.195–204.

Gens, A. & Potts, D.M., 1988. Critical state models in computational geomechanics. *Engineering Computations*, 5(3), pp.178 - 197.

Ghaboussi, J., Garret, J.H. & Wu, X., 1991. Knowledge-based modelling of material behaviour with neural networks. *Journal of Engineering Mechanics Division*, 117(1), pp.153-64.

Ghaboussi, J., Kim, J. & Elnashai, A.S., 2010. Hybrid modelling framework by using mathematics-based and information-based methods. In *IOP Conference Series: Materials Science and Engineering*., 2010.

Ghaboussi, J., Pecknold, D.A., Zhang, M. & Haj-Ali, R.M., 1998. Autoprogressive training of neural network constitutive models. *International Journal for Numerical Methods in engineering*, 42(1), pp.105-26.

Ghaboussi, J. & Sidarta, D.E., 1998. New nested adaptive neural networks (NANN) for constitutive modelling. *Computers and Geotechnics*, 22(1), pp.29-52.

Ghaboussi, J., Sidarta, D.E. & Lade, P.V., 1994. Neural network based modelling in geomechanics. In *Proceeding of the 8th International Conference on Computer Methods and Advances in Geomechanics*. Morgantown, 1994.

Giustolisi, O. & Laucelli, D., 2005. Increasing generalisation of input-output artificial neural networks in rainfall-runoff modelling. *Hydrological Sciences Journal*, 50(3), pp.439-57.

Giustolisi, O. & Savic, D., 2006. A symbolic data-driven technique based on evolutionary polynomial regression. *Journal of Hydroinformatics*, 8(3), pp.207-22.

Giustolisi, O. & Savic, D.A., 2009. Advances in data-driven analyses and modelling using EPR-MOGA. *Journal of Hydroinformatics*, 11(3-4), pp.225-36.

Goldberg, D., 1989. *Genetic Algorithms in Search, Optimization, and Machine Learning*. ADDISON-WESLEY.

Golub, G.H. & Van Loan, C.F., 1993. *Matrix Computations*. London: The John Hopkins University Press.

Haj-Ali, R. & Kim, H., 2007. Nonlinear constitutive models for FRP composites using artificial neural networks. *Mechanics of Materials*, 39(12), p.1035–1042.

Hashash, Y.M.A., Fu, Q. & Butkovich, J., 2004 b. Generalized strain probing of constitutive models. *International Journal for Numerical and Analytical Methods in Geomechanics*, 28(15), p.1503–1519.

Hashash, Y.M.A., Fu, Q., Ghaboussi, J., Lade, P.V., Saucier, C., 2009. Inverse analysis–based interpretation of sand behavior from triaxial compression tests subjected to full end restraint. Canadian Geotechnical Journal, 46(7), p.768–791.

Hashash, Y.M.A., Ghaboussi, J., Fu, Q. & Marulanda, C., 2006 c. Constitutive Soil Behavior Representation via Artificial Neural Networks: A Shift from Soil Models to Soil Behavior Data. In *Proceedings of GeoCongress 2006: Geotechnical Engineering in the Information Technology Age*. Atlanta, 2006 c.

Hashash, Y.M.A., Ghaboussi, J. & Jung, S., 2006 b. Characterizing Granular Material Constitutive Behavior Using SelfSim with Boundary Load-Displacement Measurements. In *Proceedings of the Tenth Biennial ASCE Aerospace Division International Conference on Engineering, Construction, and Operations in Challenging Environments*. Houston, USA, 2006 b.

Hashash, Y.M.A., Jung, S. & Ghaboussi, J., 2004. Numerical implementation of a neural network based material model in finite element analysis. *International Journal for Numerical Methods in Engineering*, 59(7), p.989–1005.

Hashash, Y.M.A., Levasseur, S., Osouli, A., Finno, R., Malecot, Y., 2010. Comparison of two inverse analysis techniques for learning deep excavation response. Computers and Geotechnics, 37(3), p.323–333.

Hashash, Y.M.A., Marulanda, C., Ghaboussi, J. & Jung, S., 2003. Systematic update of a deep excavation model using field performance data. *Computers and Geotechnics*, 30(6), p.477–488.

Hashash, Y.M.A., Marulanda, C., Ghaboussi, J. & Jung, S., 2006. Novel Approach to Integration of Numerical Modeling and Field Observations for Deep Excavations. *ASCE Journal of Geotechnical and Geoenvironmental Engineering*, 132(8), pp.1019-31.

Hashash, Y.M.A. & Song, H., 2008. The Integration of Numerical Modeling and Physical Measurements through Inverse Analysis in Geotechnical Engineering. *KSCE Journal of Civil Engineering*, 12(3), pp.165-76.

Hashash, Y.M.A., Song, H. & Osouli, A., 2011. Three-dimensional inverse analyses of a deep excavation in Chicago clays. *International Journal for Numercial and Analytical Methods in Geomechanics*, 35(9), pp.1059-75.

Helwany, S., 2007. *Applied Soil Mechanics with ABAQUS Applications*. John Wiley & Sons, Inc.

Hooke, R., 1675. *A description of helicopes, and some other instruments*. London.

Javadi, A., Faramarzi, A. & Farmani, R., 2011. Design and Optimization of Microstructure of Auxetic Materials. *Engineering Computations*, 29(3), In press.

Javadi, A., Johari, A., Ahangar-Asr, A., Faramarzi, A., Toll, D.G., 2010. Prediction of the behaviour of unsaturated soils using evolutionary polynomial regression: An incremental approach. In *5th International Conference on Unsaturated Soils, 6-8 September*. Barcelona, Spain, 2010.

Javadi, A.A. & Rezania, M., 2009a. Applications of artificial intelligence and data mining techniques in soil modelling. *Geomechanics and Engineering, An International Journal*, 1(1), pp.53–74.

Javadi, A.A. & Rezania, M., 2009b. Intelligent finite element method: An evolutionary approach to constitutive modeling, *Advanced Engineering Informatics*, 23(4), pp. 442-451.

Javadi, A.A., Tan, T.P. & Elkassas, A.S.I., 2004 a. An intelligent finite element method. In *Proceeding of the 11th International EG-ICE Workshop*. Weimar, Germany, 2004 a.

Javadi, A.A., Tan, T.P. & Elkassas, A.S.I., 2005. Intelligent finite element method. In *Proceeding of the 3rd MIT Conference on Computational Fluid and Solid Mechanics*. Cambridge, Massachusetts, USA, 2005.

Javadi, A.A., Tan, T.P. & Elkassas, A.S.I., 2009. Intelligent Finite Element Method and Application to Simulation of Behavior of Soils under Cyclic Loading. In A. Abraham. & a. et, eds. *FOUNDATIONS OF COMPUTATIONAL INTELLIGENCE*. Springer-Verlag. pp.317-38.

Javadi, A.A., Tan, T.P., Elkassas, A.S.I. & Zhang, M., 2004 b. Intelligent finite element method: Development of the algorithm. In *Proceeding of the 6th World Congress on Computational Mechanics-WCCM VI*. Beijing, China, 2004 b.

Javadi, A.A., Tan, T.P. & Zhang, M., 2003. Neural network for constitutive modelling in finite element analysis. *Computer Assisted Mechanics and Engineering Sciences*, 10(4), pp.375-81.

Javadi, A.A., Zhang, M. & Tan, T.P., 2002. Neural network for constitutive modelling of material in finite element analysis. In *Proceedings of the 3rd International Workshop/Euroconference on Trefftz Method*. Exeter, UK, 2002.

Jung, S. & Ghaboussi, J., 2006a. Neural network constitutive model for rate-dependent materials. *Computers and Structures*, 84(15-16), p.955–963.

Jung, S. & Ghaboussi, J., 2006b. Characterizing rate-dependent material behaviors in self-learning simulation. *Computer Methods in Applied Mechanics and Engineering*, 196(1-3), pp.608-19.

Jung, S. & Ghaboussi, J., 2010. Inverse identification of creep of concrete from in situ load-displacement monitoring. *Engineering Structures*, 32(2), pp.1437-45.

Jung, S., Ghaboussi, J. & Marulanda, C., 2007. Field calibration of time-dependent behavior in segmental bridges using self-learning simulation. *Engineering Structures*, 29(10), pp. 2692–2700.

Kessler, B.S., El-Gizawy, A.S. & Smith, D.E., 2007. Incorporating Neural Network Material Models Within Finite Element Analysis for Rheological Behavior Prediction. *Journal of Pressure Vessel Technology*, 192(2), pp.58-65.

Kim, J., Ghaboussi, J. & Elnashai, A.S., 2010. Mechanical and informational modeling of steel beam-to-column connections. *Engineering Structures*, 32(2), pp.449-58.

Koza, J.R., 1992. *Genetic Programming: On the Programming of Computers by Natural Selection*. Cambridge, MA.: MIT Press.

Kukreti, A.R. & Abolmaali, A.S., 1999. Moment–rotation hysteresis behavior of top and seat angle steel frame connections. *Journal of Structural Engineering* , 125(8), p.810–820.

Lade, P.V., 1977. Elasto-plastic stress-strain theory for cohesionless soil with curved yield surfaces. *International Journal of Solids and Structures*, 13(11), pp.1019-35.

Lade, P.V. & Jakobsen, K.P., 2002. Incrementalization of a single hardening constitutive model for frictional materials. *International Journal for Numerical and Analytical Methods in Geomechanics*, 26, pp.647-59.

Laucelli, D. & Giustolisi, O., 2011. Scour depth modelling by a multi-objective evolutionary paradigm. *Environmental Modelling & Software*, 26(4), pp.498-509.

Lu, M., AbouRizk, S.A. & Hermann, U.H., 2001. Sensitivity analysis of neural networks in spool fabrication productivity studies. *ASCE Journal of Computing in Civil Engineering*, 15(4), pp.299-308.

Mita, K.A., Dasari, G.R. & Lo, K.W., 2004. Performance of a Three-Dimensional Hvorslev–Modified Cam Clay Model for Overconsolidated Clay. *ASCE International Journal of Geomechanics*, 4(4), pp.296-310.

Najjar, Y.M. & Huang, C., 2007. Simulating the stress–strain behavior of Georgia kaolin via recurrent neuronet approach. *Computers and Geotechnics*, 34(5), p.346–361.

Nezami, E.G., Hashash, Y.M.A. & Ghaboussi, J., 2006. A Model for Large Scale Near-Real Time Simulation of Granular Material Flow. In *Proceedings of the Tenth Biennial ASCE Aerospace Division International Conference on Engineering, Construction, and Operations in Challenging Environments*. Houston, USA, 2006.

Osouli, A., Hashash, Y.M.A. & Song, H., 2010. Interplay between Field Measurements and Soil Behavior for Capturing Supported Excavation Response. *ASCE Journal of Geotechnical and Geoenvironmental Engineering*, 36(1), pp.69-84.

Owen, D.R.J. & Hinton, E., 1980. *Finite Element in Plasticity: Theory and Practice*. Swansea: Pineridge Press Limited.

Penumadu, D. & Zhao, R., 1999. Triaxial compression behaviour of sand and gravel using artificial neural networks (ANN). *Computers and Geotechnics*, 24(3), pp.207-30.

Rezania, M., 2008. Evolutionary Polynomial Regression Based ConstitutiveModelling and Incorporation in Finite Element Analysis. PhD Thesis, University of Exeter, Exeter, UK

Rezania, M., Faramarzi, A. & Javadi, A., 2011. An evolutionary based approach for assessment of earthquake-induced soil liquefaction and lateral displacement. *Engineering Applications of Artificial Intelligence*, 24(1), pp.142-53.

Schofield, D.S. & Worth, C.P., 1968. *Critical state soil mechanics*. London: McGraw-Hill.

Shin, H.S., 2001. *Neural network based constituive models for finite element analysis*. PhD dissertation University of Wales Swansea, UK.

Shin, H.S. & Pande, G.N., 2000. *Neural Network based Finite Element Analysis of Composite Materials*. CR/1011/00. Swansea: University of Wales University of Wales.

Shin, H.S. & Pande, G.N., 2000. On self-learning finite element code based on monitored response of structures. *Computers and Geotechnics*, 27, pp.161-78.

Shin, H.S. & Pande, G.N., 2001. Intelligent finite elements. In *Proceeding of Asian-Pacific Conference for Computational Mechanics-APCOM 01*. Sydney, Australia, 2001.

Shin, H.S. & Pande, G.N., 2002. Enhancement of data for training neural network based constitutive models for geomaterials. In *Proceeding of The 8th International Symposium on Numerical Models in Geomechanics-NUMOG VIII*. Rome, Italy, 2002.

Shin, H.S. & Pande, G.N., 2003. Identification of elastic constants for orthotropic materials from a structural test. *Computers and Geotechnics*, 30(7), p.571–577.

Sidarta, D.E. & Ghaboussi, J., 1998. Constitutive modelling of geomaterials from non-uniform material tests. *Computers and Geotechnics*, 22(1), pp.53-71.

Stasa, F.L., 1986. *Applied Finite Element Analysis for Engineers*. CBS College Publishing.

Timoshenko, S.P. & Goodier, J.N., 1970. *Theory of Elasticity*. McGraw-Hill.

Tsai, C. & Hashash, Y.M.A., 2008. A novel framework integrating downhole array data and site response analysis to extract dynamic soil behavior. *Soil Dynamics and Earthquake Engineering*, 28(3), p.181–197.

YU, H.S., 1998. CASM: A unified state parameter model. *International Journal For Numerical And Analytical Methods In Geomechanics*, 22(8), pp.621-23.

Yun, G.J., Ghaboussi, J. & Elnashai, A.S., 2006 a. Neural network-based constitutive model for cyclic behaviour of materials. In *Proceeding of the 1st European Conference on Earthquake Engineering and Seismology*. Geneva, Switzerland, 2006 a.

Yun, G.J., Ghaboussi, J. & Elnashai, A.S., 2006 b. Self-learning simulation for modeling of beam-column connections in steel frames. In *Proceeding of the 4th International Conference on Earthquake Engineering*. Taipei, Taiwan, 2006 b.

Yun, G.J., Ghaboussi, J. & Elnashai, A.S., 2008 a. A new neural network-based model for hysteretic behavior of material. *International Journal for Numerical Methods in Engineering*, 73(4), p.447–469.

Yun, G.J., Ghaboussi, J. & Elnashai, A.S., 2008 b. A design-variable-based inelastic hysteretic model for beam–column connections. *Earthquake Engineering and Structural Dynamics*, 37(4), p.535–555.

Yun, G.J., Ghaboussi, J. & Elnashai, A.S., 2008 c. Self-learning simulation method for inverse nonlinear modeling of cyclic behavior of connections. *Computer Methods in Applied Mechanics and Engineering*, 197(33-40), p.2836–2857.

LIST OF PUBLICATIONS

The following publications were accomplished during the author's PhD studies in University of Exeter.

Journals

- Faramarzi, A., Javadi, A. A., and Ahangar-Asr, A., *Numerical Implementation of EPR-based material models in finite element analysis*, Computers and Structures, 2011, (under review).
- Javadi, A. A., Faramarzi, A., and Ahangar-Asr, A., *Analysis of behaviour of soils under cyclic loading using EPR-based finite element method*, Finite Element in Analysis and Design, 2011, (under review).
- Javadi, A. A., Faramarzi, A., and Farmani, R. *Design and Optimization of Microstructure of Auxetic Materials*, Engineering Computations, 2011, 29(3), In Press.
- Rezania, M., Faramarzi, A., and Javadi, A. A. *An evolutionary based approach for assessment of earthquake-induced soil liquefaction and lateral displacement*, Engineering Applications of Artificial Intelligence, 2011, pp 142-153., vol. 24(1)
- Ahangar-Asr, A., Faramarzi, A., Javadi, A. A. and Giustolisi, O. *Modelling Mechanical Behaviour of Rubber Concrete Using Evolutionary Polynomial Regression*, Engineering Computations, 2011, pp 492-507, vol. 28(4).
- Ahangar-Asr, A., Faramarzi, A., Mottaghifard, N., Javadi, A. A., *Modelling of Permeability and Compaction Characteristics of Soils using Evolutionary Polynomial Regression*, Computers and Geosciences, 2011, vol. (In Press).
- Ahangar-Asr, A., Faramarzi, A. and Javadi, A. A. *A New Approach for Prediction of the Stability of Soil and Rock Slopes*, Engineering Computations, 2010, pp 878-893., vol. 27(7)
- Javadi, A. A., Mehravar, M., Faramarzi, A. and Ahangar-Asr, A. *An Artificial Intelligence Based Finite Element Method*, ISAST Transactions on Computers and Intelligent Systems, 2009, pp 1-7., vol. 1(2).

Conferences

- Javadi, A. A., Faramarzi, A., Mehravar, M. and Ahangar-Asr, A. *EPR-Based Finite Element Analysis of Soils Under Cyclic Loading*, Proceedings of the 19th ACME Conference, 5-6 April 2011, Heriot-Watt University, Edinburgh, 2011, pp 57-60
- Faramarzi, A., Mehravar, M., Veladi, H., Javadi, A. A., Ahangar-Asr, A. and Mehravar, M. *A Hysteretic Model for Steel Plate Shear Walls*, Proceedings of the 19th ACME Conference, 5-6 April 2011, Heriot-Watt University, Edinburgh, 2011, pp 69-72
- Ahangar-Asr, A., Faramarzi, A., Javadi, A. A., Mottaghifard, N. *An Evolutionary Approach to Modelling Compaction Characteristics of Soils*, Proceedings of the 19th ACME Conference, 5-6 April 2011, Heriot-Watt University, Edinburgh, 2011, pp 45-48
- Ahangar-Asr, A., Mottaghifard, N., Faramarzi, A., Javadi, A.A. *A Prediction Model for the Stability Factor of Safety in Soil Slopes*, Postgraduate Conference on Computing: Applications and Theory (PCCAT 2011), 2011, pp 37-40.
- Javadi, A. A., Faramarzi, A., Ahangar-Asr, A., and Mehravar, M. *Intelligent Finite Element Method in Geotechnical Engineering*, Proceedings of the 18th Annual Conference of the Association of Computational Mechanics in Engineering (ACME-UK), 29-31 March 2010, University of Southampton, 2010, pp 89-92.
- Javadi, A. A., Faramarzi, A., Ahangar-Asr, A. and Mehravar, M. *Finite element analysis of three dimensional shallow foundation using artificial intelligence based constitutive model*, Proceedings of the International Conference on Computing in Civil and Building Engineering, 30 June-2 July, Nottingham, UK, Nottingham University Press, 2010, pp 421., vol. Paper 211
- Ahangar-Asr, A., Faramarzi, A. and Javadi, A.A. *An evolutionary numerical approach to modelling the mechanical properties of rubber concrete*, Proceedings of the International Conference on Computing in Civil and Building Engineering, 30 June-2 July, Nottingham, UK, Nottingham University Press, 2010, pp 411., vol. Paper 206
- Javadi, A. A., Faramarzi, A., Farmani, R., Mehravar, M., and Ahangar-Asr, A. *Optimising Microstructure of Auxetic Materials*, 8th ASMO UK / ISSMO conference on Engineering Design Optimization, Queen Mary University of London, London, 8-9 July, 2010.
- Javadi, A. A., Johari, A., Ahangar-Asr, A., Faramarzi, A., and Toll, D. G. *Prediction of the behaviour of unsaturated soils using evolutionary polynomial regression: An incremental approach*, 5th International Conference on Unsaturated Soils, 6-8 September, Barcelona, Spain, 2010, pp 837-842.

- Javadi, A. A., Faramarzi, A. and Ahangar-Asr, A. *An Intelligent Finite Element Method*, Proceedings of 17th. conference on computational mechanics (ACME-UK), 6-8 April 2009, Nottingham, pp 307-310., 2009
- Javadi, A. A., Faramarzi, A., Farmani, R. and Evans, K. E. *Design of Microstructure and Topological Optimisation of Auxetic Materials*, Proceedings of 17th. conference on computational mechanics (ACME-UK), 6-8 April 2009, Nottingham, pp 251-254., 2009
- Javadi, A. A., Johari, A., Ahangar-Asr, A., Faramarzi, A. and Toll, D. G. *Using Evolutionary Polynomial Regression in Modelling of Unsaturated Soils*, Proceedings of 17th. conference on computational mechanics (ACME-UK), 6-8 April 2009, Nottingham, pp 353-356., 2009
- Javadi, A. A., Johari, A., Ahangar-Asr, A., Faramarzi, A. and Toll, D.G. *A New Approach to Constitutive Modelling of Unsaturated Soils Using Evolutionary Polynomial Regression*, Proceedings of 4th Asia-Pacific Conference on Unsaturated Soils, Newcastle, Australia., 2009
- Faramarzi, A. *Design of microstructure and topological optimisation of auxetic materials (poster presentation)*, 11th. Young Researchers Conference, 18 March 2009, London, UK., 2009
- Faramarzi, A. and Javadi, A. A. *Dynamic Analysis of Steel Plate Shear Walls (Poster Presentation)*, 10th. Young Researchers Conference, 19 March 2008, London, UK. , 2008.

UNIVERSITY OF EXETER

CONGRATULATIONS

Asaad Faramarzi

on obtaining an

Effective Researcher Award for Excellence 2011
worth £100

We are delighted that you have obtained this prestigious and highly competitive award whilst studying for your PhD at the University of Exeter.

We will do our best to ensure you have the support and training you need to succeed in your studies and in the future, and I hope that you will make full use of the resources we have on offer and will play a full part in the life of the postgraduate community at Exeter.

We wish you every good fortune for your future.

Professor Robert Van de Noort
Dean of the Faculty of Research
July 2011

UNIVERSITY OF EXETER

Advanced Technologies Research Institute

Prize for the Best PhD Student at the Final Stage

Asaad Faramarzi

In recognition of the best overall PhD student at the final stage awarded by the Advanced Technologies Research Institute

Professor K E Evans CEng CPhys
Dean of College

College of Engineering, Mathematics and Physical Sciences

UNIVERSITY OF EXETER

SCHOOL OF ENGINEERING, COMPUTING AND MATHEMATICS

Harrison Building
North Park Road
Exeter
UK EX4 4QF

Telephone +44 (0)1392 263628
Fax +44 (0)1392 217965
Web www.exeter.ac.uk/secam

06 February 2009

Mr Asaad Faramarzi
94 Mount Pleasant Road
EXETER
Devon
EX4 7AD

Dear Asaad

Advanced Technologies Research Institute Prize 2007/8

I am writing to notify you that you have been awarded the Advanced Technologies Research Institute Prize for the best PhD student at Stage 1. This award is based on your outstanding performance.

Congratulations on your award.

Yours sincerely

pp. Professor K E Evans CEng CPhys
Head of School